0119

1680

RD&E CENTER

Technical Report

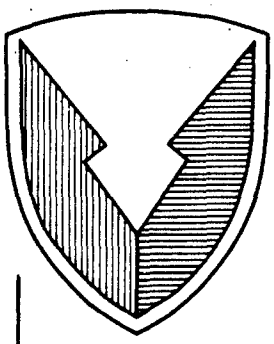

No. 13558

DEVELOPMENT OF A MODULAR TRANSIENT CYCLE ANALYSIS PROGRAM FOR THE ADIABATIC DIESEL AND OTHER COMPOUND DIESEL ENGINES

CONTRACT DAAE07-84-C-R063

JUNE 1991

Gary L. Borman
Patrick V. Farrell
David E. Foster
Jay K. Martin
and
Phillip S. Myers
Engine Research Center
University of Wisconsin-Madison
1500 Johnson Drive
Madison, WI 53706

By

U.S. ARMY TANK-AUTOMOTIVE COMMAND
RESEARCH, DEVELOPMENT & ENGINEERING CENTER
Warren, Michigan 48397-5000

NOTICES

This report is not to be construed as an official Department of the Army position.

Mention of any trade names of manufacturers in this report shall not be construed as an official endorsement or approval of such products or companies by the U.S. Government.

Destroy this report when it is no longer needed. Do not return it to the originator.

UNCLASSIFIED

SECURITY CLASSIFICATION OF THIS PAGE

REPORT DOCUMENTATION PAGE

1a. REPORT SECURITY CLASSIFICATION UNCLASSIFIED	1b RESTRICTIVE MARKINGS
2a. SECURITY CLASSIFICATION AUTHORITY	3 DISTRIBUTION / AVAILABILITY OF REPORT UNCLASSIFIED/UNLIMITED
2b. DECLASSIFICATION / DOWNGRADING SCHEDULE	
4 PERFORMING ORGANIZATION REPORT NUMBER(S)	5. MONITORING ORGANIZATION REPORT NUMBER(S)
6a. NAME OF PERFORMING ORGANIZATION Engine Research Center University of Wisconsin-Madison 6b OFFICE SYMBOL (If applicable)	7a. NAME OF MONITORING ORGANIZATION U.S. Army Tank Automotive Command
6c. ADDRESS (City, State, and ZIP Code) 1500 Johnson Drive Madison, WI 53706	7b. ADDRESS (City, State, and ZIP Code) ATTN: DRSTA-DFOA WARREN, MI 48397-5000
8a. NAME OF FUNDING / SPONSORING ORGANIZATION U.S. Army Tank Automotive Command 8b. OFFICE SYMBOL (If applicable)	9. PROCUREMENT INSTRUMENT IDENTIFICATION NUMBER DAAE07-84-C-R063
8c. ADDRESS (City, State, and ZIP Code) ATTN: DRSTA-DFOA WARREN, MI 48397-5000	10. SOURCE OF FUNDING NUMBERS PROGRAM ELEMENT NO. / PROJECT NO. / TASK NO. / WORK UNIT ACCESSION NO.

11. TITLE (Include Security Classification)
Development of a Modular Transient Cycle Analysis Program for the Adiabatic Diesel and Other Compound Diesel Engines (Unclassified)

12. PERSONAL AUTHOR(S)
Gary L. Borman, Patrick V. Farrell, David E. Foster, Jay K. Martin, Phillip S. Myers

13a. TYPE OF REPORT	13b. TIME COVERED	14. DATE OF REPORT (Year, Month, Day)	15. PAGE COUNT
FINAL	FROM 7/30/84 TO 5/30/90	June 17, 1991	123

16. SUPPLEMENTARY NOTATION

17. COSATI CODES			18. SUBJECT TERMS (Continue on reverse if necessary and identify by block number)
FIELD	GROUP	SUB-GROUP	

19. ABSTRACT (Continue on reverse if necessary and identify by block number)

This final report covers a broad range of research activities, each of which contributes to the improved application of zero-dimensional engine cycle codes and/or multidimensional computational fluid mechanics (CFM) codes to engine design. Most of the work focused on problems related to in-cylinder heat transfer.

20. DISTRIBUTION / AVAILABILITY OF ABSTRACT ☒ UNCLASSIFIED/UNLIMITED ☐ SAME AS RPT. ☐ DTIC USERS	21. ABSTRACT SECURITY CLASSIFICATION UNCLASSIFIED
22a. NAME OF RESPONSIBLE INDIVIDUAL Gary L. Borman	22b. TELEPHONE (Include Area Code) 608/263-1616 22c. OFFICE SYMBOL

DD FORM 1473, 84 MAR 83 APR edition may be used until exhausted. All other editions are obsolete.

SECURITY CLASSIFICATION OF THIS PAGE

SUMMARY

This final report covers a broad range of research activities each of which contributes to the improved application of zero-dimensional engine cycle codes and/or multidimensional computational fluid mechanics (CFM) codes to engine design. Most of the work focused on problems related to in-cylinder heat transfer. The major tasks accomplished are listed below.

(1) A cycle analysis code for a single cylinder engine was written, in a modular format, with inclusion of the ability to handle the in-cylinder effects of dynamic changes in engine operating conditions.

(2) A study of a new method of correlating cylinder pressure data during combustion in terms of engine operating parameters was conducted. The method was illustrated by application to a set of data taken on a single cylinder Cummins NH engine with simulated turbocharging.

(3) Experiments conducted on the single cylinder Cummins NH engine determined the instantaneous in-cylinder heat transfer following step changes in fueling level.

(4) Experiments were conducted on an engine with optical access through the piston and clearance volume to establish boundary layer data needed for theoretical development of heat transfer models appropriate for use in CFM codes. These data for motored conditions included velocity and velocity fluctuation data, boundary layer temperature profiles, and instantaneous heat flux data. The temperature profiles were obtained by speckle interferometry, applied to an engine for the first time.

(5) New methods for calculation of instantaneous spatially resolved heat flux in the engine cylinder were developed and incorporated into an available CFM code. The new theory incorporated the data as described in Item 4 above.

(6) The new boundary layer computational methods were exercised for variations in engine parameters and were compared with heat transfer data from motored engine experiments conducted at the University of Wisconsin-Madison Engine Research Center under Army Research Office (ARO) funding.

(7) A series of experiments were conducted on the Cummins NH engine with and without sprayed zirconia coatings on the piston, head and valve face surfaces. Data included two-color pyrometry measurements of the flame temperature and soot concentration at the outer portion of the piston bowl.

(8) Attempts to use results from CFM code calculations to upgrade models for zero-dimensional cycle codes showed that too many uncertainties still exist in the CFM codes to make such coupling practical at this time.

Each of the above listed tasks resulted in publications of theses and/or papers which are referenced in the body of the report. An abbreviated list of conclusions from the research is given below.

(1) The modular cycle analysis program results agree well with the engine data, and both show that under step changes in fueling level with constant speed and intake port conditions, imep, isfc, and volumetric efficiency jump to the new steady state values almost immediately.

(2) It is possible to correlate cylinder pressure with a simple function containing three parameters and dimensionless time. Correlations of ignition delay and combustion duration were found which fit the data for the Cummins NH engine and define the dimensionless time. The three parameters in the pressure function are correlated in terms of simple functions of the engine operating parameters. This algorithm can be used to replace correlation of heat release in the cycle analysis program.

(3) A new instrument which allows measurement of the steady state heat without using a one-dimensional approximation was constructed and tested in the Cummins NH engine. The results show that a one-dimensional approximation of steady flux, can be in error by as much as 60% at full load conditions. Thus the new instrument offers a significant improvement over conventional instruments.

(4) Experimental data for step changes in fueling level show that the surface temperature swing during a cycle reached the new steady state values after a few cycles. The cycle average surface temperature rose rapidly after the fueling change with a time constant corresponding to about 70 cycles at 1450 rpm. Although the ignition delay, the maximum rate of pressure rise, the peak heat flux and the premixed burning fraction all increased above their final steady values immediately following the step change in fueling, the increases were small and died off rapidly.

(5) It is possible to measure boundary layer temperature profiles using speckle interferometry and to use the profiles to predict heat flux in a motored engine at low to moderate engine speeds. Application of the method to fired engines was not established. This method has the advantage that it could be used to determine heat transfer effects of roughness and porosity of ceramic surfaces.

(6) Laser Doppler velocimeter (LDV) measurements of turbulence at the edge of the boundary layer when incorporated in boundary layer models resulted in very accurate predictions of motored engine heat flux. Prediction of these values from theory alone is reasonably good for motoring and spark ignition (SI) combustion, but has not been validated for diesel combustion. Recent LDV position corrected measurements indicate that the boundary layer thickness on smooth surfaces is very thin (0.2 mm). Similar corrected measurements for surfaces which are rough have not been completed.

(7) Several improved methods of heat flux calculation for use in the CFM code KIVA were produced by the work of this contract. Calculations using these models show good agreement with motored data and with spark ignition engine data. Comparisons with diesel data are confounded by inadequate combustion models in KIVA. Comparisons for low swirl motored engines are also confounded by lack of intake flow models in KIVA.

(8) Experiments were conducted on a Cummins NH single cylinder engine with an air gap piston, partially stabilized zirconia (PSZ) coatings (1.3 mm on piston and fire deck and 0.76 mm on valves) and reduced cooling of the head. Premixed burning was reduced, indicated fuel consumption increased slightly, and closed cycle global heat transfer increased slightly for the insulated case. In-cylinder measurements of soot concentration using a two-color pyrometer showed no significant effect of insulation on soot concentration. Careful consideration of these and other data led to the conclusion that too many confounding factors are present to make any positive conclusion concerning the potential for low heat rejection designs. It is clear, however, that new ceramic materials with much lower thermal response factor (product of conductivity, density, and specific heat) and a smooth nonporous gas-side surface are required. It is then necessary to develop a high temperature combustion chamber design (injector, bowl geometry, and flow characteristics) suited to such a material.

PREFACE

This final technical report was prepared by the University of Wisconsin-Madison, Engine Research Center, for the U.S. Army Tank-Automotive Command (TACOM) under Contract DAAE-07-84-C-R063. Much of the work reported here has been greatly augmented by the Army Research Office Center of Excellence Contract DAAL03-86-K-0174.

The work was carried out under the direction of Professors G. Borman, P. Farrell, D. Foster, and J. Martin. Professor P. Myers supplied invaluable advice throughout the contract period. Four doctoral students worked on the contract projects; I-Ping Chang, J. Lin, P. Pierce, and J. Yang. Mr. Chang received his salary support from Chung Cheng Institute of Technology, Taoyuan, Taiwan. Mr. Pierce, received three years of stipend as an Army Research Fellow. Four masters degree students completed theses based on the contract work, they are; D. Cook, M. Mueller, L. Ning, and D. Verhoeven. Mr. H. Paulson worked on the contract as a visiting research student from Norway. Mr. S. Yamada worked on the contract for two years as a visiting research scientist supported by his employer, Kubota Corporation. Dr. Sung Soo Kim worked on the contract while he spent a year in Madison as a visiting professor, supported by his university, the Korean Advanced Institute of Science and Technology, Seoul, Korea. Dr. Kang Huh was supported by the contract for a period of one year as a post-doctoral fellow.

TABLE OF CONTENTS

Section		Page
1.0.	INTRODUCTION	15
2.0.	OBJECTIVES	17
3.0.	CONCLUSIONS	17
3.1.	Modular Cycle Analysis	17
3.2.	Application: Transient Load	18
3.3.	Energy Balances in an Insulated Engine	19
3.4.	Models for Spatially-Resolved Heat Transfer	19
4.0.	RECOMMENDATIONS	20
4.1.	Engine Analysis	20
4.2.	Heat Transfer Analysis	20
4.3.	Heat Transfer in Insulated Engines	20
5.0.	DISCUSSION	21
5.1.	Modular Cycle Analysis	21
5.1.1.	Steady State Code	21
5.1.2.	Dynamic-State Code	21
5.1.3.	Pressure Fitting	26
5.1.4.	Application to Design	29
5.1.5.	Combining CFM and Cycle Codes	29
5.2.	Application: Transient Load	31
5.2.1.	Background	31
5.2.2.	Experimental Design	32
5.2.3.	Other Measurements and Data Acquisition	40
5.2.4.	First Law Energy Balances	51
5.2.5.	Overall Long Term Response of the Engine	51
5.3.	Energy Balances and Particulate Temperature Measurement in an Insulated Engine	57
5.3.1.	Background	57
5.3.2.	PSZ Tests	58
5.3.3.	Reasons for Conflicting Results	64
5.3.4.	Observations	70
5.4.	Models for Spatially-Resolved Heat Transfer	71
5.4.1.	Need for Spatially-Resolved Predictions	71
5.4.2.	Engine Measurements to Support Development of Heat Transfer Models	78

TABLE OF CONTENTS (Continued)

Section		Page
5.4.3.	Comparisons with Experimental Data	101
5.4.4.	Comparisons with KIVA II Predictions	104

LIST OF REFERENCES 115

DISTRIBUTION LIST Dist-1

LIST OF ILLUSTRATIONS

Figure	Title	Page
5-1.	FORTRAN program flow chart for steady state cyclic simulation program	22
5-2.	FORTRAN program flow chart for the transient cycle simulation program	23
5-3.	FORTRAN program flow chart for the transient wall temperature calculation	24
5-4.	The influence of individual engine operation parameter on parameter "A"	28
5-5.	Comparison of heat release rates for a case with small premixed combustion and comparison of pressures calculated from cycle simulation program by using these two AHRR respectively. (ϕ = 0.398, RPM - 1500, P_o = 0.2 MPa, T_o = 333.3 K)	30
5-6.	Locations of the Pressure Transducer and Instrumentation Plug, Top View	34
5-7.	Finite Difference Model Used in the Analysis of the Three-Dimensional Heat Flux Probe Data	35
5-8.	Schematic Diagram of Fuel Supply System for Step Load	37
5-9.	Fuel Line Pressure Before, During and After Step-Up Operation	38
5-10.	Engine Control Parameters Before, During and After Step-Up Operation	41
5-11.	Air Flow Rate, Air Delivery, Fuel Delivery and Equivalence Ratio Before, During and After Step-Up Operation	42
5-12.	Cylinder Pressure, IMEP and ISFC During Step-Up and at High Load Steady State. Low Load Steady State ISFC is 202 g/kW-hr, Low Load Steady State IMEP is 580 kPa, Low Load Steady State Cylinder Pressure is 6.89 MPa	43

LIST OF ILLUSTRATIONS (Continued)

Figure	Title	Page
5-13.	Ignition Delay During Step Up and at High Load Steady State. Low Load Steady State Ignition Delay is 8.4 Degrees	45
5-14.	Rate of Cylinder Pressure Rise of Step Up Cycle #3 vs High Load Steady State	46
5-15.	Normalized Heat Release Rates of Low Load, High Load Steady State and Step Up Cycle #3	47
5-16.	Surface Temperature Response Before, During and After Step Up Operation	49
5-17.	Cycle Averaged Surface Temperature and Surface Temperature Swing Before, During and After Step Up Operation	50
5-18.	Comparison of Surface Heat Flux at Low Load, High Load Steady State and Step Up Cycle #3	53
5-19.	Averaged and Maximum Surface Heat Flux Before, During and After Step Up Operation	54
5-20.	Cycle Averaged Surface Temperature and Back Side Junction Temperature of Long Transient Step Up Test Result	55
5-21.	Description of the Purdue Experimental Engine and the Matrix of Conditions Tested	59
5-22.	Comparison of Apparent Heat Release Rates, Base Engine (cooled/ metal) versus the Ceramic Coated Engine (LHR). The graph shows the results for 1300 rpm, 25% load. The table gives the results for both 25 and 50% load	60
5-23.	Summary of the Heat Transfer and Indicated Specific Fuel Consumption of the Ceramic Coated and Base Engine	61
5-24.	Description of the Wisconsin Experimental Engine and the Matrix of Conditions Tested	62

LIST OF ILLUSTRATIONS (Continued)

Figure	Title	Page
5-25.	Schematic of the Engine Test Stand and Cross Section of the Cylinder with Air-Gap Piston and Radiation Probe Assembly	63
5-26.	Apparent Heat Release and Tabulated Results for the Uncoated (LHR-1) and the Coated (LHR-2) Air-Gap Piston. The Conditions are Heavy Load (ϕ=0.5) and 1500 rpm	65
5-27.	Comparisons of Heat Transfer and Indicated Specific Fuel Consumption at Different Loads and Speeds for the Uncoated Air-Gap Piston (LHR-1) and the Ceramic Coated Air-Gap Piston (LHR-2)	66
5-28.	Cross Section Schematic of the Coolant-Wall-Gas Interface and an Equivalent Electrical Analogy	69
5-29.	Bottom View of Cylinder Head	80
5-30.	Cross Section of Clearance Volume Showing Location of Windows (Areas With Dots), Valves, and Instrumentation Port	81
5-31.	Side View of the Instrumentation Plug	82
5-32.	Experimental Set Up for Speckle Interferometry in an Engine	84
5-33.	Set Up for Reconstruction from Speckle Interferograms	85
5-34.	Thermal Boundary Layer Thickness Estimates from Speckle Data.	88
5-35.	Wall Heat Transfer Estimates from Speckle Data	89
5-36.	Wall Heat Transfer Estimates from Speckle Data for Different Engine Operating Conditions	91
5-37.	Comparison of Heat Flux Estimates from Speckle Interferometry and Heat Flux Probe Measurements	92

LIST OF ILLUSTRATIONS (Continued)

Figure	Title	Page
5-38.	McLaughlin and Tiederman Weighting Function (Dashed Line) and Modified Weighting Function Applied to Measurements (Solid Line)	94
5-39.	Velocity Data Taken 50 Microns From the Wall at 750 RPM, High Swirl	95
5-40.	Phase-Averaged Surface Temperature Swing	97
5-41.	Comparison of Bias Corrected and Uncorrected Phase Averaged Velocity Data, 50 Microns From Wall at 750 rpm, High Swirl	98
5-42.	Phase-Averaged Velocity Profiles With Bias Correction for Two Different Crank Angles and Two Engine Speeds	99
5-43.	Friction Velocities Calculated by Matching Law-of-the Wall at Different Distance from the Wall	100
5-44.	Averaged Friction Velocity vs Crank Angles for Two Engine Speed at High Swirl Conditions	102
5-45.	Comparisons of Measured Heat Flux with Model Calculations	103
5-46.	Sensitivity of Heat Flux Predictions to Value of u*	106
5-47.	Measured and Calculated Values of Heat Flux for a Change in Comparison Ratio	107
5-48.	Measured and Calculated Values of Heat Flux for a Change in Engine Speed	108
5-49.	Comparison of Heat Flux Predictions and Measurements in the Motored Pancake Engine	110
5-50.	Comparison of Different Heat Flux Model Predictions on the Cylinder Head of a Motored Deep-Bowl Engine	111

LIST OF ILLUSTRATIONS (Continued)

Figure	Title	Page
5-51.	Comparison of Different Heat Flux Model Predictions on the Cylinder Head of a Motored Deep-Bowl Engine	112
5-52.	Comparison of Different Heat Flux Model Predictions on the Cylinder Head of a Motored Deep-Bowl Engine	113

LIST OF TABLES

Table		Page
5-1.	NH Engine Specifications	33
5-2.	First Law Analysis of Step Up Transient and High Load Steady State	52
5-3.	See-Through Engine Specifications	79
5-4.	Measurement Conditions	105
5-5.	Bowl-in-Piston Geometry Specifications and Operating Conditions	105

1.0. INTRODUCTION

This report gives an overview of the research conducted under the TACOM Contract DAAE-07-84-C-R063 over the six-year period of the contract from 1984 to 1990. The primary subject of the research was heat transfer in engines and application of heat transfer models to both zero-dimensional cycle models (cycle analysis) and multidimensional in-cylinder models (the computer code KIVA). A more detailed understanding of the work may be obtained by consulting the resulting theses[1-8] and published papers.[9-18] A comprehensive review of engine heat transfer prior to 1986[19] and a brief overview of heat transfer research conducted at the Engine Research Center from 1986 to 1990[20] can be obtained from the listed references. As shown in this overview, much of the work reported here has been greatly augmented by work done under the Army Center of Excellence Contract, DAAL03-86-K-0174.

To understand the objectives of the research conducted under this contract, it is necessary to know the types of engine modeling tools available at the start of this report and their limitations. This introduction thus briefly discusses the two major modeling tools, cycle analysis, and computational fluids modeling, with emphasis on the limitations important to Army needs and the role of this contract work in removing some of these limitations.

The modeling tool, which is called cycle analysis here, is a zero-dimensional, thermodynamic model of the working fluid in the engine. Such models came into prominence in the 1960's and TACOM played a major role in their development[21] for use in diesels. During the 1970's the emphasis of research on these models was to improve the prediction of combustion and heat transfer; again TACOM played a major role, as illustrated by the work reported.[22] Despite the many attempts to improve the predictive nature of cycle analysis, the modeling of combustion and emissions did not yield to such approaches[23] because fluid mechanics and fluid mixing play a dominant role in diesel combustion and fluid behavior must be treated by multidimensional models. Thus, in the 1980's, a new generation of CFM models were introduced which eventually led to such three-dimensional codes as KIVA.[24,25] Despite the potential of the CFM codes, they require the use of supercomputers and until very recently could only deal with the closed portion of the cycle. Thus even at the time of this report, June, 1991, cycle analysis is used for understanding basic engine design questions. The work reported here thus deals with cycle analysis upgrades and validations as well as CFM code issues.

The original TACOM sponsored cycle codes[26,27] were written in a format which did not allow for easy change of the code for purposes of upgrading. The code for a single cylinder engine was thus revised into a modular format.[28] Because the Army had an interest in engine response to dynamic changes in load, the new program includes the ability to model in-cylinder effects due to sudden changes in load. The Army already had a code called TRANSENG[29] which predicts turbocharger response factors and inertial response to speed changes. This program, however, ignores possible in-cylinder heat transfer transients due to the thermal response of the metal surfaces, and possible coupling between combustion and heat transfer dynamic response. Because some of these coupling effects could not be predicted by modeling alone, it was proposed to also study the engine response to sudden load changes, at constant speed and inlet conditions, experimentally. An important aspect of this result was to obtain a better means of comparing the response of diesels and gas turbines to sudden changes in operating conditions.

The calculation of heat transfer in the cycle analysis programs is based on simple algebraic relationships and thus cannot be expected to properly reproduce any dramatic change in the physics of the governing processes. One such change of particular importance to the Army is that which takes place when using low heat rejection (LHR) technologies such as ceramic coatings, air gap pistons, etc. The problem may be pursued by trying to obtain some simple correlation based on global balances for a specific LHR design.[30] Such a correlation is unlikely to be general, however, in that the heat transfer is driven by the combustion events and such events will be greatly influenced by design changes. A more promising approach is thus to use a CFM code with a fundamentally derived heat transfer model. Unfortunately, computational times do not allow using a boundary layer grid which can resolve the heat transfer and thus a sub-grid model is needed for the boundary layer. One such model is the law-of-the-wall which is an empirical relationship obtained from steady flow data. Theoretical considerations cast extreme doubt on the validity of such a correlation when applied to engine conditions. The approach used here was thus to find improved boundary layer models and at the same time examine engine boundary layers in detail using optical diagnostic methods.

The optical methods, unfortunately, restricted the boundary layer study to motored engine cases. Thus it was decided to also make flux measurements in an insulated fired diesel engine.

2.0. OBJECTIVES

The following are the objectives of the research performed under the contract.

(1) Write a new cycle analysis code in a modular format including the ability to model in-cylinder effects of dynamic changes in load.

(2) Conduct experiments on a single cylinder engine to determine in-cylinder effects caused by dynamic changes in load.

(3) Obtain fundamental data on engine boundary layer temperature and velocity profiles and turbulence.

(4) Produce new boundary layer models for use in CFM codes, such as KIVA, and compare computations using these models with experimental data.

(5) Run experimental engine tests with and without LHR technologies to determine effects of such technologies on heat transfer, in-cylinder particulates, and performance.

(6) Find methods to use CFM code results to upgrade computational models used in cycle analysis codes.

3.0. CONCLUSIONS

The conclusions are given below for each topic as designated in Section 5, Discussion.

3.1. Modular Cycle Analysis

The modular cycle analysis program results are in good agreement with the engine data, and both show that under step changes in fueling level with constant speed and intake port conditions, imep, isfc, volumetric efficiency jump to the new steady state values almost immediately.

The cycle analysis developed under this contract is to be used for research and development of single cylinder engines and does not incorporate systems questions such as turbocharger matching or manifold design. Dynamic changes for multicylinder engines are dominated by such system question and thus are not appropriately addressed by the modular program.

Prediction of in-cylinder heat transfer and combustion from basic design parameters such as chamber geometry, injector characteristics, etc., is best left to

3-D computational fluids codes. They are not possible to predict reliably from zero dimensional diesel cycle codes. However, it is possible to correlate cylinder pressure with a simple function containing three parameters and dimensionless time. Correlations of ignition delay and combustion duration were found which fit the data for the Cummins NH engine and define the dimensionless time. The three parameters in the pressure function are correlated in terms of simple functions of the engine operating parameters. This algorithm can be used to replace correlation of heat release in the cycle analysis program.

3.2. Application: Transient Load

This research has reported the results of experiments run to quantify the response and combustion characteristic of a single cylinder diesel engine during a dynamic adjustment to a step change in load. The data were analyzed by ensemble averaging individual cycles after a sequence of load changes from a repetitive "hopping" operation. The heat transfer data were corrected for three dimensional heat transfer effects and the effects of surface deposits on the heat flux probe. The following conclusions resulted.

(1) The peak cylinder pressure, IMEP and ISFC responded immediately by essentially jumping to the new steady state value.

(2) The ignition delay during the response to a step increase in load was longer than the corresponding steady state value. This difference was attributed to the lower gas temperature at the time of injection. We believe that the higher level of heat transfer was ultimately responsible.

(3) The maximum rate of pressure rise, the peak heat flux and the premixed burning fraction all increased during the dynamic response. The higher rate of pressure rise will tend to cause more noise and the higher premixed burning fraction may impact the transient cycle NO_x.

(4) The surface temperature swing was not affected by the dynamic operation. The cycle averaged temperatures responded more slowly, taking approximately 2000 cycles to reach the new steady state value.

(5) The cycle averaged temperature responded in a manner that could accurately be modeled with a double time constant exponential decay. Although not shown, this double time constant exponential response was also discussed for the dynamic response in ignition delay, rate of pressure rise, premixed burning fraction and global heat transfer.

3.3. Energy Balances in an Insulated Engine

An analysis of data in the literature, plus new data taken for this contract, indicate that it is impossible to draw a general conclusion concerning the effects of insulation on closed cycle heat transfer at this time. The reason for this is probably that various engine designs can produce different results due to complex interactions with the surfaces and combustion. However, two observations can be made.

(1) Insulation changes combustion, typically decreasing premixed burn and increasing combustion duration. Such combustion changes are known to affect heat transfer.

(2) Existing data do not indicate the effects of engine designs optimized for insulated chambers and utilizing very high pressure injection with significantly large amounts of exhaust gas recirculation.

3.4. Models for Spatially-Resolved Heat Transfer

Three new models for spatially-resolved heat transfer predictions have been developed. Each model is based on a different set of assumptions regarding the in-cylinder state. To produce accurate spatial predictions of engine heat transfer, it will be necessary to use a combination of models because of the large differences in the heat transfer physics from one location in the chamber to another, and from one time in the cycle to another.

Measurements of thermal and momentum boundary layers in a motored four-stroke engine have shown that typical engine port and in-cylinder geometries result in extremely thin boundary layers, with the possibility of direct interaction of the turbulent flow and the wall. In fact, it is likely that engine boundary layers can display behavior that ranges from being very similar to flat-plate steady state boundary layers to direct turbulent interactions at the walls.

Comparisons of these model predictions showed good agreement with experiments under some motoring conditions. However, heat transfer predictions under firing conditions remain very difficult because of the unknown interactions between the combustion, wall temperature, and gas flow.

4.0. RECOMMENDATIONS

4.1. Engine Analysis

Improvements in cycle analysis programs should be sought by use of results from CFM such as KIVA. However, progress on this approach must await further improvements in CFM codes. It is thus recommended that the Army expand its work on CFM code improvement, particularly on improved combustion models.

4.2. Heat Transfer Analysis

The spatially resolved models developed under this contract can produce reasonably good results for both motored engines and fired homogeneous charge spark-ignited engines when incorporated into the CFM code KIVA.

The application of the new models to diesel combustion will undoubtedly require different models for various portions of the cylinder surface. In particular, the piston surface may require special models. It should be noted that for full load, steady state operation with high pressure injectors, liquid may not reach the piston bowl. However, in many other modes of operation, particularly during cold starting, liquid strikes the bowl. Each of these cases will require different models.

Appropriate instrumentation for radiation heat transfer measurements now exists, but calculation of radiation awaits appropriate soot models to be developed for KIVA. Work on such models should include validation for engines with high pressure injection, insulation, and turbocharging.

4.3. Heat Transfer in Insulated Engines

The measurements of heat transfer in insulated engines must be done in coordination with work on improving the combustion under conditions of high temperature combustion. The engine insulation design must allow significant levels of insulation, rather than the rather small insulating effects of the 1.27 mm thick PSZ coatings, which were used in this research.

Additional fundamental work on the effects of surface roughness and porosity need to be carried out. Deposit effects for high temperature, low sooting engines do not appear to be significant.

5.0. DISCUSSION

5.1. Modular Cycle Analysis

5.1.1. Steady state Code. The cycle analysis methods and equations given in references 31 and 32 were used to obtain a modular code for steady state operation of a single cylinder open chamber diesel engine. The major modification in the code of reference 33, other than the new modular organization, was to use the IMSL library subroutine DVERK[34] to solve the differential equations. Figure 5-1 shows the flow chart for the program. The thesis of Ning Lei[35] gives a users guide and listing of the FORTRAN code. In this version of the program, the surface temperatures for each zone are computed from a simple lumped resistance network. Resistances can be estimated from past experience, but require adjustment by comparison with engine data at a set point to obtain the best results. The program was run for the Cummins NH single cylinder and compared with experimental data. Accuracy was similar to that previously reported.[36,37]

5.1.2. Dynamic-State Code. The modular cycle program was written in a second version which includes the effects of dynamic load changes. The program starts with the engine at a steady state condition. The user must supply the operating condition history such as fueling level change and speed. The purpose of the program is to explore in-cylinder transients for a single cylinder engine on a test stand in a research environment. Users who do not care about these in-cylinder details, but who need to understand effects of turbocharger transients, etc. for a multicylinder engine, should use the program of reference 38.

The primary difference between the steady state and dynamic codes is the handling of the part temperatures. The simplification which ignores surface temperature swings during a given cycle is maintained. However, as the load is changed dynamically the surface, and eventually the entire part temperatures will change from cycle-to-cycle. The piston and valves are modeled using a finite difference code given in reference 39. The models are axisymmetric and highly simplified. The concept is to reproduce the general change in part temperatures without introducing large computational times. The resulting temperature distributions are thus intended to give cycle trends rather than temperature distributions for purposes of thermal stress calculations. The gas-side boundary conditions are computed from effective gas temperatures and heat transfer coefficients averaged over a given cycle. The boundary condition thus consists of a series of step changes, each step being one cycle (two engine revolutions) long. Figures 5-2 and 5-3 show the flow charts for the dynamic program and wall

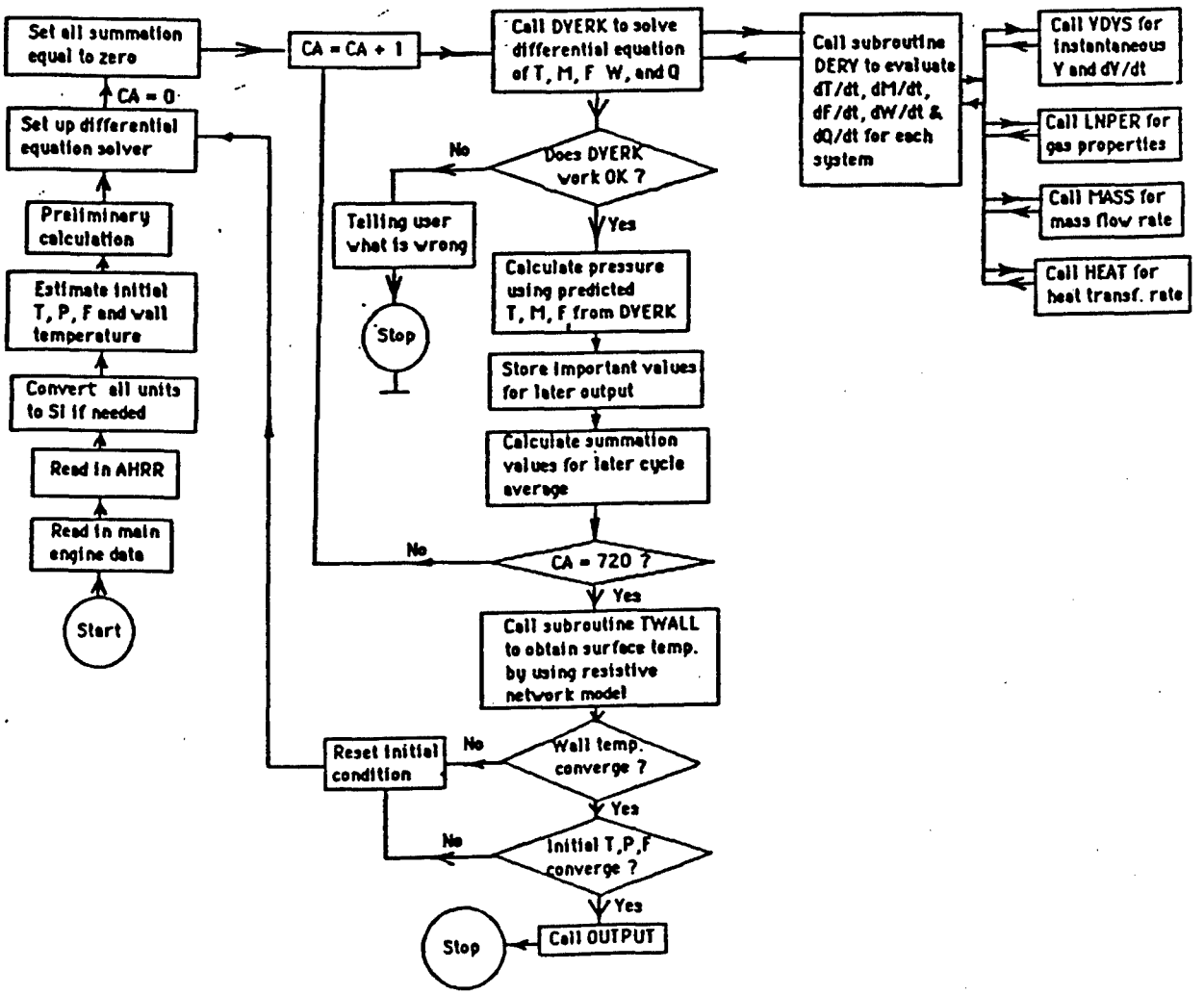

Figure 5.1. FORTRAN Program Flow Chart for Steady State Cycle Simulation Program

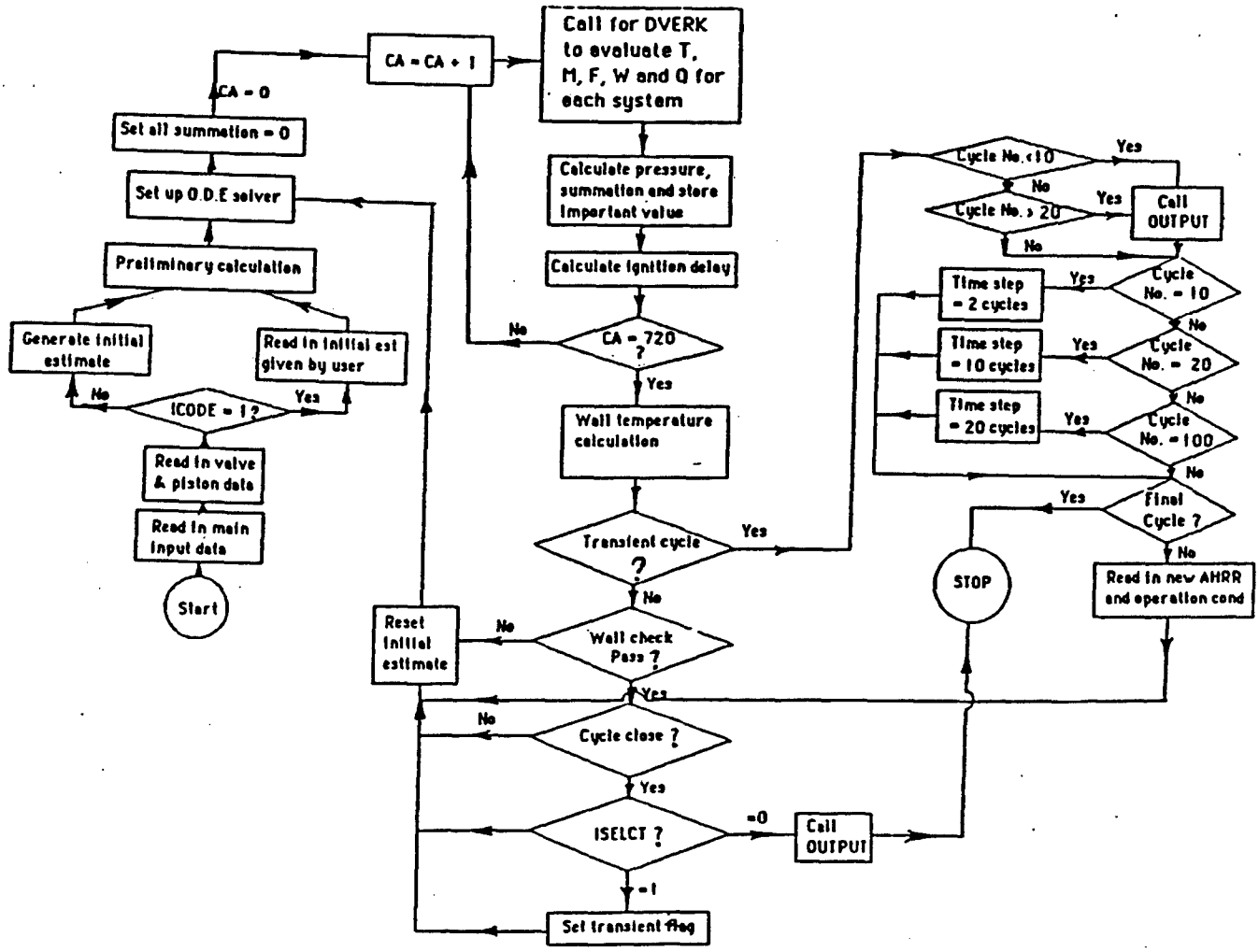

Figure 5-2. FORTRAN Program Flow Chart for the Transient Cycle Simulation Program

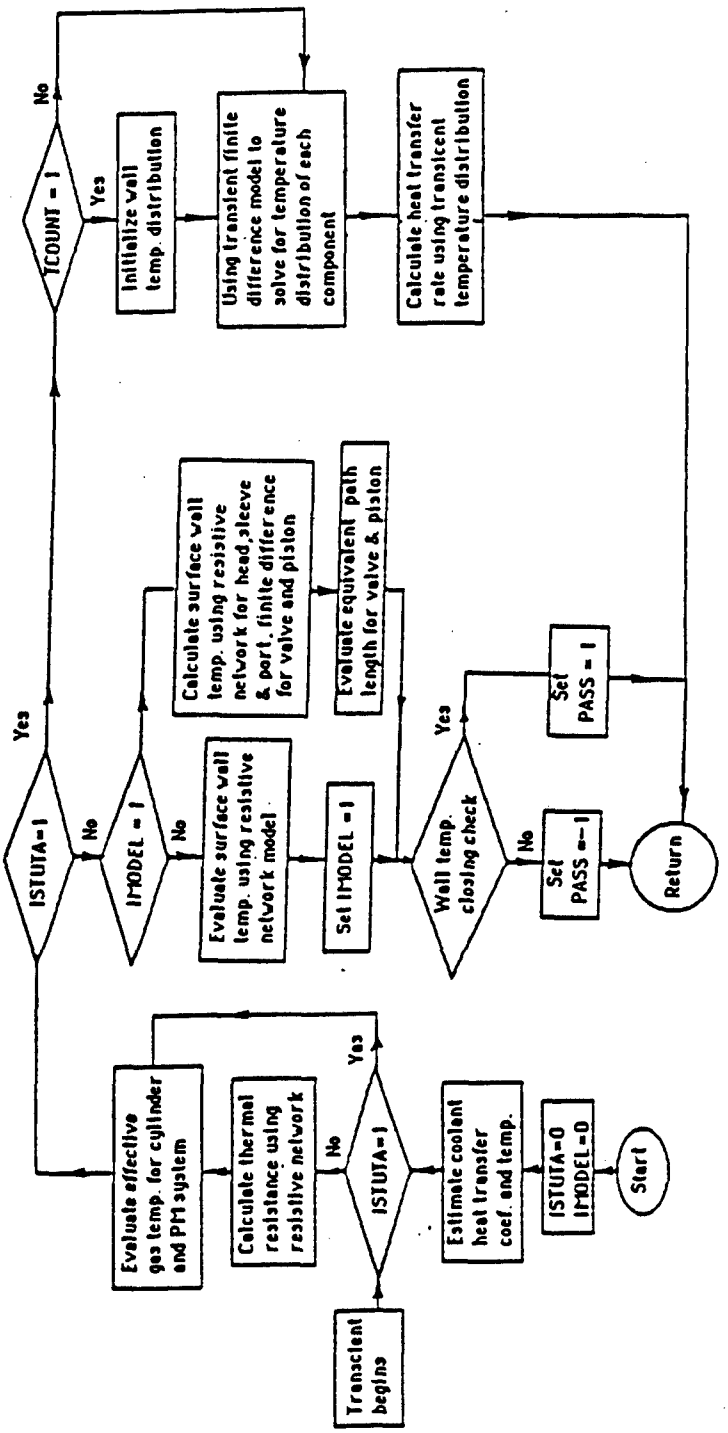

Figure 5-3. FORTRAN Program Flow Chart for the Transient Wall Temperature Calculation

temperature calculations respectively. The results from these calculations are in good agreement with the experimental results which are discussed in another section of this report.

Although the effects of load change on the cycle turn out to be small, there are some changes in the combustion which result from changes in ignition delay. When the load is stepped up, the wall temperatures are lower and result in lower gas temperatures and thus longer ignition delays. This results in a change in the time of the start of combustion and increased premixed burning. It is important to note, however, that these small changes are masked by cyclic variability. For example, a change in load from 0.3 to 0.6 equivalence ratio gives only a one crank

degree increase in ignition delay between the third cycle after the step and the steady state high load value. The change in the pressure trace, due to such a difference, is very small. Thus simply phasing the heat release properly, but using the steady state heat release shape, gives an adequate model for the imep response to the transient load, but does not predict the small changes in peak pressure due to the slightly increased premixed burn fraction.

In order to correct the phasing of the start of heat release, a formula for prediction of ignition delay is needed. The ignition delay (ID) in crankdegrees was fit using steady state data from the NH engine and the equation

$$ID = 0.075 p^{-1.637} \phi^{-.445} \exp(3811.9 / T) \qquad (1)$$

where p = the average pressure during the delay, MPa
T = the average temperature during the delay, K
ϕ = equivalence ratio

The formula fits the NH data base very well, but the constants are engine specific.

There is no doubt that fitting the heat release using two Weibe functions, as done by Miyamoto, et al.,[40] would allow correlation of the heat release shape change with ignition delay, but again the resulting constants would be engine specific. It is our judgment that all such approaches using cycle analysis will be engine specific and thus not predictive for new engine designs. The best use of cycle analysis is thus to understand trends or to analyze a specific engine for which a data base already exists. It is not yet known if CFM codes will eventually be predictive, but they do offer that potential.

5.1.3. Pressure Fitting. The approach to modeling combustion typically used in cycle analysis follows that of Ref. 41. The method uses engine specific pressure data to generate a single zone heat release rate. Generalized forms of the heat release shape may be used to give trends, but predictions for different engine designs are not trustworthy.[42] Furthermore, the algorithm for generating the heat release from the pressure data requires computation of the pressure derivative (time rate-of-change of pressure). The accuracy is uncertain because noise and pressure waves must be filtered out prior to the calculation. A different approach is offered in this report which can be used as an alternative for those wishing to reproduce performance factors without regard to details of the combustion process. In this approach, the pressure data are fit directly in terms of a normalized crankangle, X, and three constants, A,B,C. The three constants are then each fit empirically in terms of engine operating parameters.

The cylinder pressure measured during combustion is normalized by a scaling factor, p_o, to give the dimensionless pressure P. The reciprocal of P is then fit in terms of X.

$$1/P = p_o/p = AX^2 + BX + C \tag{2}$$

where p_o = 6.895 MPa (1000 psi) is used here.

The dimensionless crankangle X is defined as

$$X = (\theta - \theta_1)/(\theta_2 - \theta_1) \tag{3}$$

where θ = crankangle
θ_1 = crankangle at ignition
θ_2 = crankangle at end of combustion

Thus we see that X = 0 at start of combustion and X = 1 at end of combustion and $\theta_2 - \theta_1$ is the combustion duration. The value of θ_1 is obtained directly from analysis of the data and determines C.

$$C = p_o/p(\theta_1) = p_o/p_1 \tag{4}$$

Exact determination of θ_1 is not easily accomplished because the processes of cooling by fuel vaporization and heating by combustion are competitive during the delay period. An alternative which does not use energy analysis was recently proposed by I.S. Mohammad.[43] In this analysis, the statistical deviation of the

pressure for many (300) cycles shows a slight hump at the start of combustion and thus identifies θ_1.

The value of B was determined by noting that the maximum value of P from Eq. 2 is given by

$$B = -2AX_m \tag{5}$$

where X_m is the value of X at the peak (maximum) pressure, P_m.

Using Eqs. (4) and (5) gives

$$B = -\left[4A(1/P_1 - 1/P_m)\right]^{1/2} \tag{6}$$

Given P_1 and P_m, the constant A remains to be determined. The method recommended here is to select A such that the work done during combustion, W_{12}, determined from

$$W_{12} = \int_{\theta_1}^{\theta_2} p(dV/d\theta), \tag{7}$$

where V is the cylinder volume, is the same as the work computed using the formula of Eq. (2) to determine p.

The combustion duration was determined by selecting θ_2 as the value corresponding to 99% heat release as determined from a single zone model. The duration was then fit using the Cummins NH data.

$$\theta_2 - \theta_1 = 3.\theta^{0.303}(\text{rpm})^{0.174} p_i^{0.25} T_i^{0.45} \tag{8}$$

where rpm = engine speed, revolutions per minute
p_i = intake pressure, MPa
T_i = intake temperature, K.

As in the case of ignition delay, the formula constants are engine specific. The formula error is less than 5% for all data and less than 2.5% for 80% of the data.

The values of the constant A were fit in terms of p_i, T_i, rpm, and ϕ. Figure 5-4 shows the resulting plots of A which were fit with straight lines. The constant A is fit to within 2% error over the ranges shown in Fig. 5-4 by,

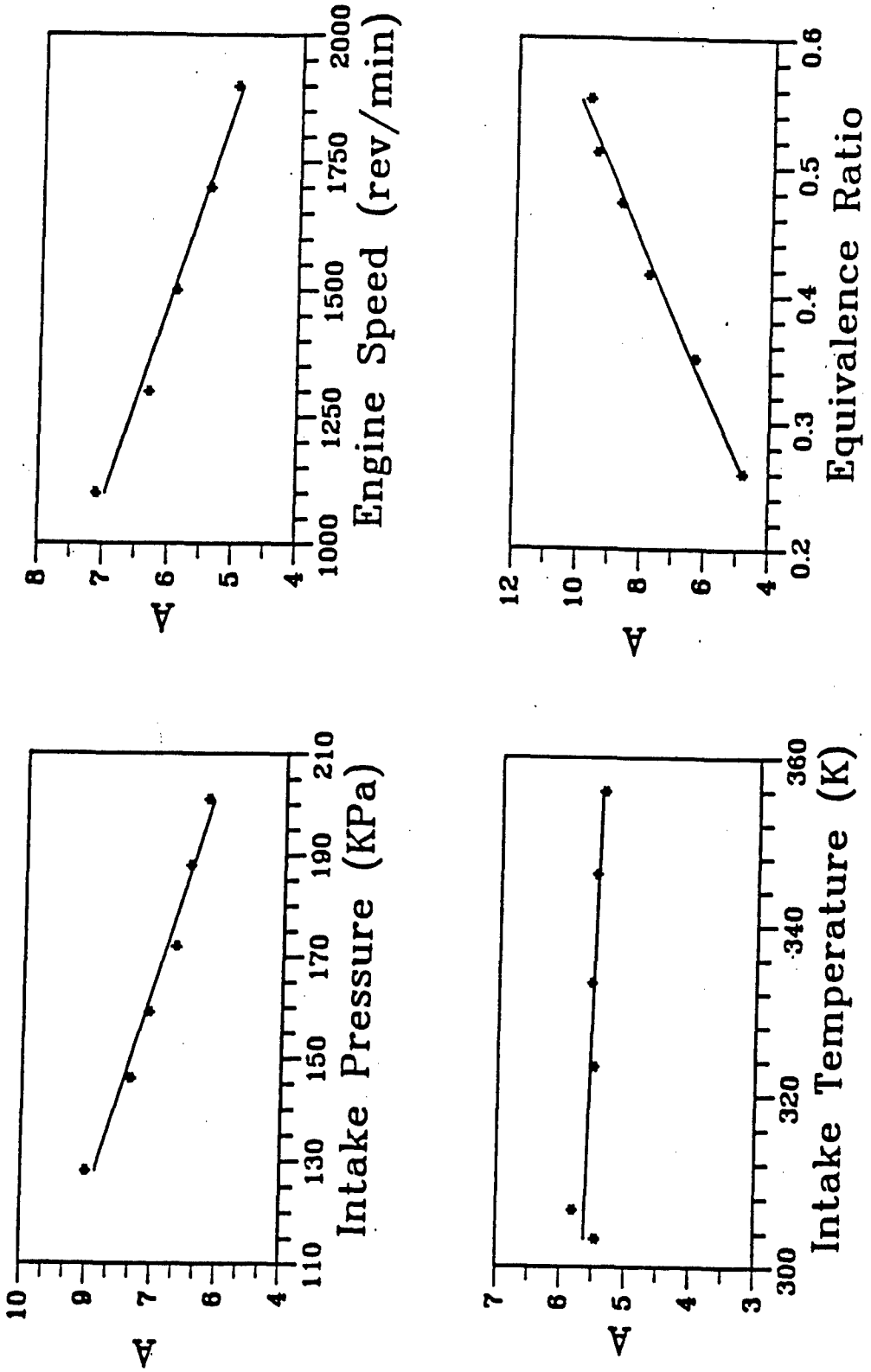

Figure 5-4. The Influence of Individual Engine Operation Parameter on Parameter "A"

$$A = 10.14 + 9.33\phi - 31.476 p_i - 0.00123 rpm \quad (9)$$

The fits of pressure agree extremely well with the data except in the region of the initial (premixed) burning. This is illustrated in Fig. 5-5 for a typical case. The deviation would be larger for a naturally aspirated engine, but for modern turbocharged engines it is too small to see on all but a very large plot. The resulting heat release analysis, also shown in Fig. 5-5, shows that this small deviation causes the characteristic "premixed burn spike". Clearly, the simple fitting procedure is not useful if one wishes to study the premixed burn fraction characteristics.

5.1.4. Application to Design. The algorithm, given in the previous section, may be applied as a design procedure when combined with the cycle analysis program. The concept may be applied to study the data base engine or could be extrapolated to an engine of the same family. The procedure steps are listed below.

(1) Using the cycle analysis determine θ_1 and θ_2 using Eq. (1) and Eq. (8), respectively, for a selected injection timing. This gives p_1.

(2) Select a maximum (peak) pressure, p_m, and find A,B,C using it and Eq. (9). This allows generation of $p(\theta)$ for $\theta_1 \le \theta \le \theta_2$.

(3) Compute the heat release rate from the $p(\theta)$ equation and use it in the cycle analysis.

Following these steps, the designer can generate trends using the cycle code. It is obvious that this does not help to design the combustion system (injector hole number, swirl, bowl shape, etc.). To design the combustion system from analysis requires use of CFM codes such as KIVA which incorporate details of the spray, fluid mechanics, and combustion kinetics.

5.1.5. Combining CFM and Cycle Codes. It is possible to run CFM codes such as KIVA for design purposes, however, it may not be cost or time effective. It may be possible, however, to use the CFM code as a substitute for experimental data to build better cycle analysis codes. The possibility for this in application to zonal heat transfer models has already been discussed in the section on heat transfer modeling. A similar technique could be applied to zonal combustion models. Such models have been attempted many times, but cannot be generalized, because methods for determining mixing models are inadequate.

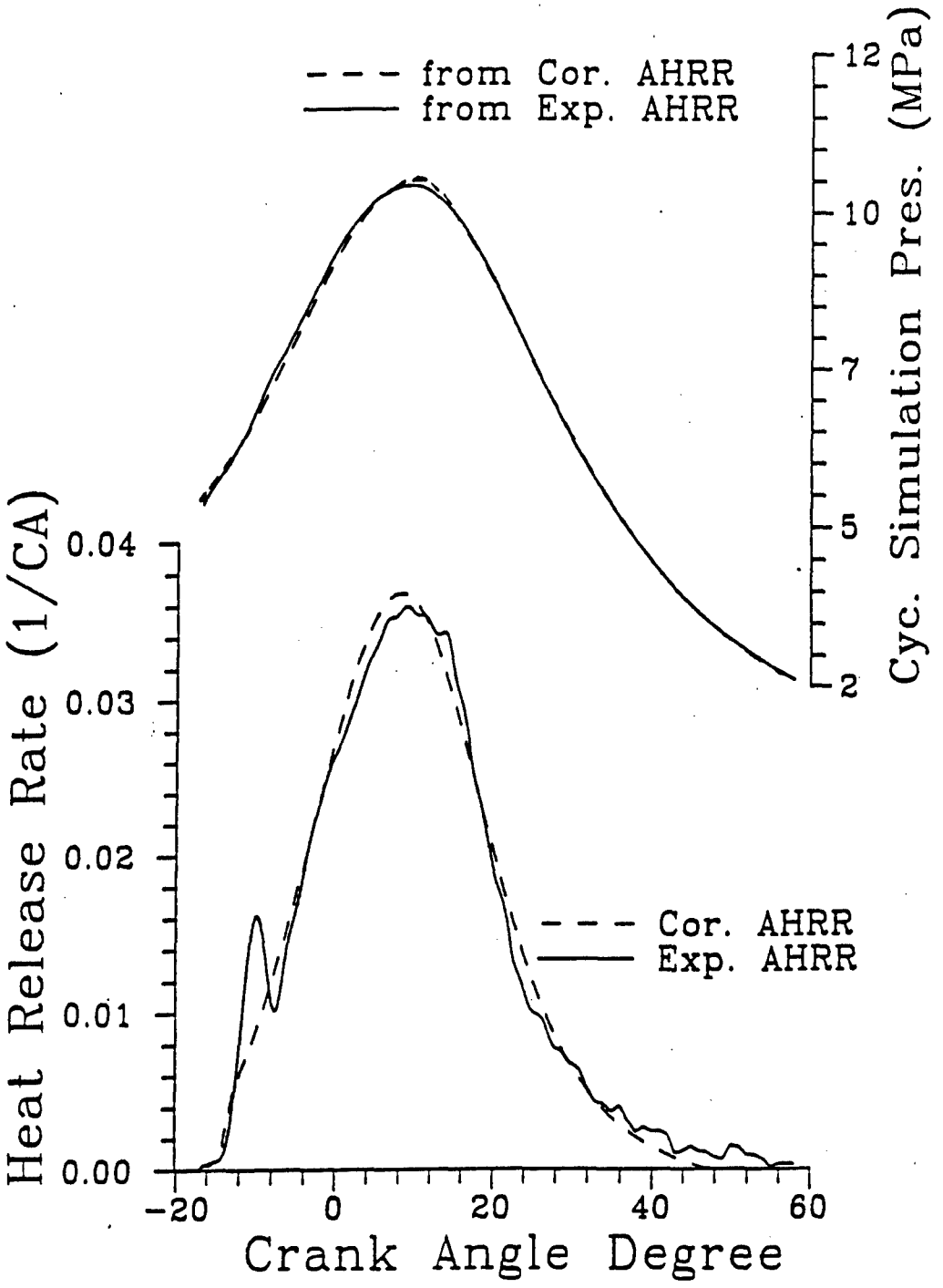

Figure 5-5. Comparison of Heat Release Rates for a Case with Small Premixed Combustion and Comparison of Pressures Calculated from Cycle Simulation Program by using these Two AHRR Respectively (ϕ = 0.398, RPM = 1500, P_o = 0.2 MPa, T_o = 333.3 K)

However, CFM codes could guide such mixing parameter selection. Computations run with KIVA at the ERC have, however, shown that present spray models lack the ability to be predictive. Thus it is premature to use KIVA for cycle analysis improvement.

5.2. Application: Transient Load

Historically, diesel engine research has focused on steady state operation. However, in practice, most of the diesel engine's operation is under transient operating conditions. Typically for engine simulations, the transient operation has been modeled as a sequence of quasi-steady state operating conditions. The research conducted for this aspect of the project addressed the issue of combustion and heat transfer during the transient (dynamic) operation of a direct injection diesel engine. In particular, a single-cylinder, direct-injection, quiescent-chamber diesel engine was used.

Of particular interest was the in-cylinder phenomena; the change of air delivery due to the turbocharging system or the change of fuel delivery caused by a governor was not included. Our purpose was to determine the time required for parameters such as ignition delay, heat release rates, instantaneous heat flux, peak pressure, and other combustion phenomena to reach their steady state values after the engine experienced a step change in load. These data would then be used to assess to what extent the steady state assumptions used in current engine simulations accurately models the actual process and what changes, if any, need to be incorporated into the simulations. If the response of the in-cylinder engine phenomena to dynamic load changes is accurately modeled then the turbocharger and governor response will follow naturally from their respective models.

5.2.1. Background. Although not studied extensively there has been some reporting in the literature of the engine response to dynamic changes in load. Watanabe, et al.[44] have studied the dynamic behavior of a variety of engines including direct and indirect injection naturally aspirated and direct injection turbocharged diesel engines. Although noise was the focus of their work some results on combustion were also reported. They found that during acceleration the ignition delay of the DI-NA engine increased by two crank angle degrees and the rate of change of pressure (dP/dt) increased two to three times relative to steady state operation. It was also reported that the combustion phenomena observed during the acceleration could be reproduced during steady state operation by using lower coolant temperatures. The authors suggested that the combustion characteristics of acceleration deviates from steady state mainly because of the lower cylinder wall temperature.

Sawa[45] discussed the behavior of exhaust smoke under accelerating conditions similar to those of Watanabe, et al. The results not only show that during acceleration the smoke level was much higher but also that the peak pressure was higher and there was a larger premixed burning portion of the heat release diagram.

Samria, et al.[46] reported that the ignition delay was longer by three crank angle degrees and the first peak in the heat release rate diagram (the premixed burning portion of the diagram) was higher during acceleration than in steady state (similar to Watanabe, et al.[47]).

5.2.2. Experimental Description. For our research a single cylinder Cummins NT855 engine was used. This engine is similar to the engines used in many Army vehicles. In its production configuration the NT855 engine is an in-line six-cylinder turbocharged engine. Our research engine was a single cylinder version of this same engine. Except for the block, crankshaft and flywheel all the engine parts used were original production engine parts. The engine specifications are given in Table 5-1.

The original NT855 cylinder head had four valves, two intake and two exhaust valves. To make room for our heat flux probe and pressure transducer we modified the head by removing an intake and exhaust valve on the exhaust port side of the cylinder head. A schematic of the top view of the cylinder head is given in Fig. 5-6.

5.2.2.1. In-cylinder instrumentation. The cylinder pressure was measured with an AVL model 8QP500ca piezo-electric transducer along with an AVL model 3059 charge amplifier.

The most unique transducer used in this work was our heat flux probe. In the more common heat flux probe a single surface thermocouple and a backside thermocouple are used along with a Fourier decomposition of the data to calculate the average and instantaneous heat flux. In this analysis one assumes that the heat transfer is one-dimensional.

With this new probe, the temperature data from each surface thermocouple can be time averaged and used with the backside temperature in a six node 3-D finite difference calculation of the average heat flux from the engine cylinder at that location. A schematic of the model and the equation for calculating the average heat flux are given in Fig. 5-7. Once the probe was constructed it was calibrated with an oven soak and an ice bath. Its accuracy was found to be typical of surface thermocouples, always within 1 K of the thermometer with which the probe was compared.

Table 5.1. NH Engine Specifications

Cycle	4-Stroke
Bore	139.7 mm (5.5 in.)
Stroke	152.4 mm (6.0 in.)
Compression ratio	13.4
Displacement	2.336 1 (142.5 $in.^3$)
Rated output	50 kW (67 hp) at 1900 RPM
Combustion Chamber	Quiescent type
Fuel injector	PTD injector
Number of orifices	8
Orifice diameter	0.2 mm
Spray angle from head	18°
Spray plume cone angle	20°-25°
Valve Timing	
Intake valve	opens at 23° before TDC (517°)*
	closes at 33° after BDC (33°)
Exhaust valve	opens at 46° before BDC (314°)
	closes at 39° after TDC (579°)

* BDC before compression as 0°.

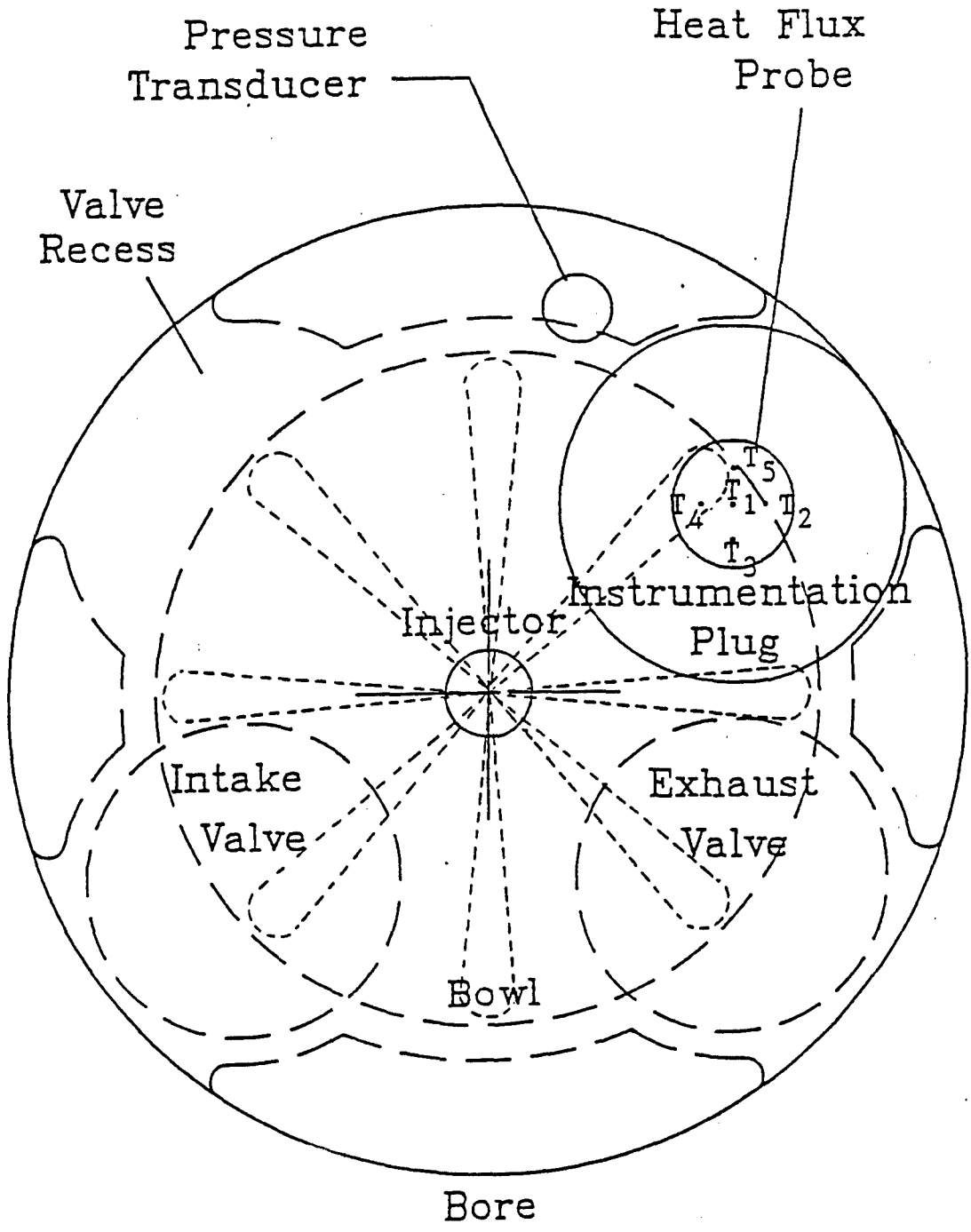

Figure 5-6. Locations of the Pressure Transducer and Instrumentation Plug, Top View

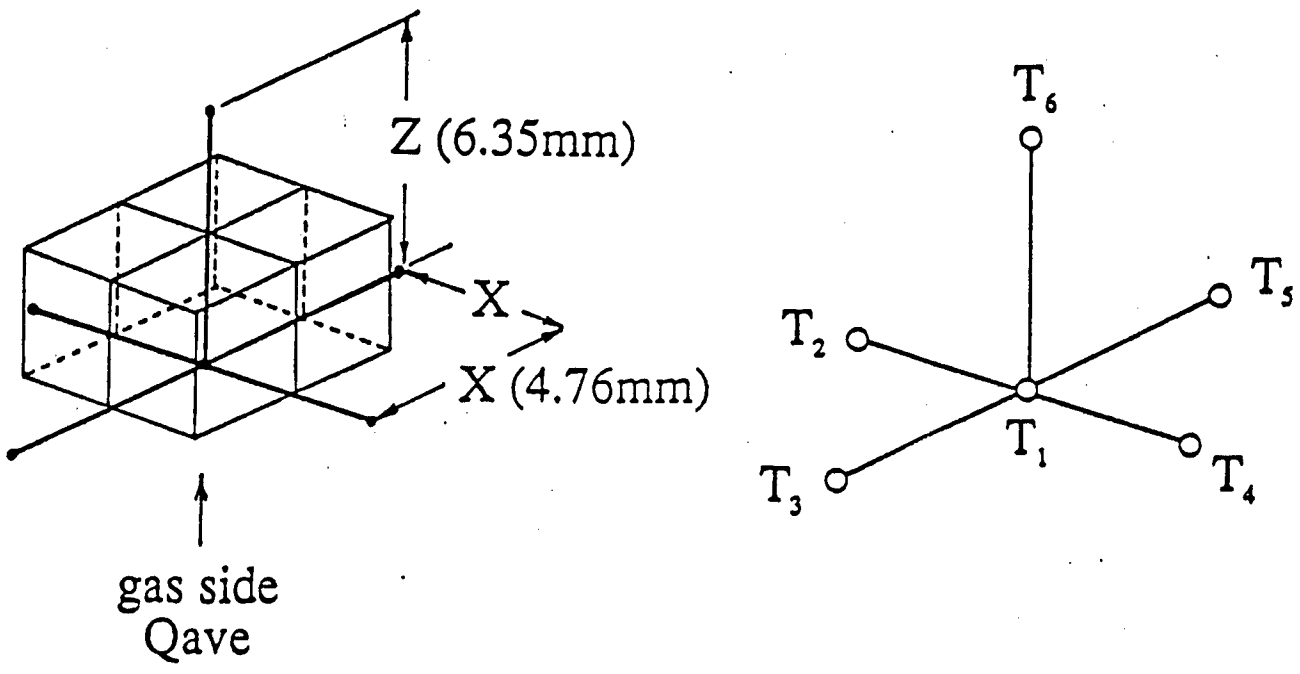

$$Qave = K(T_1-T_6)/Z + 2KZ[T_1-(T_2+T_3+T_4+T_5)/4]/X^2$$

Figure 5-7. Finite Difference Model Used in the Analysis of the Three-Dimensional Heat Flux Probe Data

5.2.2.2. Dynamic load control. There are numerous types of dynamic operation; the engine can undergo a speed change at constant load, a load change at constant speed or a simultaneous load and speed change for example. In this work the dynamic load change was simulated by subjecting the engine to a step change in load while holding the engine speed as constant as our dynamometer would allow.

Figure 5-8 shows a schematic representation of the fuel system we used to bring about the step change in load. The two fuel tanks, pressurized by inert gas cylinders, were used to replace the fuel supply pump in the original system. The two solenoid valves, one normally closed, one normally open, were installed so that one or the other of the fuel supply tanks would always by supplying the fuel to the injector. The solenoid valves activate in approximately 10 ms. This results in the fuel pressure at the inlet of the engine reaching its new level in approximately 50 ms. Fifty milliseconds is slightly shorter than the period of one engine cycle.

By controlling the solenoids the engine load could be stepped up or down in a repetitive or "single shot" operation. When operated in this fashion there would be one intermediate cycle, during which the step load change was occurring, before the fuel flow reached the new load condition. Pressure traces of the fuel line pressure are shown in Fig. 5-9. It is readily seen that by the second cycle after the step load change the fuel flow rate is identical to that of the steady state at the new load.

During the dynamic response of the engine the instantaneous fuel flow rate was estimated by assuming that the fuel flow could be treated as quasi-static. The pressure at the cylinder head fuel inlet was monitored using a T-Hydronics model TH-2V strain gage pressure transducer with a built in amplifier. Using this pressure and the engine speed the fuel flow rate was taken from a steady state calibration of flow rate versus speed and fuel line pressure.

5.2.2.3. Other measurements and data acquisition. The start of injection was determined by monitoring the output of strain gages mounted on the push rod between the rocker arm and the injector.

The intake air flow was controlled via a set of choked flow nozzles which fed a large surge tank. Under dynamic conditions the engine speed would change slightly (approximately 2%). This would perturb the steady state condition of the surge tank and piping down stream of the choked nozzles. Adjustments for this change in storage of the mass of air was made by monitoring the surge tank pressure, assuming ideal gas behavior and performing a mass balance on the system.

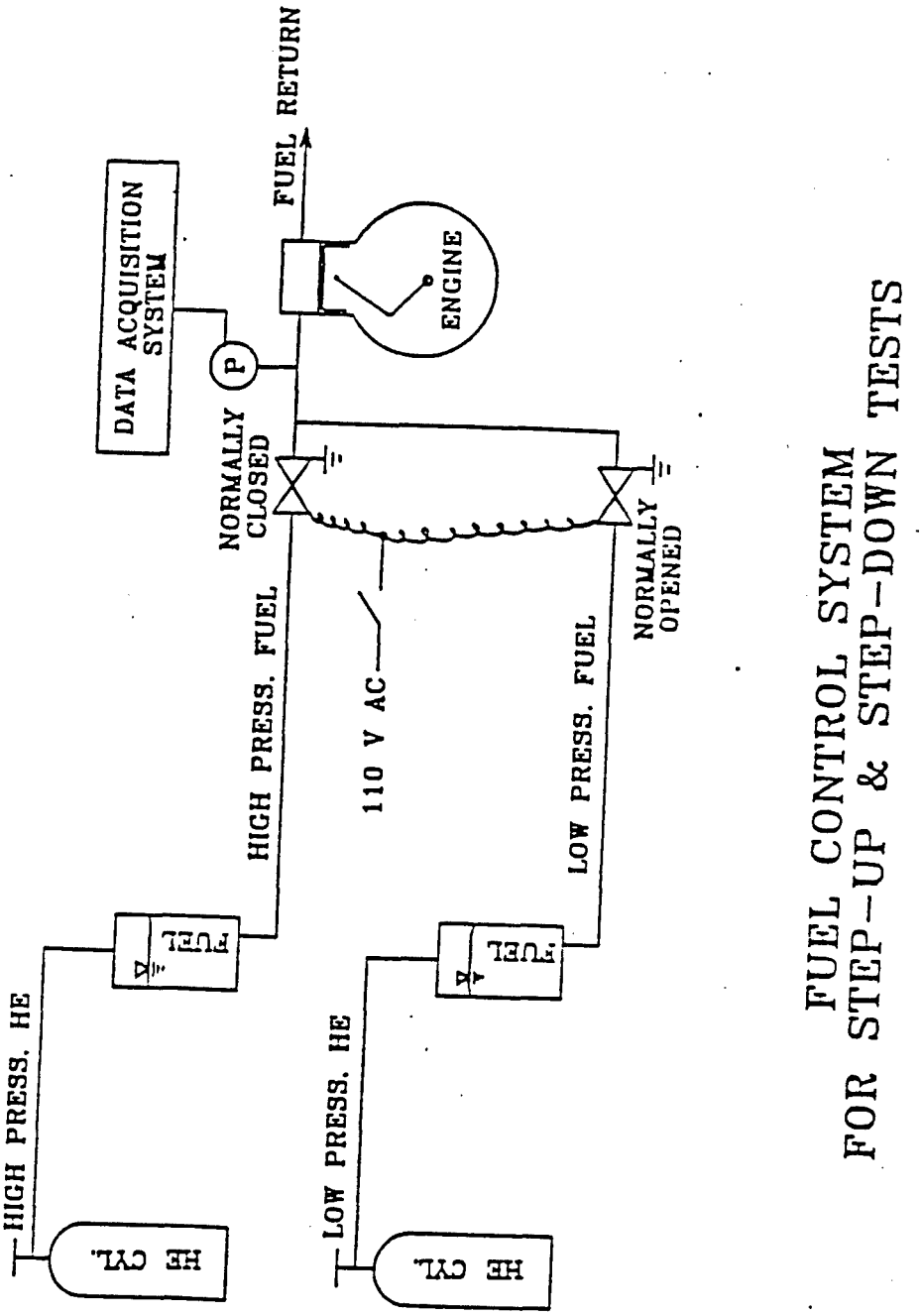

Figure 5-8. Schematic Diagram of Fuel Supply System for Step Load

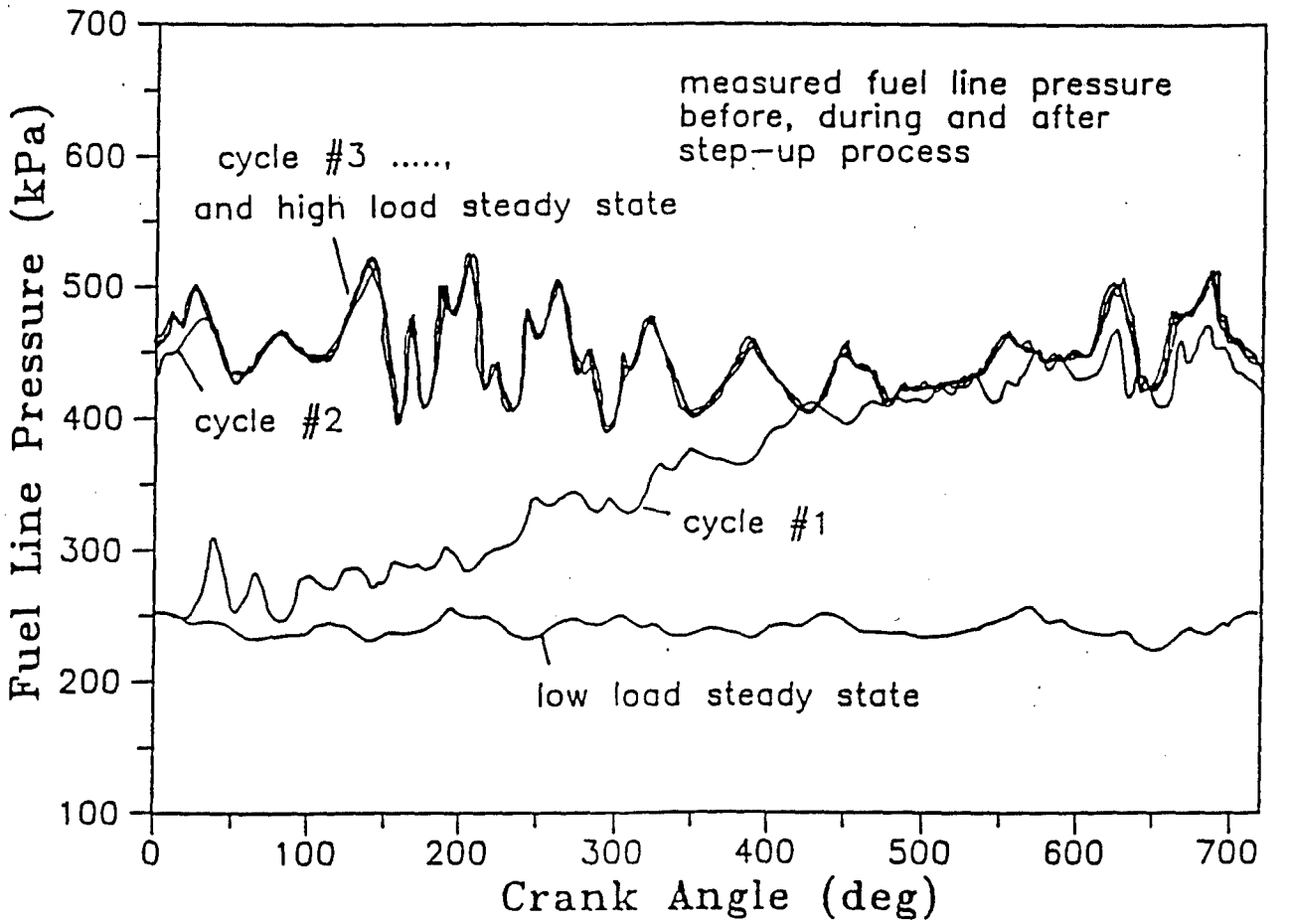

Figure 5-9. Fuel Line Pressure Before, During and After Step-Up Operation

The intake air was not heated for any of these tests. The intake temperature of approximately 300 K is lower than the typical air intake temperatures of a turbocharged engine without an aftercooler. However, some air-to-air aftercoolers can provide temperatures in this range for continuous rated load conditions.[48]

Two different PC based data acquisition systems were used during the experiments. Eight channels of temperature pressure and injector link load were taken at 0.5 crank angle intervals using a Power and Energy International (PEI) Incorporated data acquisition systems. The data of fuel line pressure, engine speed, intake and exhaust surge tank pressures, exhaust port wall temperature, and the back side temperature of the heat flux probe were taken using a low speed (6 kHz) data acquisition system, a PC based system with a DT2805 Data Translation board. Complete details of the experimental set-up and the data acquisition system can be found in the doctoral thesis of C. S. Lin.

5.2.2.4. Experimental matrix and procedures. It was expected that the changes in combustion, i.e. ignition delay, rates of pressure rise, heat release rates, etc., and heat transfer that occurred during the dynamic transient would be small. Early tests indicated that cycle to cycle variation were large enough to obscure the changes we were looking for. To overcome this problem we devised a "hopping" control strategy to run the dynamic load change many times in succession. In this procedure we operated the engine to steady state at the initial load, then upon command from a controller a step change in load was brought about and the new load was held for 15 engine cycles and then the engine was returned to the original load for 950 cycles before the "hop" was repeated.

Individual cycles of data were recorded with the data acquisition system while the engine was operating in the 15 cycle step. After this "hopping" had been repeated 50 times and the individual cycles had been recorded we formed ensemble averages of the individual cycles of data after the step. In this way we attempted to average out cycle to cycle variation to examine the trends of combustion and heat transfer during the dynamic response.

The response of the engine to a dynamic load change requires more than 15 cycles to reach the new steady state. To establish the overall rate at which the engine reached the new steady state operating condition we ran longer term transient responses in which the data was taken in short bursts of 30 consecutive cycles at 750 cycle intervals. Also, data was taken for 500 consecutive cycles after the step load change to provide information on the cycles in the mid-range of the transient.

In addition to the dynamic response data we also took sets of data during cold motoring. These data sets were conducted with a clean heat flux probe and with a probe which had steady state surface deposits from the different loads tested in our experimental matrix. By comparison of the temperature response for the clean and surface deposited probe we were able to correct for the attenuation and phase lag of the deposit.

In all of the tests reported, the fuel used was Amoco Premium #2 diesel fuel.

5.2.3. Results and Discussion.

5.2.3.1. Overall engine behavior. Figures 5-10 and 5-11 show the overall engine response during the first 11 cycles of a step change in load from an equivalence ratio of 0.3 to 0.6. In these figures the step is triggered at cycle number zero, cycle number one is the intermediate cycle in which the fuel pressure has not yet reached the new high load value and cycle number two is the first cycle of the new load. This is easily seen in the top graph of Fig. 5-10. One can also see from the figure that our dynamometer control allowed a slight (approximately 2%) increase in the engine speed during the first 11 cycles. Also shown is the slight decrease in the intake surge tank pressure, due to the increased engine speed and fixed inlet flow through the choked flow nozzles, and the increased back pressure as a result of the higher load.

In Fig. 5-11 one observes that the air flow into the engine is increased on a per unit time basis because of the increased speed but when considered on a per cycle basis it remained approximately constant. Because the Cummins PT injection system relies on the fuel pressure and time available to fill the injector volume to determine the fuel delivery per cycle, the increased engine speed caused a slight decrease in the fuel delivery per cycle. The combination of the above effects caused a slight decrease in the equivalence ratio from cycle to cycle, primarily driven by the decrease in fuel delivery per cycle.

Figure 5-12 shows the measured peak cylinder pressure, IMEP, and IFSC for the first 10 cycles after the step up in load. The peak cylinder pressure jumped immediately to the steady state value but then decreased slightly. We believe that this was caused by the changing fuel delivery per cycle. We also believe that this was responsible for the decrease in IMEP shown in the figure. What is interesting is that the ISFC, which is proportional to fuel delivery per cycle divided by the IMEP, jumped from the steady state value at low load (202 g/kW-hr) to the high load steady state value and remained approximately constant.

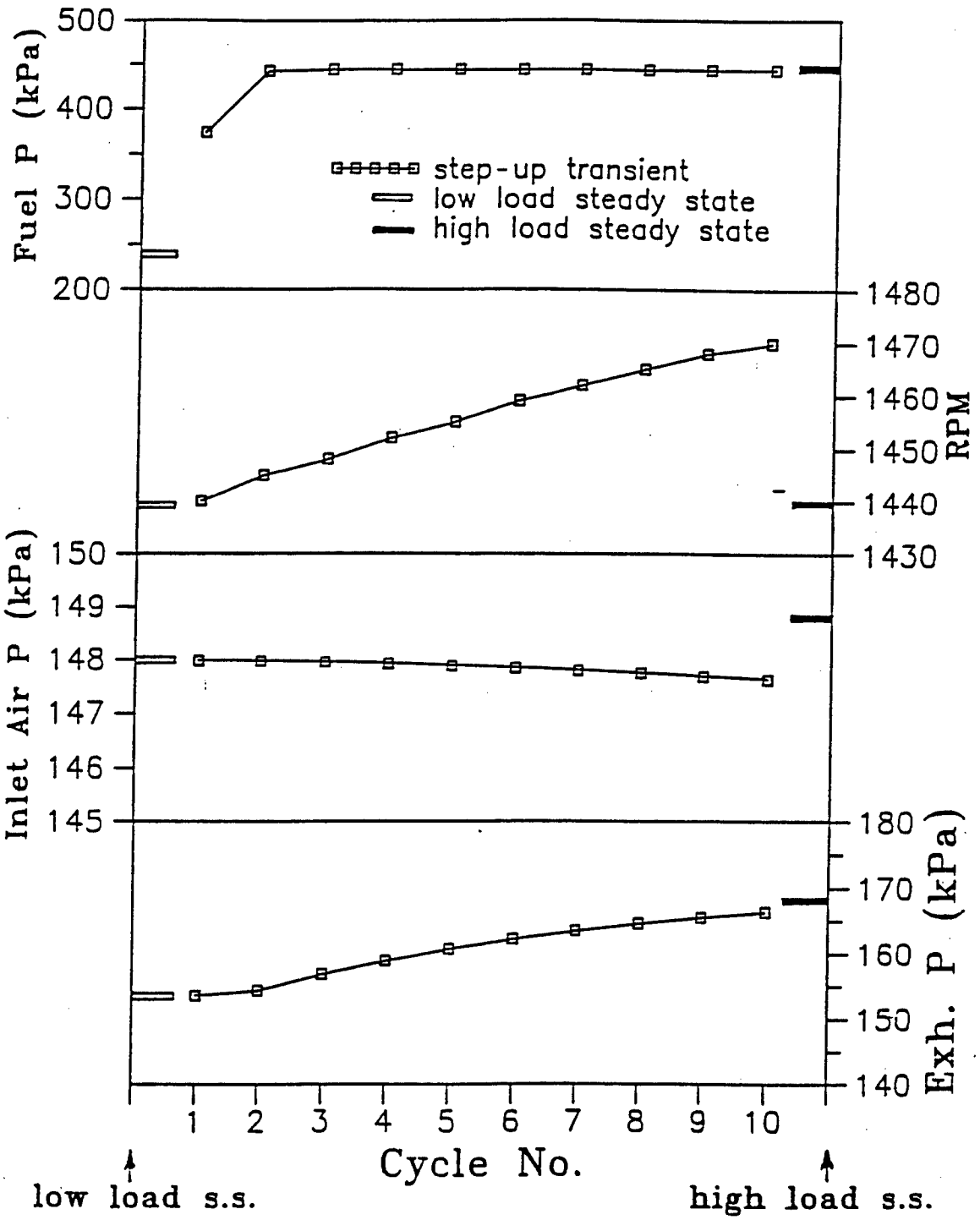

Figure 5-10. Engine Control Parameters Before, During and After Step-Up Operation (Measurement error is ± 1%)

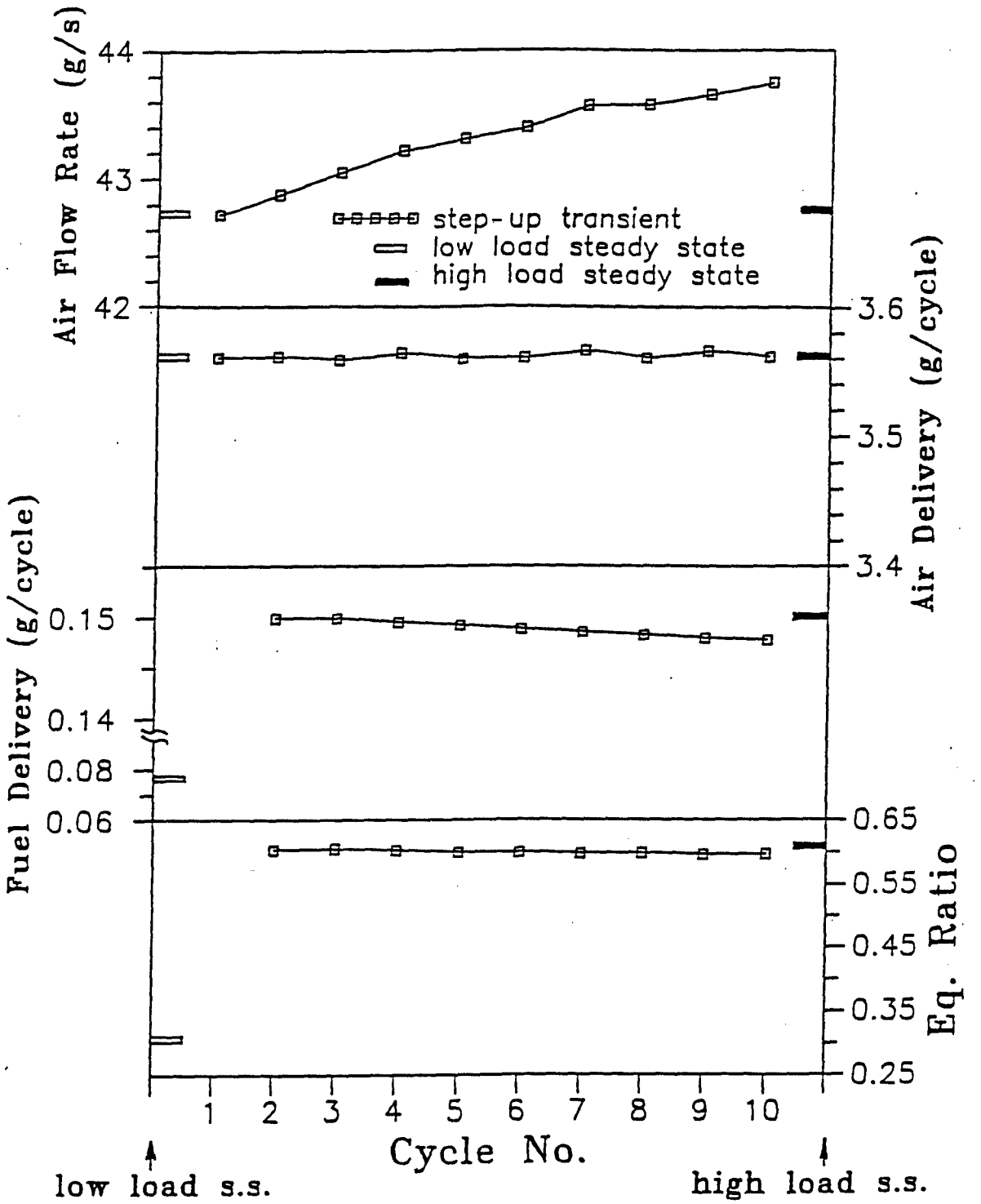

Figure 5-11. Air Flow Rate, Air Delivery, Fuel Delivery and Equivalence Ratio Before, During and After Step-Up Operation (Measurement error is ± 1%)

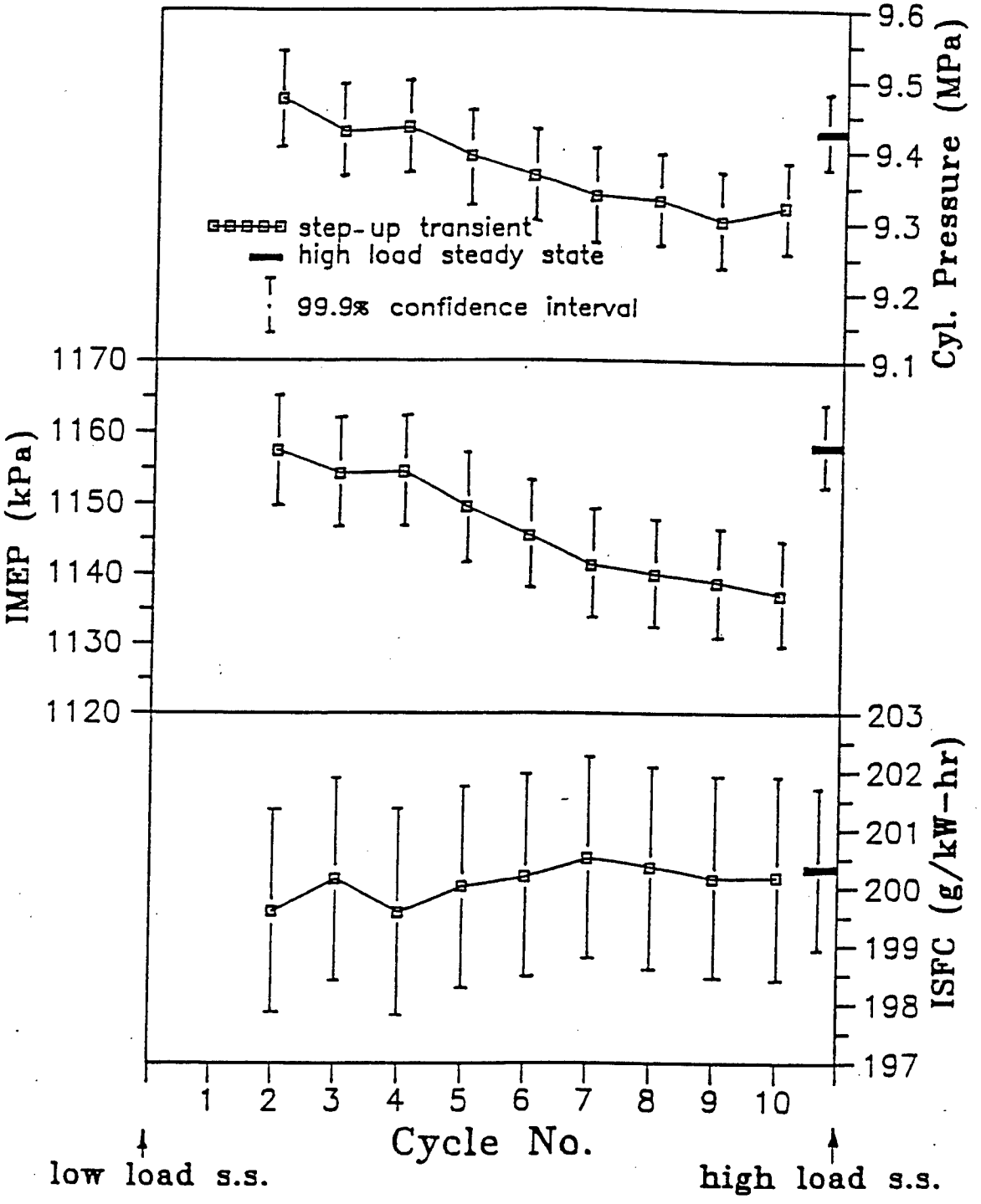

Figure 5-12. Cylinder Pressure, IMEP and ISFC During Step-Up and at High Load Steady State, Low Load Steady State ISFC is 202 g/kW-hr, Low Load Steady State Cylinder Pressure is 6.89 MPa

5.2.3.2. Ignition delay. The ignition delay of the individual cycles during the dynamic response are shown in Fig. 5-13. For these data the ignition delay was determined by measuring the time from the start of injection, determined by the link load data, to the point of 10% of the maximum heat release rate [a technique found to be very sensitive by Van Gerpen[49]]. The data shown in Fig. 5-13 were obtained by ensemble averaging the ignition delays of the 50 individual cycles of data of that particular cycle number after the step change in load. It is readily apparent from the figure that ignition delay during the dynamic response is longer than the steady state high load value and the time response to reach the new steady state is much longer than 10 cycles.

5.2.3.3. Rate of pressure rise and heat release. The rate of pressure rise is considered to be a main source of engine combustion noise; the faster the pressure rise the higher the noise. A comparison of the rates of pressure rise between the high load steady state and a representative cycle of the step-up transient (cycle #3) is shown in Fig. 5-14. It is noted that the largest maximum rate of pressure rise during the step-up transient was 17% higher than that of steady state. The relationship between the rate of pressure rise and the sound level depends on engine structure, no general correlation is available. However, the results of this research are consistent with the results of Watanabe, et al.[50]

Heat release rate calculations were done using a one-zone heat release model similar to that originally proposed by Krieger and Borman.[51] The results of the heat release analysis for the low load steady state, the high load steady state and cycle number three of the dynamic response are shown as normalized heat release rates in Fig. 5-15. It is observed that the premixed burning fraction and the peak of the heat release rate were significantly higher during the dynamic response than they were at the steady state high load condition. We estimate that 13.3% of the fuel was consumed in the premixed burning portion of the dynamic response as opposed to 9.8% in the high load steady state condition. These results can be explained by the larger ignition delay observed during the dynamic response relative to the high load steady state.[52] These results are also consistent with an analysis we did in which the additional fuel injected during the longer ignition delay was calculated from a fuel delivery curve for our injector.

5.2.3.4. Surface temperature and heat transfer. The data of surface temperature was analyzed. We examined the average surface and backside temperatures and how they changed, how the surface temperature swing changed, and how the instantaneous and average heat flux changed during the dynamic response.

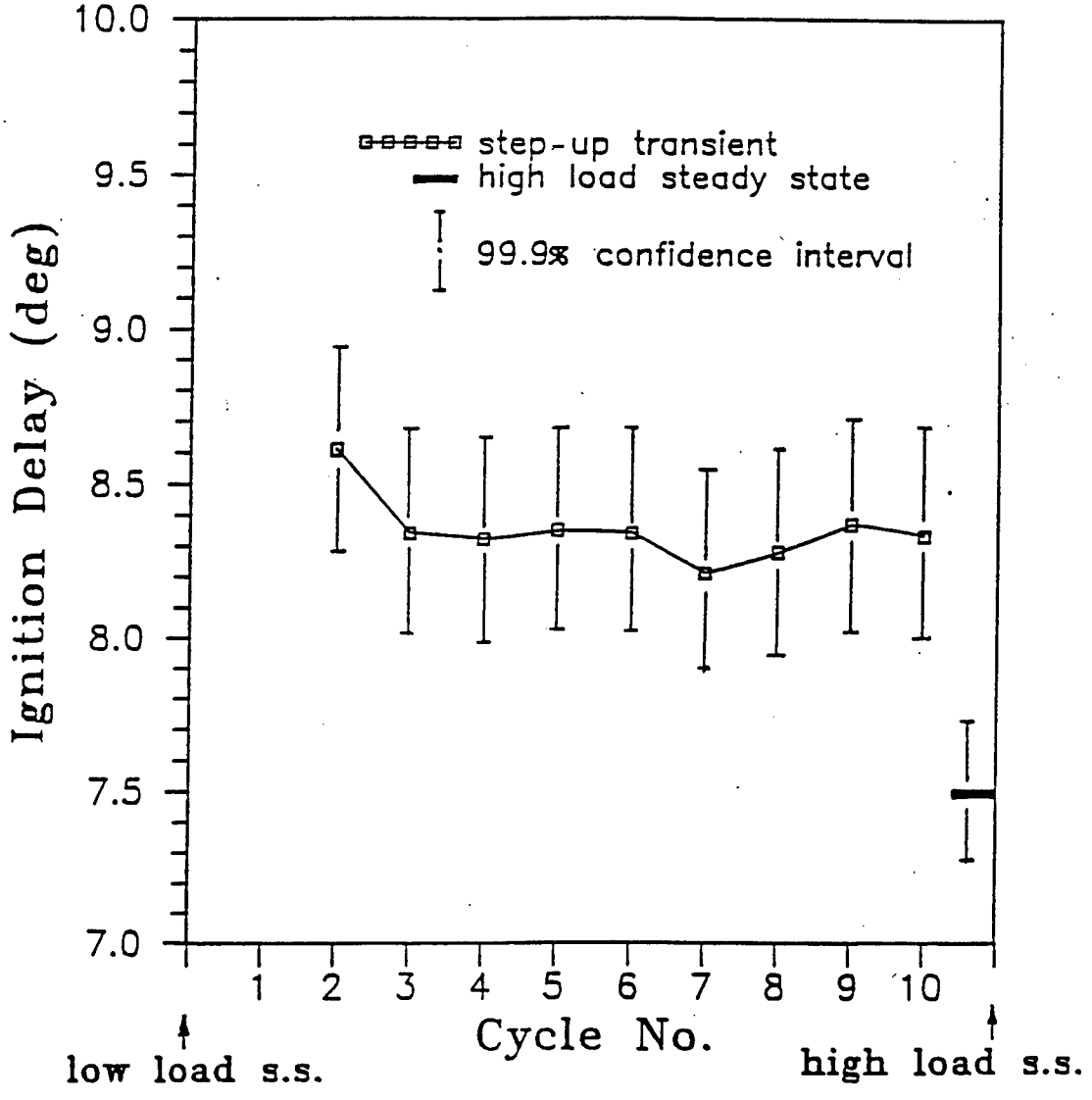

Figure 5-13. Ignition Delay During Step-Up and at High Load Steady State, Low Load Steady State Ignition Delay is 8.4 Degrees

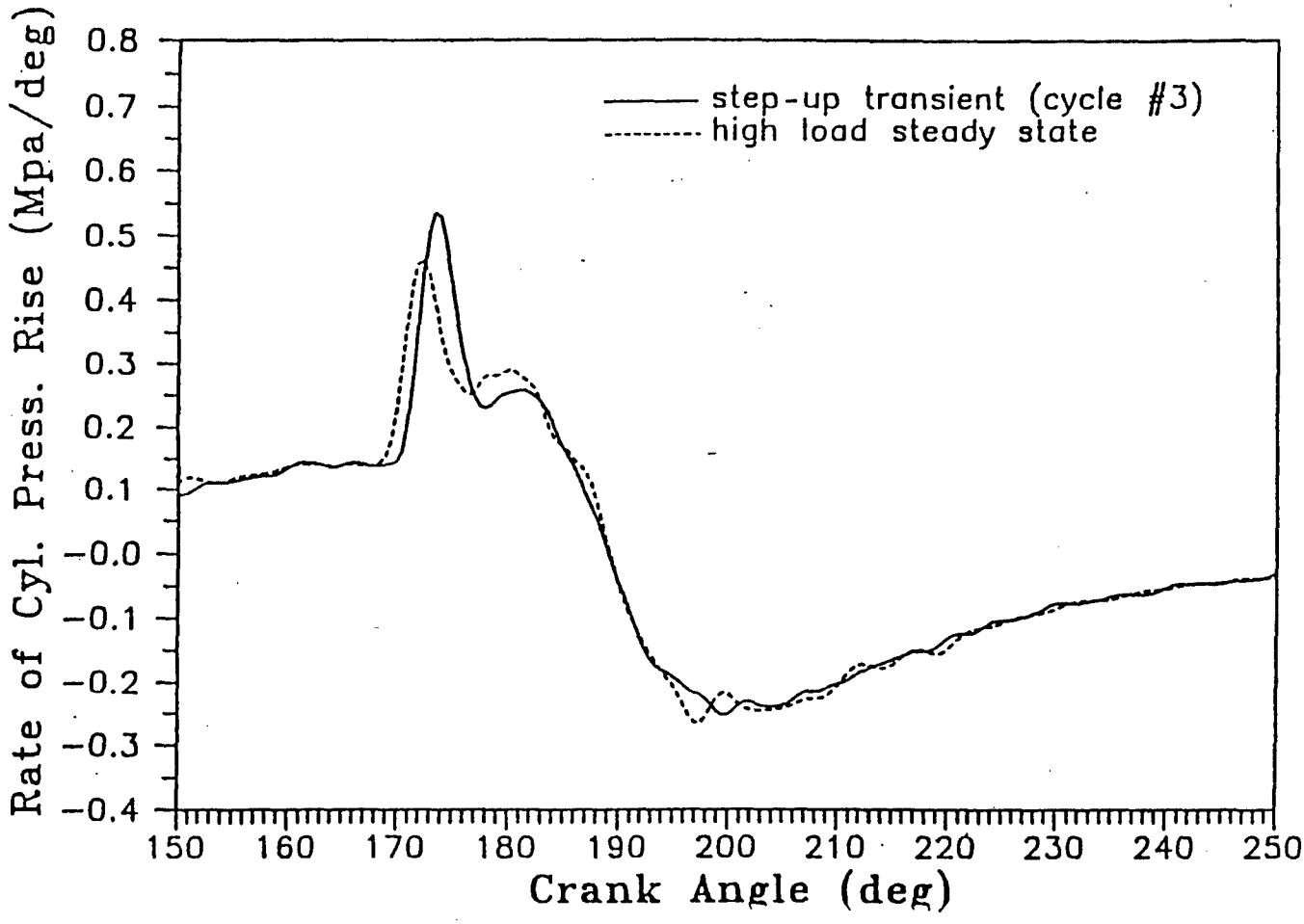

Figure 5-14. Rate of Cylinder Pressure Rise of Step-Up Cycle #3 vs High Load Steady State

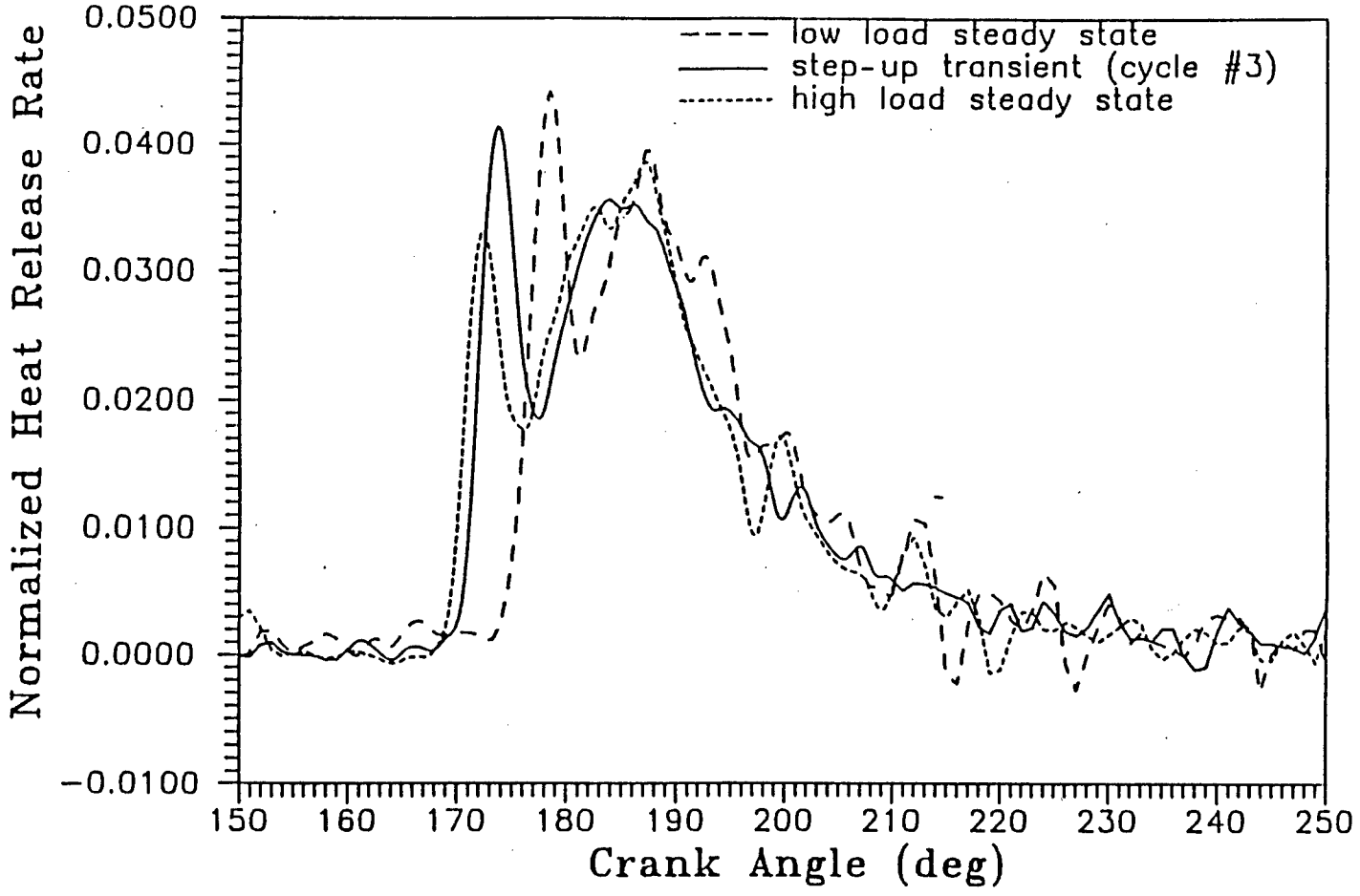

Figure 5-15. Normalized Heat Release Rates of Low Load, High Load Steady State and Step-Up Cycle #3

The surface temperature history measured by the center surface thermocouple is shown in Fig. 5-16. The lowest curve is the low load steady state, the next 10 curves above it are from the transient cycles after the step-up, and the curve at the very top is that of the high load steady state. Excluding cycle #1 which is an intermediate cycle, the magnitude of the temperature swing jumped from its low load to its high load value almost immediately following the load change. But the cycle averaged surface temperature rose gradually due to the thermal capacity of the metal. During this part of the dynamic response the back side temperature did not change. These data are plotted in Fig. 5-17 in terms of the magnitude of the temperature swing and the average surface temperature.

Calculation of the surface heat flux during the dynamic response required a different calculation procedure than the fourier decomposition, which is typically used under steady state conditions. Morel, et al.[53] have used a finite difference discretization of the energy equation to solve transient problems. We did not use this approach because the fine node spacing required near the combustion chamber surface and the continually changing boundary conditions resulted in excessively long computational times.

Instead we used an exact solution technique. A brief overview of the approach is given below. The energy equation for each nodal system was rearranged into matrix form. The general form of the matrix included a thermal capacitance term, a conductance term, and a forcing function. The solution to this set of linear ordinary differential equations was expressed as the sum of homogeneous and particular solutions. The particular solution depends solely on the forcing function, which was determined from the surface temperature data, and the homogeneous solution was written in terms of a series summation of eigenfunctions and eigenvalues. The advantage of this method is that if the material properties are treated as constant, the solution of the eigenfunctions and eigenvalues only need to be determined once.

Furthermore, since the overall solution is analytical there is no need to sub-divide the time steps of the calculation. We assumed that the material properties were constant, fit the surface temperature data with a linear interpolation between data points, which then became our forcing function and solved the system of equations at one crank angle degree intervals. We compared the results with the fourier decomposition method and the finite difference approximation method for steady state operation. The results of the three techniques were essentially identical. Under dynamic response, when the analytical solution is not applicable, the exact solution was 40 times faster than the finite difference solution using a Crank-Nicolson numerical routine.

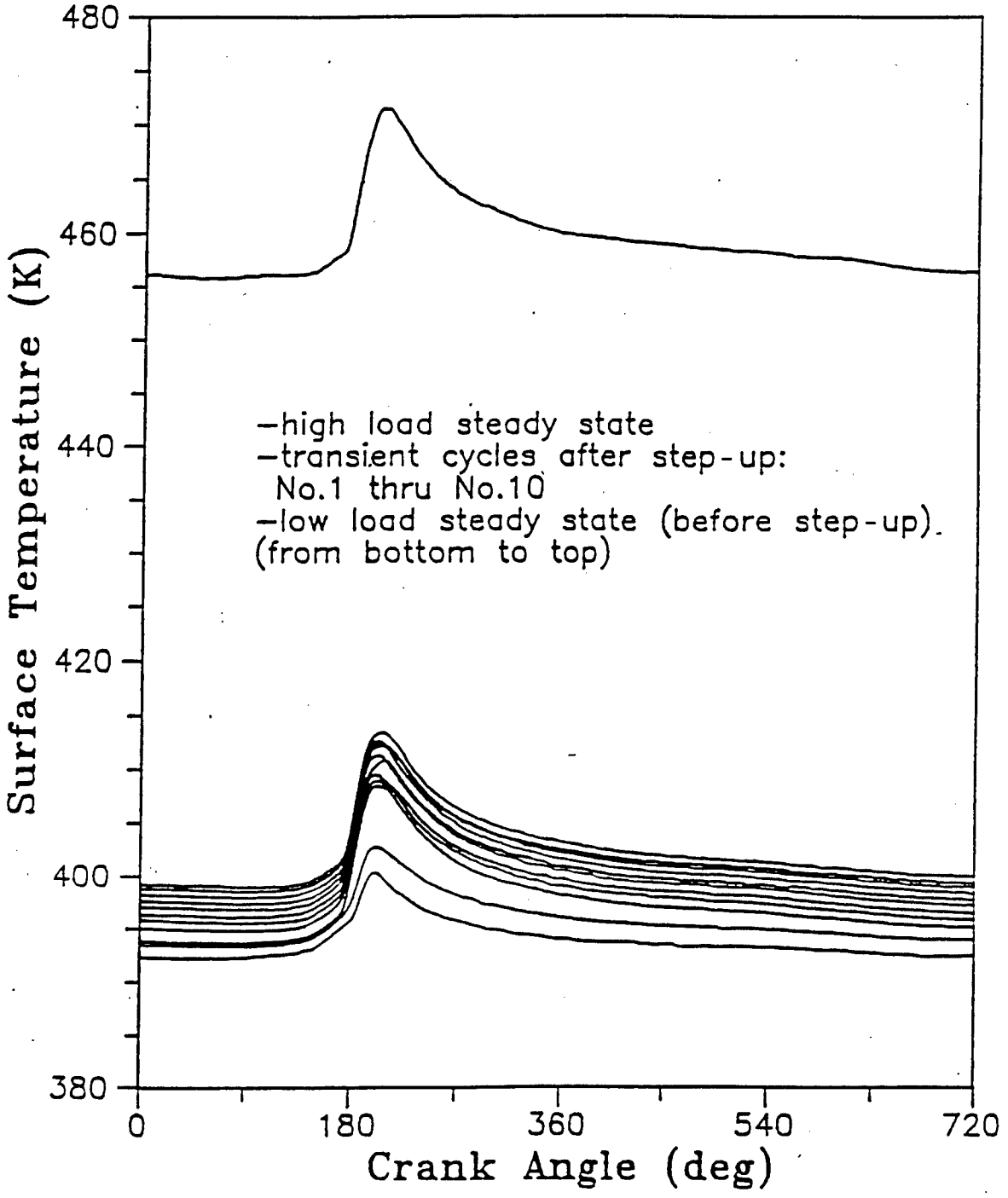

Figure 5-16. Surface Temperature Response Before, During and After Step-Up Operation

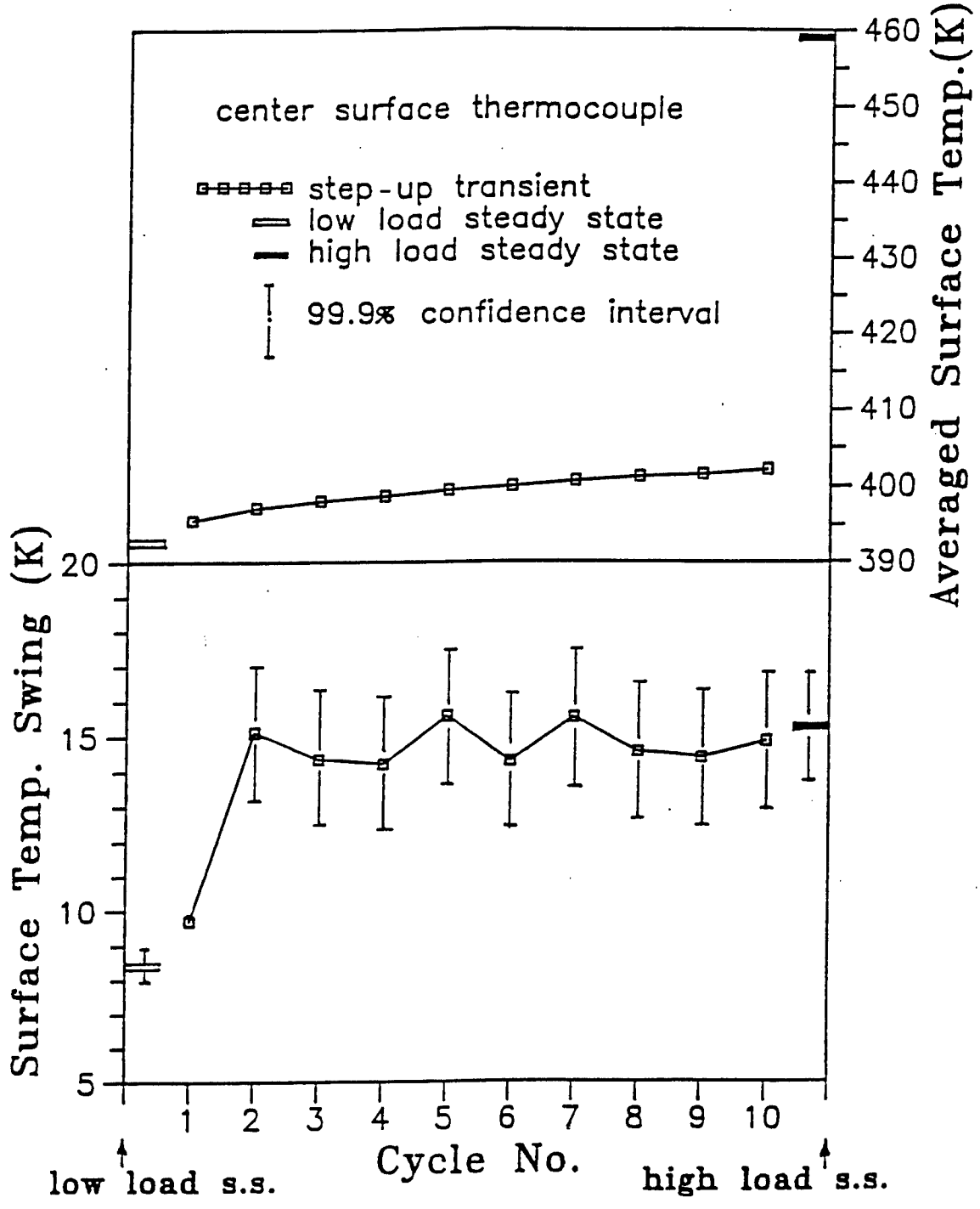

Figure 5-17. Cycle Averaged Surface Temperature and Surface Temperature Swing Before, During and After Step-Up Operation

A comparison between the steady state instantaneous heat flux at low load steady state, high load steady state and the third cycle of the dynamic response are shown in Fig. 5-18. What is most striking about this figure is that the instantaneous heat flux of the third cycle of the dynamic response is very close to that of the steady state high load. Note also that the peak value of the heat flux for the dynamic cycle was higher than the corresponding value for the steady state operation.

Figure 5-19 shows the maximum and average heat flux during the first 10 cycles of the transient. Again, it is apparent that the heat flux jumped almost immediately to values that are slightly higher than the steady state values.

5.2.4. First Law Energy Balance. The data shown in Figs. 5-19 and 5-20 are for the local heat flux at the probe position. We also performed a first law analysis of the data during the closed portion of the cycles. The results of this analysis for cycle number three (TR) and the high load steady state (SS) are presented for intake valve closing (IVC), start of fuel injection (INJ), and exhaust valve opening (EVO) in Table 5-2. Since the work (WK) and total heat transfer (Qtotal) are integrated quantities it is necessary to choose a reference point, IVC was chosen for this. The lower cylinder pressure for the transient cycle at INJ along with the lower gas temperature, which caused longer ignition delays, are seen by looking in the first and second columns of Table 5-2. The most interesting results are the calculated total global heat transfer. It is shown that the total heat transfer for the transient cycle was higher at both INJ (IVC to INJ) and EVO (IVC to EVO). There was approximately a 12.6% increase in the heat transfer in the transient operation compared to the steady state.

A comparison between the value of the global heat transfer calculated via the first law and that calculated using the results of the heat flux probe were consistent in trend but different in magnitude. For our data the estimate of the heat transfer from the probe was consistently 65% to 70% of the magnitude of the first law results. These results emphasize the three dimensional nature of the heat transfer.

5.2.5. Overall Long Term Response of the Engine. In order to obtain long term transient data, longer than the first ten cycles, an intermediate range and a long time transient set of tests were conducted. The approach followed for both the intermediate and long transient tests was to take 30 consecutive cycles of data then let an interval of cycles pass before taking data again. These 30 cycles data bursts were then ensemble averaged to give a representative cycle for that portion of the transient; it was assumed that changes during these 30 cycles were small relative to the change over the entire transient. For the intermediate range,

Table 5-2. First Law Analysis of Step-Up Transient and High Load Steady State

C.A.		P(kPA)	T (K)	Mass (g)	U (J)	Wk (J)	Qtotal (J)
	SS	161	363	3.67	610	0	0
33	TR	160	358	3.71	645	0	0
(IVC)	diff	-1	-5	0.04	35	0	0
	SS	3612	889	3.67	2102	-1447	-45
162	TR	3497	852	3.71	2055	-1392	-18
(INJ)	diff	**-115**	**-37**	0.04	-47	55	**27**
	SS	564	1155	3.82	-3206	2590	1225
314	TR	531	1079	3.86	-3321	2588	1379
(EVO)	diff	-33	-76	0.04	-115	-2	**154**

Remarks:
SS - high load steady state
TR - step up transient
diff - TR minus SS
WK - work output as positive, integrated from IVC
Qtotal - total heat transfer out as positive, integrated from IVC

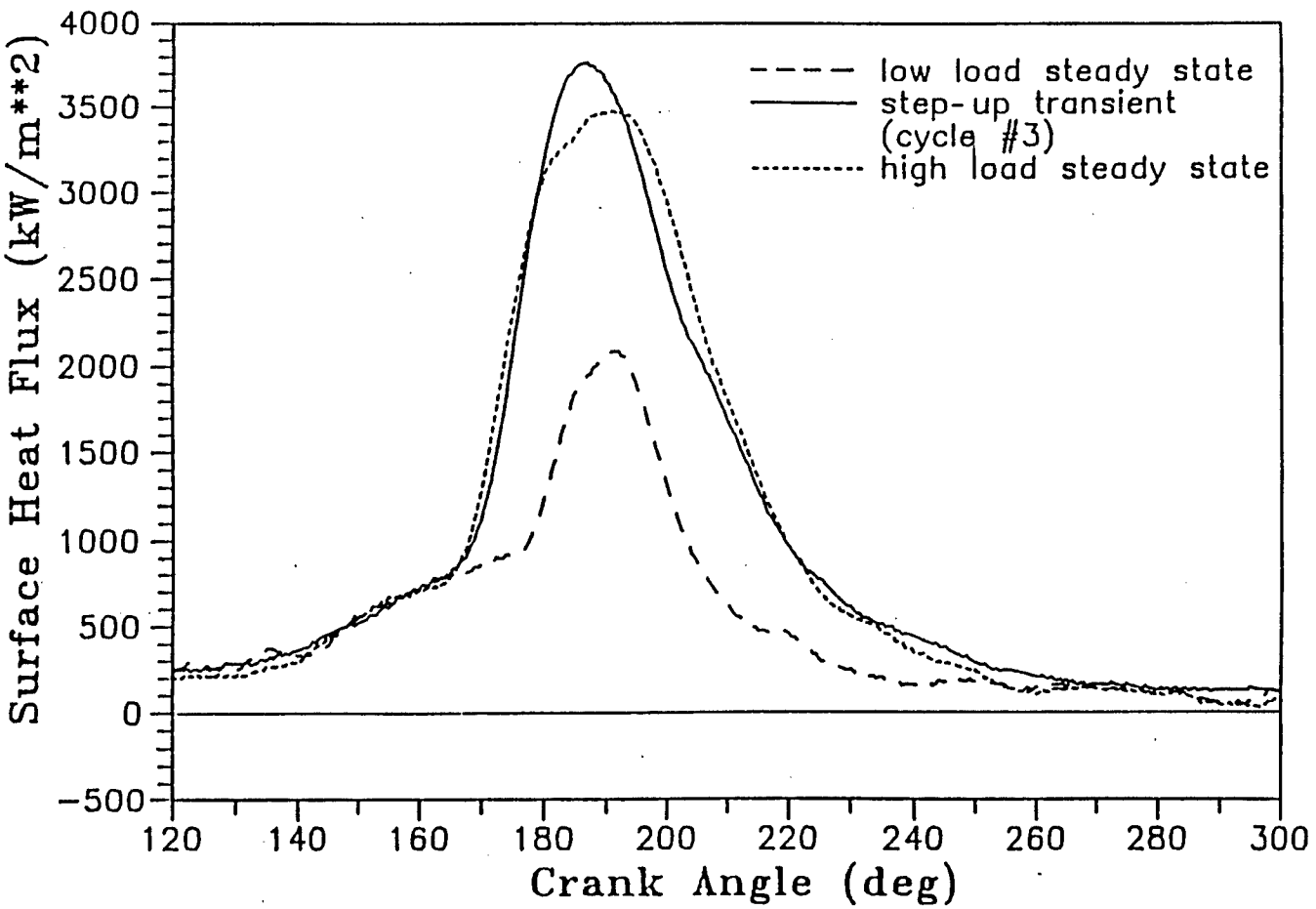

Figure 5-18. Comparison of Surface Heat Flux at Low Load, High Load Steady State and Step-Up Cycle #3

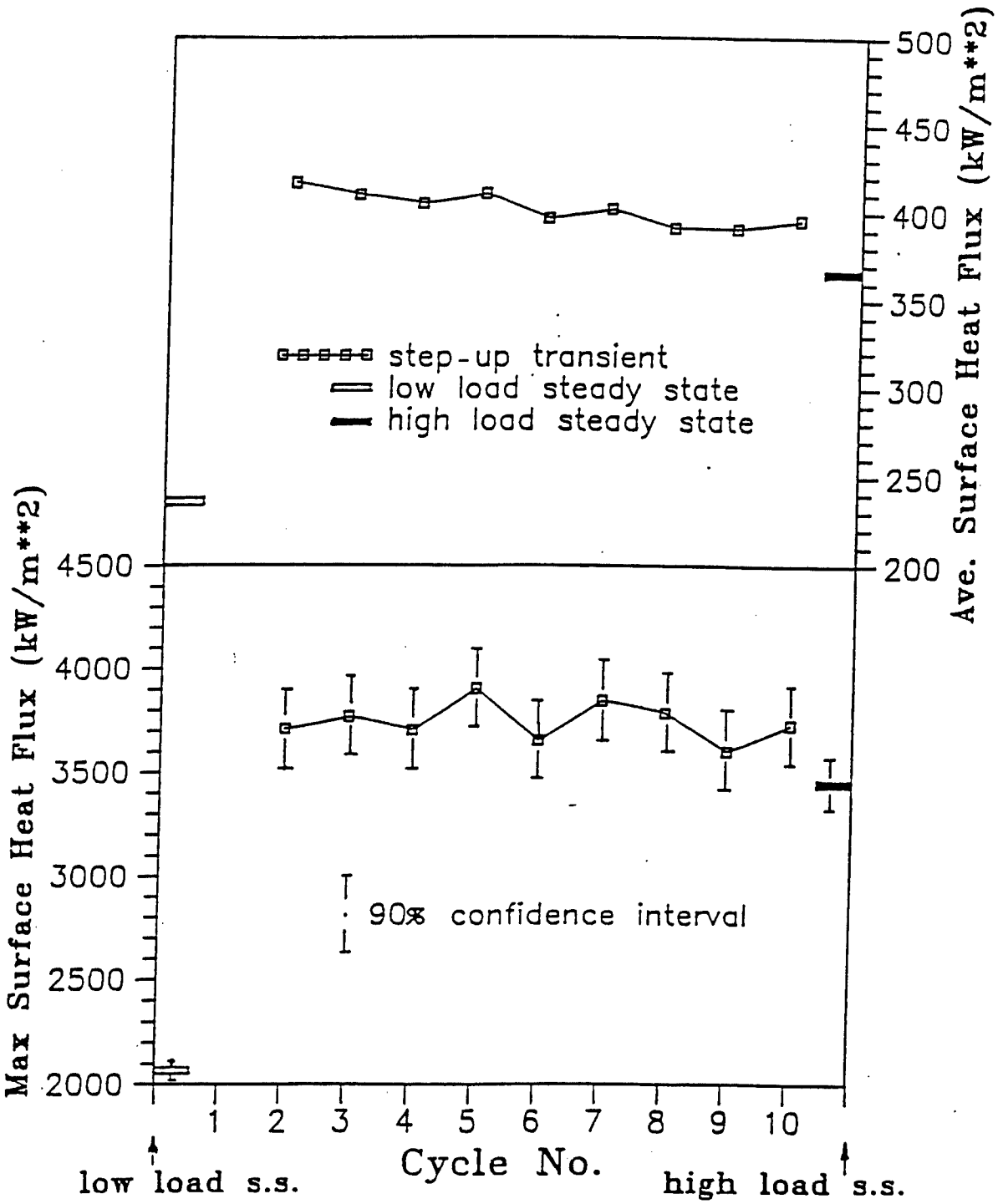

Figure 5-19. Averaged and Maximum Surface Heat Flux Before, During and After Step-Up Operation

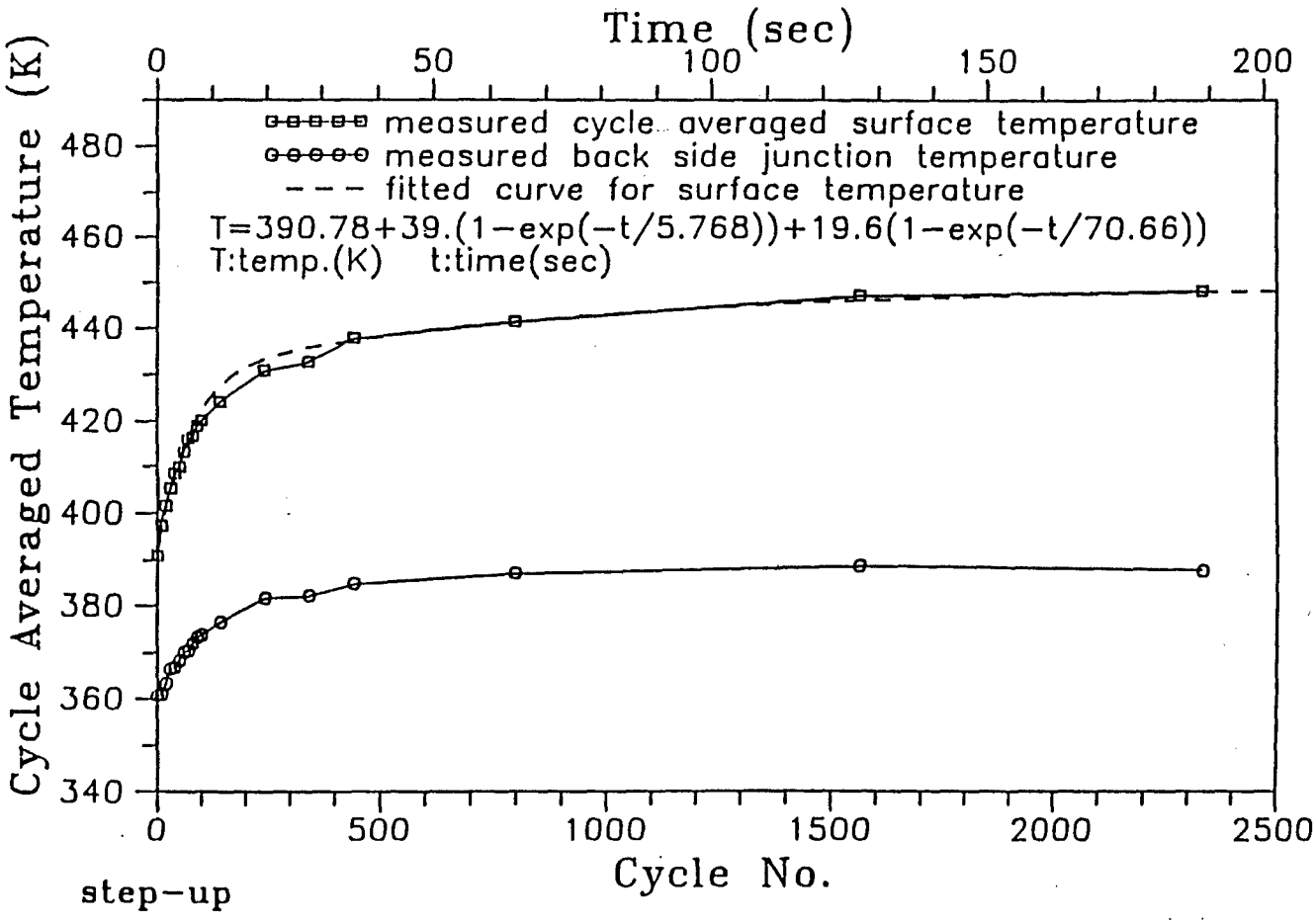

Figure 5-20. Cycle Averaged Surface Temperature and Back Side Junction Temperature of Long Transient Step-Up Test Results.

data were taken continuously from 0 to the 500th cycle, then cycle numbers 151 - 180, 251 - 280, 351 - 380, and 451 - 480 were taken for ensemble averaging. For the long transient case the data acquisition systems were set up to take 30 consecutive cycles as a set at 750 cycle intervals. A total of 15 sets of data were taken and then ensemble averaged.

Figure 5-20 gives the cycle averaged surface and backside temperatures during the transient. The most rapid change in temperature occurred during the first 100 cycles, and after approximately 2000 cycles the surface temperatures were essentially steady state. We determined that a double time constant exponential fits the data very accurately:

$$T = 390.78 + 39.0*(1-\exp(-t/5.768)) + 19.6*(1-\exp(-t/70.66)) \qquad (10)$$

where T = cycle averaged surface temperature (K)
t = time (sec.).

Such an expression could be useful in heat transfer models for dynamic operation.

The data for ignition delay, maximum rate of cylinder pressure rise, premixed burning fraction, localized instantaneous, and total heat transfer were analyzed in the same manner as the average surface temperature (Fig. 5-20). The resulting profiles were very similar to Fig. 5-20 in their characteristics.

In all cases the most rapid change occurred during the first 100 cycles, with the rate of change decreasing and asympotically approaching the new load steady state value in approximately 2000 cycles. This suggests to us that a double time constant experimental response, analogous the one fit to the temperature data of Figure 5-20, may be appropriate for modeling the general behavior of engine dynamic response.

An analogous set of data was taken for a condition of dynamically changing from a high load to a low load. The results and conclusions were identical to the step-up results in their characteristics. The only difference was in the direction of change. The interested reader is referred to the reference of the doctoral thesis of C.S. Lin.[54]

5.3. Energy Balances and Particulate Temperature Measurement in an Insulated Engine

The background leading to the experiments reported in this section is the current unresolved controversy as to whether or not the use of ceramics in the walls of an engine combustion chamber actually reduces the net heat transfer to the coolant.

The object/motivation of the experiments was to: evaluate the effectiveness of selected thermal barriers, assess particulate loading in normal and insulated engines, measure particulate temperature and radiation, and conduct global heat transfer analysis.

5.3.1. Background. A background a review of a few recent experiments on comparative heat transfer rates in insulated and normal engines is given below.

Huang and Borman,[55] making localized measurements, found that heat transfer through an insulated plug in a normal engine was lower than through a normal plug. Extrapolated to a global basis, this would indicate less heat transfer to the coolant in an insulated engine.

Woschni, et al.[56] using an air gap piston for insulation and making a global energy balance during the closed portion of the cycle, found higher wall temperatures but greater heat transfer to the coolant for the insulated case.

Morel, et al.[57] using local measurements, found that in the insulated case localized temperatures were higher and the local heat flux was lower. Again, this would indicate less heat transfer to the coolant in the insulated case.

Alkidas[58] and Gatowski,[59] recognizing that past experiments had not generally optimized the combustion process, attempted to optimize combustion for both the normal and insulated configuration and found: lower volumetric efficiency for the insulated case - this same result has been found by numerous other persons; premixed burn was the same or less for the insulated case; burning time was longer for the insulated case; lower smoke and higher NO_X for the insulated case; and more heat rejection for the insulated case.

Yang and Martin[60] modeled heat transfer using similar conditions for both insulated and normal engines. Their variables were wall temperature, flow velocity, and quench distance. They predicted that lower wall temperatures and higher velocities increased the rate of heat transfer and, if the quench distance became very small, peak heat transfer became larger than for the normal case. In all cases the time-averaged heat flux was lower for higher wall temperatures, i.e., there was less heat transfer for insulated case.

Both the above, as well as other data not presented, show conflicting results as to whether less heat is rejected to the coolant with insulated engines. Consequently, at Wisconsin, it was decided to conduct global heat transfer measurements on a single-cylinder version of the Cummins NH-250 engine.[61] The first tests were done cooperatively with Purdue University since they and Ricardo-ITI had accumulated a large amount of archival data on their normal metal engine. It was also decided to use three different nozzle configurations in an attempt to optimize the combustion system for the insulated engine. Injection timing was varied in each case to establish the NO_X-smoke trade-off curve.

Data on the engine and the thermal barriers used are summarized in Fig. 5-21. As can be seen from Fig. 5-21, tests were conducted using different nozzle configurations, loads, and speeds. Differences in combustion were observed between the normal and insulated engines. Figure 5-22 shows some of these differences for the nozzle configuration used for the normal engine. As can be seen there were differences in the premixed burning, the duration of heat release and in burning schedule. The most obvious and largest difference is in the extent of premixed burning.

A global heat transfer analysis, which is basically the First Law applied to the closed portion of the cycle, was used to estimate the heat transfer in both the insulated and normal engine at Purdue. The heat transfer results, as well as fuel consumption data, are presented in Fig. 5-23. It can be seen that in all cases the heat transfer, as a fraction of fuel energy, was greater for the insulated engine. It can also be seen that, at the lower rpm, the fuel consumption was higher for the insulated engine but that the fuel consumption was lower at the higher rpm.

5.3.2. PSZ Tests. In view of the confusing nature of the reviewed results, additional tests were run on another, single-cylinder, low heat rejection, eight-hole, NH-250 engine located at the University of Wisconsin. As can be seen from Fig. 5-24, the compression ratio of this engine was higher than the previous engine. In addition, an air gap piston, as well as a PSZ coating for some of the tests, was used for insulation. Thus the data from the two insulated engines are not comparable. For the tests at Wisconsin, radiation measurements were also made with the injector rotated to enable radiation measurements to be made on and in between the spray axes.

A schematic of the system and a cross section of the combustion chamber are shown in Fig. 5-25. Note the air gap insulation for the piston and the location of the radiation probe. While not shown in Fig. 5-25, in addition to the piston top, the firedeck, valves and top portion of the liner were coated with PSZ.

PURDUE EXPERIMENTAL ENGINE

- Single-cylinder diesel based on Cummins six-cylinder NH-250 engine
- Compression ratios: 15.3 Baseline
  15.7 LHR configuration
- Thermal Barriers: 0.050 in. PSZ on piston and firedeck
  0.030 in. PSZ on valves
  Decreased cooling in engine head

PURDUE EXPERIMENTAL MATRIX

INJECTOR	SPEED (RPM)	PERCENT LOAD
8-.007-17°	1300	25
	1300	50
	2100	25*
	2100	75*
10-200-17°	1300	25
	1300	50
	2100	50
12-195-16°	1300	25
	1300	50
	2100	50

* these runs are not optimized

Figure 5-21. Description of the Purdue Experimental Engine and the Matrix of Conditions Tested

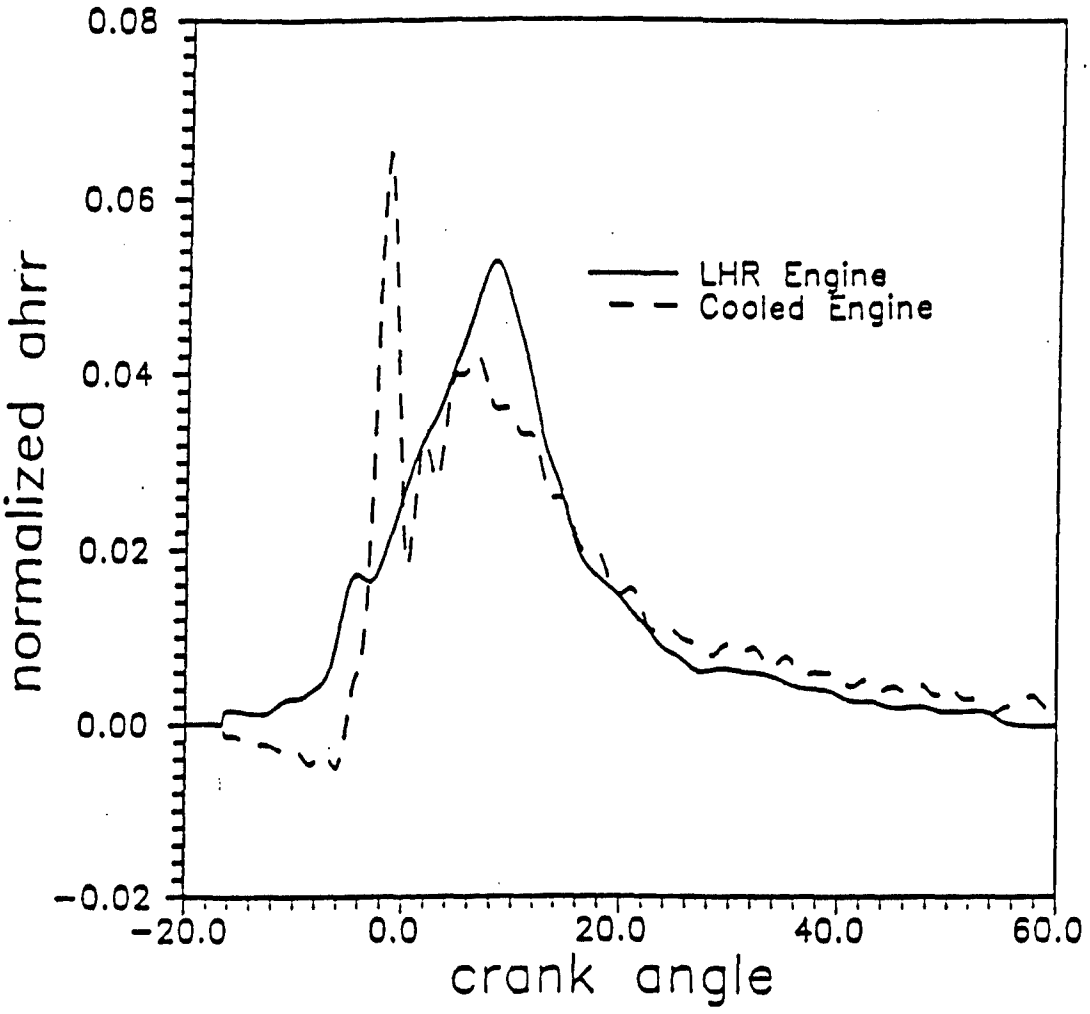

Percent Load	25		50	
	ceramic	metal	ceramic	metal
Peak Premixed AHRR	0.0173	0.0653	0.0069	0.0326
Premixed Burn Percent	5.32	15.92	2.27	8.60
Duration of HR [ca°]	21.24	23.35	28.61	26.31
Burning Schedule				
0%	-7.14	-3.98	-11.68	-10.18
50%	9.04	11.02	11.69	8.05
70%	14.11	19.37	16.93	15.95

Figure 5-22. Comparison of Apparent Heat Release Rates, Base Engine (cooled/metal) versus the Ceramic Coated Engine (LHR), the graph shows the results for 1300 rpm, 25% load. The table gives the results for both 25 and 50% load

COMPARISON OF PREFORMANCE PARAMETERS

	Percent Cycle Energy Input as Heat Transfer		ISFC (kg/hp-hr)	
Speed, Load	ceramic	metal	ceramic	metal
1300, 25%	0.208	0.145	0.138	0.135
1300, 50%	0.152	0.100	0.133	0.130
2100, 25%	0.198	0.136	0.136	0.137
2100, 75%	0.135	0.082	0.135	0.138

Figure 5-23. Summary of the Heat Transfer and Indicated Specific Fuel Consumption of the Ceramic Coated and Base Engine

WISCONSIN EXPERIMENTAL ENGINE

-- Single-cylinder diesel based on Cummins six-cylinder NH-250 engine

-- Compression ratios: 20.09 LHR-1
20.45 LHR-2

-- Thermal Barriers: LHR-1: Air-gap piston
LHR-2: Air-gap piston with 0.030 in. PSZ coating

Each LHR configuration had 0.030 in. PSZ applied to firedeck, valves, and top 0.40 in. of liner

WISCONSIN EXPERIMENTAL MATRIX

Speed [rpm]	Equivalence Ratio	Radiation Probe Location
1300	0.30 0.40 0.50	on spray axis
1500	0.30 0.40 0.50	between sprays
1700	0.30 0.40 0.50	on spray axis

Figure 5-24. Description of the Wisconsin Experimental Engine and Matrix of Conditions Tested

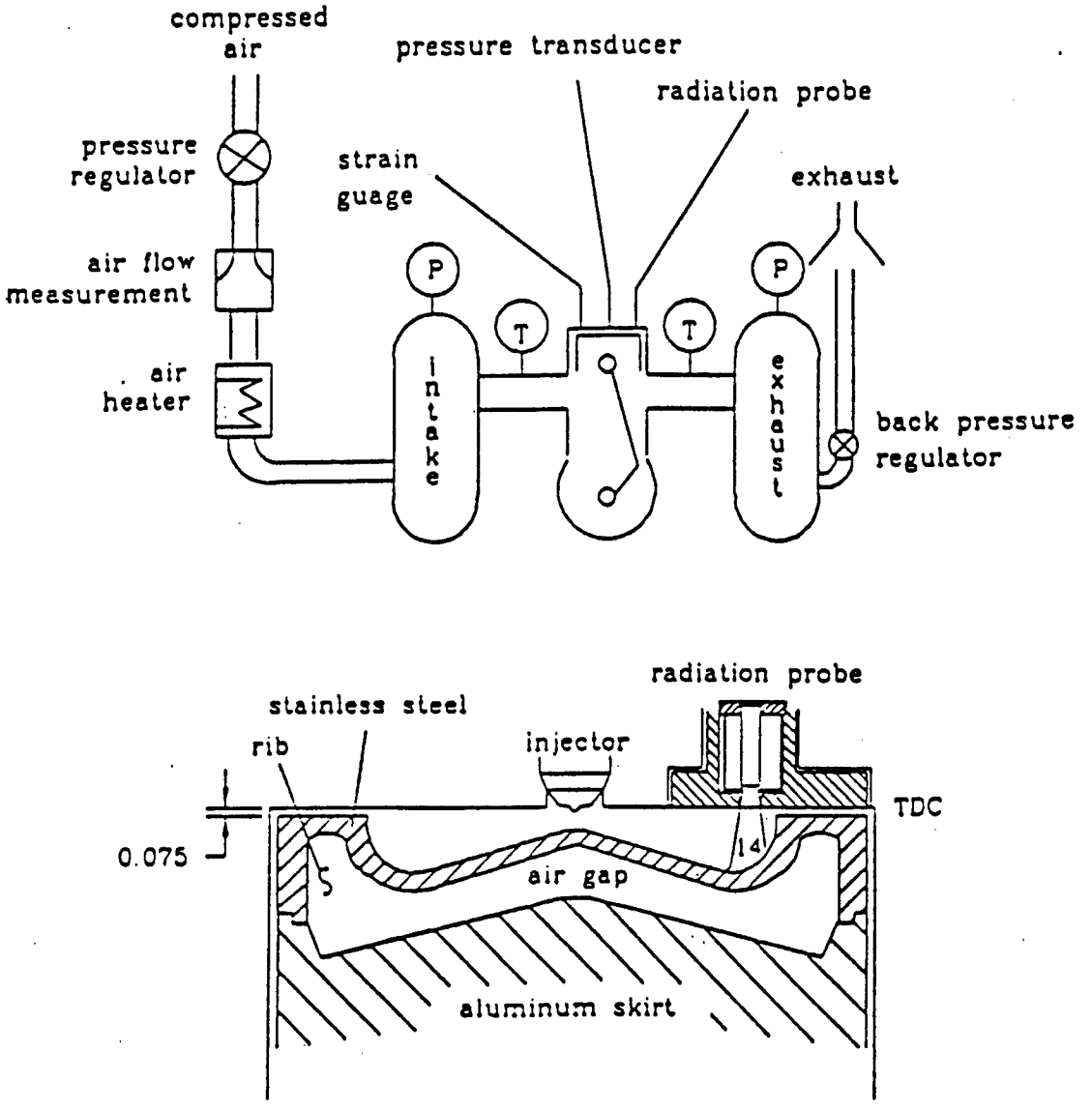

Figure 5-25. Schematic of the Engine Test Stand and Cross Section of the Cylinder with Air-Gap Piston and Radiation Probe Assembly

As shown in Fig. 5-26 there was little difference in combustion with and without the coating on the piston. There is essentially no difference even in the extent of premixed burning.

Figure 5-27 compares global heat transfer and fuel consumption for the two different insulated configurations of the Wisconsin engine. With the exception of the first row of Fig. 5-27, in all cases both global heat transfer and fuel consumption were increased when the PSZ coating was applied.

Two-color radiation and temperature measurements from the carbon particles in the diesel combustion chamber are usually characterized by what is called the KL factor where K physically represents the number of carbon particles per unit path length and L is the path length. Measurements were made of KL for the Wisconsin insulated engine with the high compression ratio and were also available from previous experiments on the normal metal engine at Wisconsin with a compression ratio of 13.3. In spite of the differences in compression ratio, comparisons were made between the insulated and normal engine. They gave approximately the same value for K indicating that the soot concentration per unit length was approximately the same in the insulated high-compression-ratio engine and the lower compression-ratio normal engine.

5.3.3. Reasons for Conflicting Results. The data we have discussed above and, the data previously summarized, as well as other data in the literature were taken by presumably competent investigators but are conflicting and contradictory. Therefore, assuming the data are correct, the reasons why conflicting results might be obtained by competent investigators are discussed below.

First of all, note that heat transfer from the hot gases to the wall affects efficiency and that the net heat transfer to the coolant is the sum of both the heat transfer to and from the wall. Next note that two different types of experiments have been run by investigators to evaluate the effect of insulation on the net heat transfer rate between the gases and the wall. The first type of experiment is measurement of local instantaneous heat transfer rates. For local heat transfer measurements there is the fundamental question as to whether a local heat transfer rate measurement is characteristic of the complete combustion chamber heat transfer rate. This question is particularly pertinent since it is well established that there is considerable variation in heat transfer in the chamber from point to point.

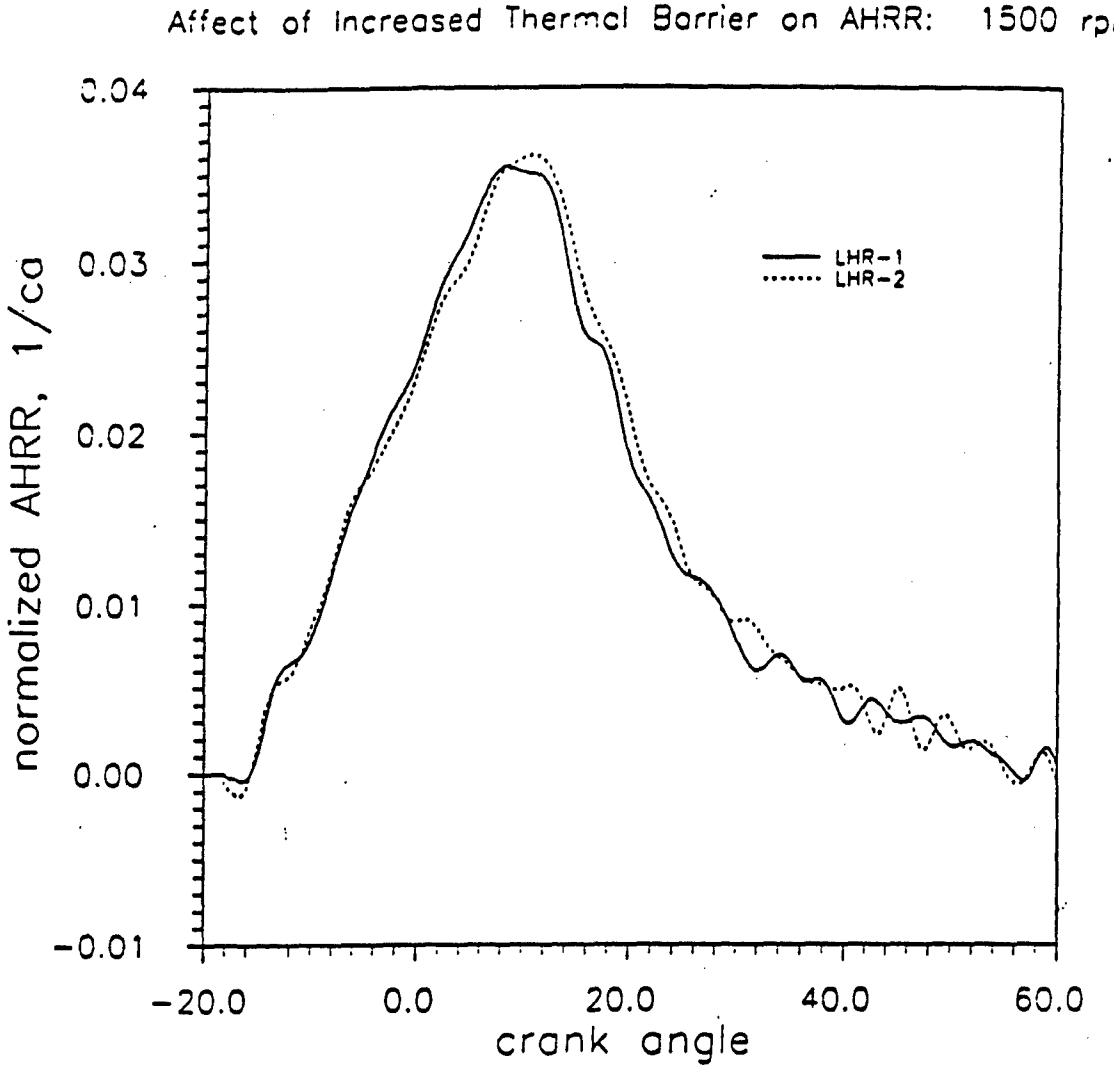

LHR configuration	LHR-1	LHR-2
Peak Premixed AHRR	0.006	0.005
Centroid of AHRR	13.91°	13.97°
Duration of HR [°ca]	29.86	30.20
Burning Schedule 0% 50% 70%	 -14.07 9.57 15.79	 -14.33 9.91 15.86

Figure 5-26. Apparent Heat Release and Tabulated Results for the Uncoated (LHR-1) and the Coated (LHR-2) Air-Gap Piston, the Conditions are Heavy Load (ϕ = 0.5) and 1500 rpm

COMPARISON OF PERFORMANCE PARAMETERS

		Percent Cycle Energy Input as Heat Transfer		ISFC (kg/hp-hr)	
speed rpm	equivalence ratio	LHR-1	LHR-2	LHR-1	LHR-2
1300	0.30	0.2878	0.2796	0.1323	0.1318
1300	0.40	0.2689	0.2888	0.1337	0.1377
1300	0.50	0.2610	0.3228	0.1366	0.1463
1500	0.30	0.2796	0.2924	0.1306	0.1331
1500	0.40	0.2489	0.2855	0.1332	0.1390
1500	0.50	0.2327	0.2815	0.1349	0.1390
1700	0.30	0.2566	0.3008	0.1311	0.1413
1700	0.40	0.2365	0.2512	0.1322	0.1348
1700	0.50	0.2186	0.2532	0.1362	0.1382

LHR-1: Air-gap piston

LHR-2: PSZ coated air-gap piston

Figure 5-27. Comparison of Heat Transfer and Indicated Specific Fuel Consumption at Different Load and Speeds for the Uncoated Air-Gap Piston (LHR-1) and the Ceramic Coated Air-Gap Piston (LHR-2)

On the plus side, it is true that local heat transfer rates can be measured quite precisely. However, especially when ceramics are used for insulating purposes, there can be questions as to whether the sensor itself affects the heat transfer rate. For example, does even a thin coating on the surface of a ceramic affect the emissivity of the surface and the porosity of the wall? Additionally, it is known that in steady heat transfer there is a transition region where heat transfer rates are different when flow passes over a temperature discontinuity. Thus, if the surface is insulated locally and is surrounded by cooler surfaces, there is a question as to whether local heat transfer is affected.

The second type of experiment uses global heat transfer measurements representing an average heat transfer rate for the entire combustion chamber. Basically, for global measurements, a First Law balance is written for the time interval during which both the intake and exhaust valves are closed. All terms in this energy balance, except the heat transferred, are evaluated from experimental data and the heat transferred can then be computed.

The global measurement gives directly the heat transfer rate from the hot gases to the wall but there are a number of uncertainties that affect the precision of the measurement.

First, the trapped mass must be estimated very accurately. For example, a one percent error in the trapped mass estimate can manifest itself as an error greater than five percent in the global heat transfer.

Work must be evaluated from the pressure-time diagram. This evaluation depends upon the dubious accuracy of the pressure pick up.

It must be assumed that the same amount of fuel is injected each cycle. Also, estimations must be made of the chemical energy in the exhaust gas just before the exhaust valve opens. Cycle analysis is of little help in either case.

Blowby must also be estimated. Blowby is affected by cylinder and piston distortion and they, in turn, may be affected by insulation. For example, Gatowski[62] found blowby to increase three per cent when thermal barriers were introduced into the engine.

However, even if very precise and detailed measurements were possible for global analysis purposes, conflicting results could still be obtained. This is because of changes occurring between normal and insulated engines in the extremely complex heat transfer occurring in engines and the many interactions

that affect heat transfer. Figure 5-28 attempts to illustrate the complexities and interactions. The top portion of the diagram shows the physical situation while the bottom portion shows an electrical analog of the system.

Looking at the top portion of the diagram, note that wall materials affects and changes everything to the right of the wall, as well as the wall itself. To illustrate the point, assume that when wall materials are changed, coolant temperatures change in such a manner as to keep the coolant-wall interface temperature constant. It is well established that when insulating materials are used in the combustion chamber the mass of air inducted during the intake process is decreased, i.e. higher gas temperatures exist during the intake stroke and, therefore, during compression. The changed density of air in the combustion chamber affects the fuel spray, including impingement on the walls. The thickness of the boundary layer may be affected by changes in spray impingement as well as by changes in quench distance due to different wall temperatures. If the same amount of fuel is injected per cycle the stoichiometry of combustion will be changed. If the wall temperature is increased the character of the combustion chamber wall deposits may be changed or deposits may even be eliminated. If the ignition delay is changed the phasing of the temperature-time curve is changed. It is clear that a change in wall material has feedback effects on all of the other physical elements of the system and can cause unexpected heat transfer effects.

Possible interactions by the electrical analog of the physical situation are shown in the lower portion of Fig. 5-28 where it is seen that there are a number of energy (voltage) generators present and that they are affected by a change in wall material.

Consider the bulk gas on the right hand side. Two sources of energy are shown in the bulk gas - one convective and one radiative. Note that the radiant source is not significantly affected by the resistance of the boundary layer. As mentioned above, the shape and the magnitude of both of these generators is potentially affected when we change wall material. Gas temperatures at the time of injection of the fuel affects ignition delay, premixed burning, and bulk gas temperature thereby affecting the shape and magnitude of both the convective and radiant heat transfer generators. Similarly, if volumetric efficiency is changed, both convective and radiant heat transfer generators are changed.

Looking next at the boundary layer, the long row of generators in the boundary layer represents the fact that differing amounts of compression work are done in differing portions of the boundary, i.e., compression of the boundary layer varies from approximately isothermal to isentropic. Note that this distribution of work

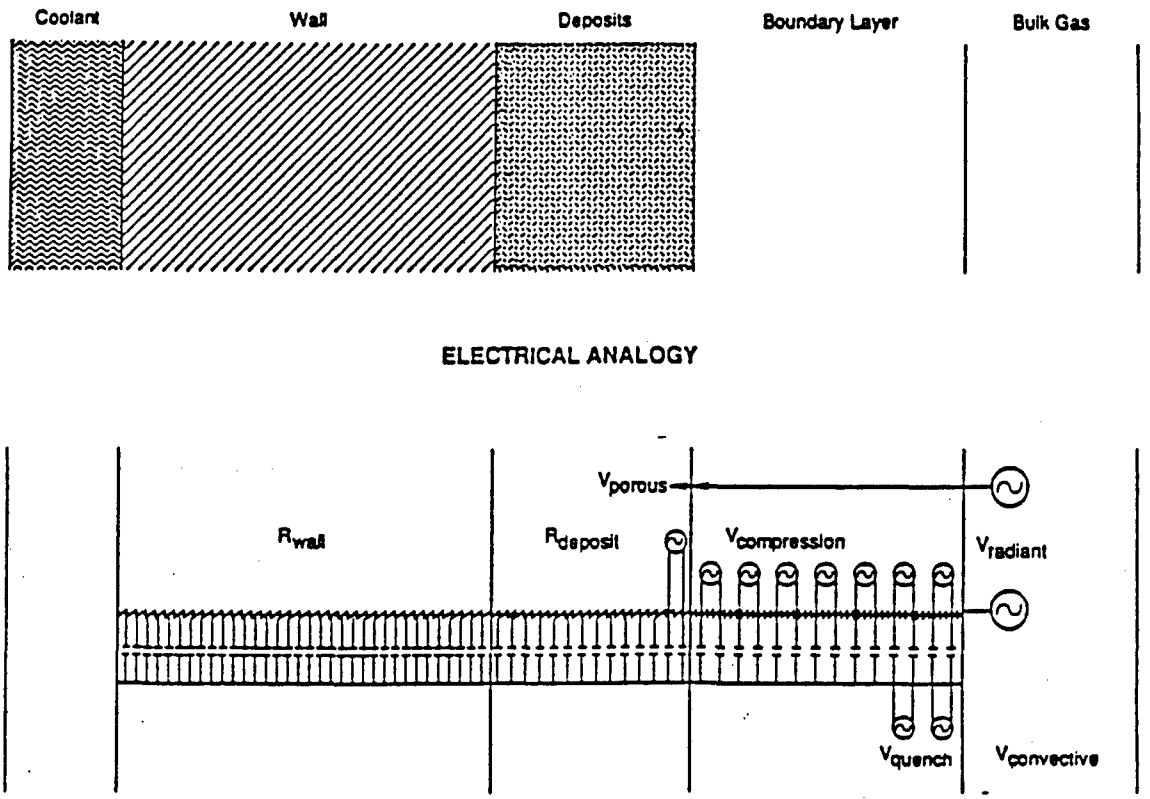

Figure 5-28. Cross Section Schematic of the Coolant-Wall-Gas Interface and an Equivalent Electrical Analogy

in the boundary layer is affected by a change in wall material, i.e., if the wall material is a better insulator the wall temperature swing increases and compression at the wall departs from approximately isothermal compression.

The shorter row of generators in the boundary layer represents the fact that, if the change in wall material (or other factors such as removal of coolant) cause higher wall temperatures, the thickness of the quench zone, and therefore the effective boundary layer thickness, may be changed. In addition, if the changes in the bulk gas conditions affect the extent of spray impingement on the wall the thickness and the energy generation in the boundary layer may be changed. It is well established that the atomization because of surface impingement depends upon the surface temperature. This could have a pronounced effect on the energy release in the boundary layer. There is interaction and feedback between impingement, wall temperature, the bulk gas temperature, and heat transfer.

Looking next at the deposits, they can be changed, or even eliminated, by a change in wall material. Deposits are physically thin but their thermal conductivity and heat capacity are low so that they are thermally much thicker than they appear physically. It has often been observed that higher wall temperatures can change the properties of deposits, or even eliminate them, with obvious effects on heat transfer. The deposit voltage generator reflects the possibility that deposit porosity could result in gas flow into and out of the deposits with a consequent energy exchange. Incidentally, although not shown, the same phenomena could occur if the wall is porous. In addition, the deposit voltage generator includes the possibility that introduction of oxygen into the deposits by gas flow could cause chemical reactions in the deposits which would, in turn, affect heat transfer.

The double-headed arrow on the radiant heat transfer reflects the possibility that longer wave length radiation may penetrate below the gas-deposit interface decreasing the effective thermal thickness of the deposit. Again, although not shown, the same affect may be present in some wall materials.

5.3.4. Observations. With all of this complexity of heat transfer in engines what general observations can be reached with regard to the net heat transfer in insulated versus normal engines?

The first observation is that insulating the combustion chamber does affect combustion and that combustion affects heat transfer. This effect of insulation on combustion was noted in the experiments reported here as well as by many other investigators. In general, insulating the chamber significantly reduces premixed burning. There are less certain indications that it also increases the duration of burning.

The second observation is that existing comparisons of heat transfer in insulated and in normal engines have been made using current rather than future combustion chambers. Because of the severe future limits on particulates and NO_X, diesel combustion chamber design and therefore diesel combustion, is rapidly changing. Higher injection pressures, more rapid introduction of the fuel, and changes in combustion chamber shape are being used. These changes will undoubtedly affect such factors as spray impingement, location of initiation of combustion, combustion chamber particulate loading, etc., and they, in turn, affect heat transfer. Thus, in addition to all of the uncertainties discussed above, there is uncertainty as to the applicability of the existing data to future combustion chambers.

These two general observations lead to the third. This third observation is that no general conclusion can be reached about the question of whether the net heat transfer is smaller for insulated engines than for normal engines. Because of the complexities and numerous feedback mechanisms in engine heat transfer, it appears that there is no general answer to this question. This viewpoint is supported by existing data. It appears logical and probable that these various complexities and feedbacks can be manipulated to produce reduced heat transfer in insulated engines. However, the available data make it clear that simply using insulation without concern for these complexities and feedbacks does not inevitably produce reduced heat transfer in insulated engines.

What are the implications of these general conclusions for engine design? Probably the most significant implication is that, even in insulated engines, one must experimentally optimize a chamber from the standpoint of low heat transfer as well as from the standpoint of fuel consumption and emissions. It follows that there may be trade offs between heat transfer and other optimizing factors just as there is a trade off between NO_X and particulates.

5.4. Models for Spatially-Resolved Heat Transfer Predictions

5.4.1. Need for Spatially-Resolved Predictions. To predict engine efficiency, exhaust emissions, and thermally-induced stresses, accurate spatially-resolved models of engine heat transfer are required. Experimental studies have shown differences in the magnitude of the heat transfer for different locations within the combustion chamber of 50 percent or more.[63] This variation occurs because of differences in the gas-side boundary conditions that arise from spatial dependence in the local fluid mechanics, local fluid thermophysical properties, and combustion.

5.4.1.1. Need for heat transfer modeling. Multidimensional hydrodynamic models of in-cylinder events may eventually solve the momentum and energy equations for the boundary layers numerically. Due to limitations of existing computers in speed and memory, however, it is not feasible to do this now, or in the foreseeable future. Even if computers capable of carrying out the calculations existed, turbulence models would be necessary, and the application of turbulence models to the boundary layer region is a subject of much intense research itself.

The approach adopted here for the development of a method for spatially-resolved predictions of engine heat transfer has been to recognize that modeling will be required, and that simple models are necessary if they are to be used in actual engine heat transfer predictions. However, as has been stated, spatially-dependent physical environments exist in the combustion chamber of an engine. For example, in a typical DI diesel engine, the mechanisms of heat transfer in the squish region can be dominated by the squish flow and the associated pressure gradients. This is in contrast to the bowl region, where the heat transfer is controlled by interactions with the spray and combustion. Thus it is unlikely that a single simple model will be able to accurately account for these different physical environments. In this work, three different models have been developed, each in response to a different set of physical environments observed to occur in the chamber of an internal combustion engine. These different models can be used where the restrictions inherent in their formulation have been met to produce predictions from different regions of the chamber, which can then be coupled. The selection of which model to use where is dependent upon a determination of the characteristics of the in-cylinder physical state, either through trial numerical calculations, or experimental results, or both.

5.4.1.2. Approximate solution - 1-D energy equation (AS1DEE). For this model, the specific issues of the local fluid mechanics, energy transfer due to piston motion, and combustion effects on the convective heat transfer have been addressed. In the development of this model, the following assumptions were necessary: 1) All gradients parallel to the wall were assumed to be zero, i.e. the boundary layers were assumed to be one-dimensional; 2) relationships relating the turbulent viscosity to the absolute viscosity from incompressible flow were assumed to be applicable, and the turbulent Prandtl number was assumed to be constant; 3) the pressure was assumed to be uniform in space; 4) the gas conductivity was assumed to be proportional to the absolute gas temperature; 5) the gases in the chamber were assumed to be ideal; and 6) additional heat flux from interdiffusion of species and from the Dufour or diffusion-thermo effect were neglected.[64]

With these assumptions the energy equation with a source term from combustion can be expressed in a one-dimensional form:

$$\rho C_p \frac{\partial T}{\partial t} + \rho v C_p \frac{\partial T}{\partial y} = \frac{\partial}{\partial y}\left[(k + k_t)\frac{\partial T}{\partial y}\right] + \frac{dP}{dt} + \rho \dot{q} \tag{11}$$

In the following, only those equations that are necessary to perform the heat flux calculation are presented. A complete derivation can be found in Reference 65.

To begin with, equation (11) was transformed to Lagrangian coordinates, then was linearized and normalized by introducing an empirical relation for the ratio $\mu_t / \mu = f(y^+)$, a characteristic length given by:

$$\ell = \frac{\mu_w}{\kappa \rho_o u^*} \tag{12}$$

and a transform time equal to:

$$\tau = \int \frac{P}{P_o} \frac{\alpha_o}{\ell^2} dt \quad . \tag{13}$$

The boundary condition at the wall surface becomes:

$$\Phi(0, \tau) = \frac{T_w}{T_{p\infty}} - 1 = f(\tau) \tag{14}$$

where $T_{p\infty}$ is defined as:

$$T_{p\infty} = T(\infty, 0)\left(\frac{P}{P_o}\right)^{\frac{\gamma - 1}{\gamma}} \tag{15}$$

and the heat-release rate becomes:

$$\dot{Q} = \frac{P_o \dot{q} \ell^2}{C_p T_{p\infty} \alpha_o P} \tag{16}$$

The linearized equation, boundary, and initial conditions were divided into three parts specifically to separate the nonhomogeneities. In each case, the response of the individual equation set to a unit-step function was determined numerically. Then multiparameter fits to the numerical solutions were performed to find

approximate analytical forms. Duhamel's theorem allowed these approximate solutions to determine the response of each equation set to an arbitrary input. Finally, the solutions were combined to produce the model for prediction of the total heat flux.

The approximate solution for the one-dimensional energy equation to predict the surface heat flux can then be calculated according to:

$$
\begin{aligned}
Tq_w = \kappa\, T_{0,\infty} &\left(\frac{P}{P_o}\right)^{\frac{2\gamma-1}{\gamma}} \frac{\kappa \rho_o u^*}{\mu_w} \\
&\left[-f(0)\left(\frac{1}{\sqrt{\pi(\tau+\tau_o)}} + 0.082\left(1-\exp\left(-\frac{\sqrt{\tau+\tau_o}}{3}\right)\right)\right)\right. \\
&-\int_{\theta=0}^{\tau}\left(\frac{1}{\sqrt{\pi(\tau+\tau_o)}} + 0.082\left(1-\exp\left(-\frac{\sqrt{\tau-\theta}}{3}\right)\right)\right)\frac{df(\theta)}{d\theta}d\theta \\
&+\int_{\theta=0}^{\tau}\left(\sqrt{\tau-\theta} + 0.084(\tau-\theta)\right) \\
&\left.\exp\left(\frac{-1.1\, d^{0.79}}{\sqrt{\tau-\theta}+0.084(\tau-\theta)}\right)\frac{d\dot{Q}}{d\theta}d\theta\right]
\end{aligned}
\qquad (17)
$$

where the three terms represent the heat flux due to the initial boundary layer, pressure work, and heat release, respectively. The initial thermal boundary layer is assumed to be formed in a period of dimensionless time, τ_o, before compression. The period of time, τ_o, can be determined from a measured initial thermal boundary layer thickness, or estimated as 180 degrees, for example, using Eq. (13). The temperature profiles in the boundary layer can also be estimated using this model, although the emphasis of this work is on the prediction of heat flux.

5.4.1.3. Modified Law-of-the-Wall (MLAWAL). Currently, most hydrodynamic calculations of in-cylinder events use laws-of-the-wall to model the momentum and thermal boundary layers. In KIVA-II, an explicit form of the law-of-the-wall is used to determine the shear stress at the wall by determining u*:

$$U/u^* = 0.75 + 2.19\ln(yU/\nu) \qquad (18)$$

which is a function of the mean velocity U at a distance y from the wall. The kinematic viscosity used here includes contributions from the molecular viscosity and turbulence. Using a modified Reynolds analogy formula, the heat flux can be shown to be:

$$q_w'' = 1.125(\tau_w/U)c_p(T-T_w) \tag{19}$$

If the first computational node away from the wall is inappropriately placed in the laminar sublayer, then a different model is used to predict the wall shear stress.

Consideration of the heat transfer problem in engines leads to questions about the applicability of these laws for the prediction of engine heat transfer. Under motoring conditions the boundary layer can be characterized as turbulent, non-steady, and compressible because of piston motion, and scrubbing from intake and squish flows. For fired conditions, there are further complications including direct effects of combustion, radiation heat transfer, and such problems as spray impingement on combustion chamber surfaces. Combustion has a dominate influence on the boundary layer, not only as a heat source, but also in the effects on turbulence and work on the gases in the boundary layer.

The law-of-the-wall for velocity is based on the assumptions of steady state, incompressible flow, with zero pressure gradient along the wall. The law-of-the-wall for the boundary layer temperature distribution was derived with the additional assumptions that there is no heat release from combustion, and no pressure work, such that Reynolds analogy holds. However, for the engine situation, this analogy is not valid, and modifications to the law of the wall formulation must be made. To do this, a source term, S, is added to account for additional diffusion of thermal energy from the pressure work, transient effects, and combustion. Formally this is given by:

$$S=\left(\frac{C_p}{R}-1\right)\frac{dp}{dt}+\frac{\rho C_p}{R}\nabla\bullet\vec{v}-q''' \tag{20}$$

With this source term, the dimensionless temperature profile in the boundary layer is:

$$T^+=13.2\,Pr + 2.2\ln y^+ - 5.7 - S^+(87.1Pr + 2.2y^+ - 29.0) \tag{21}$$

which is applicable for $y^+ > 13.2$ and:

$$T^+=Pry^+-0.5PrS^+(y^+)^2 \tag{22}$$

for the laminar sublayer, $y^+< 13.2$. For these equations, the following definitions apply:

$$T^+ = \frac{(T_w - T)\, u^* \rho C_p}{q''_w} \tag{23}$$

and:

$$S^+ = \frac{S\upsilon}{q''_w\, u^*} \tag{24}$$

These expressions can then be differentiated and rewritten in terms of the wall heat flux q'':

$$q''_w = (T - T_w)\rho C_p\, u^* + \left(S\upsilon\, Pr\, y^{+2} / 2u^*\right) \tag{25}$$

and for $y^+ > 13.2$:

$$q''_w = \frac{(T - T_w)\rho C_p\, u^* + \left(87.1\, Pr + 2.2\, y^+ - 29.0\right)\left(S\upsilon / u^*\right)}{13.2\, Pr + 2.2\, \ell n\, y^+ - 5.7} \tag{26}$$

5.4.1.4. Pressure gradient correction model (PGC). As has been noted, for engine flows, the simple wall functions are usually adopted. With these wall functions, pressure is assumed to be uniform in space. This means that the ordinary law of the wall functions are also unable to account for the effects on momentum and heat transfer from local flow acceleration and deceleration. In an engine with a geometry designed to produce squish flows as the piston approaches TDC, flow acceleration will strongly influence thermal transport. Pressure gradients in the streamwise direction are the driving force for the flow acceleration or deceleration. Thus, it is important to account for these effects in the formation of an accurate method for the prediction of spatially-resolved heat transfer. Here, following Launder and Spalding,[66] the assumption is made that although the freestream flow is complicated, the flow within the boundary layer can be assumed to be a simple Couette boundary-layer type flow with the stress gradient balanced by the pressure gradient. This concept was used to develop a

further modification to the law of the wall that includes effects of the local pressure gradient.

The thermal wall functions of the PGC model is also a two-layer type wall function separated at a critical nondimensional distance $y^+=13.2$, where:

$$T^+ = Pr\, y^+ (1+S^+ y^+/2) \qquad y^+ \le 13.2 \tag{27}$$

and for $y^+ > 13.2$:

$$T^+ + \left(Pr\, y_c^+ \left(1+S^+ y_c^+/2\right)\right) + \frac{Pr_t}{\kappa} \ell n\left(\frac{\sqrt{1+p^+ y^+}-1}{\sqrt{1+p^+ y^+}+1}\right) + \frac{S^+ Pr_t}{\kappa}\left(\frac{2\sqrt{1+p^+ y^+}}{p^+}\right) -$$

$$\left[\frac{Pr_t}{\kappa} \ell n\left(\frac{\sqrt{1+p^+ y_c^+}-1}{\sqrt{1+p^+ y_c^+}+1}\right) + \frac{S^+ Pr_t}{\kappa}\left(\frac{2\sqrt{1+p^+ y_c^+}}{p^+}\right)\right] \tag{28}$$

Here the nondimensional pressure gradient p^+ is defined:

$$\frac{V_w}{\tau_w u^*}\frac{dp}{dx} = \frac{V_w}{\rho_w u^{*3}}\frac{dp}{dx} \tag{29}$$

Rewriting these two equations from the definitions of T^+ and S^+, the heat flux at the wall is expressed as:

$$q_w'' = \frac{(T-T_w)\rho\, Cp\, u^* - \left(S\upsilon\, Pr\, y^+/2u^*\right)}{Pr\, y^+} \tag{30}$$

$y^+ \le 13.3$, and:

$$q_w'' = \frac{(T-T_w)\rho\, Cp\, u^* - T_b\left(S\upsilon/u^*\right)}{T_a} \tag{31}$$

for $y^+ > 13.2$. The PGC model has been compared with experimental data from both fundamental boundary-layer experiments and engine test data.[67] The recommended range of application is $-0.2 < p^+ < +0.2$.

5.4.2. Engine Measurements to Support Development of Heat Transfer Models.

5.4.2.1. Description of see-through engine . In order to study boundary layer phenomena in engines, a see-through engine has been developed which has full optical access to allow measurements of the temperature distribution by a speckle interferometric technique[68] and velocity and turbulence by laser Doppler velocimetry. Table 5-3 lists details of the engine. A sapphire annular ring can be mounted between the cylinder head and the cylinder block such that the entire clearance volume at TDC is optically-accessible. Two silver-plated metal O-rings, set in grooves machined in the head and cylinder block, seal the sapphire window. In addition, the engine has a Bowditch-type piston for optical access through the piston into the combustion chamber. Finally, the cylinder head of the see-through engine has a large instrumentation port, as shown in Fig. 5-29, which can accommodate additional windows, or a transducer for the measurement of surface temperature and surface heat flux.

The velocity, temperature, and heat flux measurements to be reported here were obtained when the engine was motored and equipped with a steel ring holding two small quartz windows aligned on a diameter, as shown in Fig. 5-30. Heat flux and temperature measurements were made using a water-cooled probe, shown in Fig. 5-31, fitted to the instrumentation port. The heat-flux probe consists of a J-type thin-film surface thermocouple and 3 K-type junctions 3.2 mm from the surface. The probe itself was positioned 2 mm out from the head to allow for its use with the speckle interferometry.

5.4.2.2. Heat transfer measurements using speckle interferometry. Heat transfer measurements were made in a motored engine as part of this contract. Since some of the emphasis of the heat transfer experiments was on heat transfer from non-metallic surfaces, there was some concern that conventional heat transfer measurement techniques would not provide accurate results for these surfaces under diesel engine conditions. Many heat flux gages used in engines consist of one or more surface thermocouples placed flush with the surface of interest. Since the thermocouple junction is itself a metallic surface, when mounted on a non-metallic engine surface, the measured surface temperature may not be representative of the surface temperature of the substrate itself. This is especially true if effects of ceramic transparency to radiation, porosity to gas, and surface roughness have significant effects. The work described in this section involved development and application of a technique to estimate surface heat flux without using a surface thermocouple.

Table 5-3. See-Through Engine Specifications

Engine:	GM Triptane
Bore (mm)	91.9
Stroke (mm)	76.2
Displacement (cc)	505
Clearance volume (cc)	63.8
Compression ratio	8.92
Swirl ratio	variable with intake valve position
Valve Timing:	
Intake opens	40 deg BTDC
Intake closes	100 deg BTDC
Exhaust opens	60 deg ATDC
Exhaust closes	80 deg ATDC

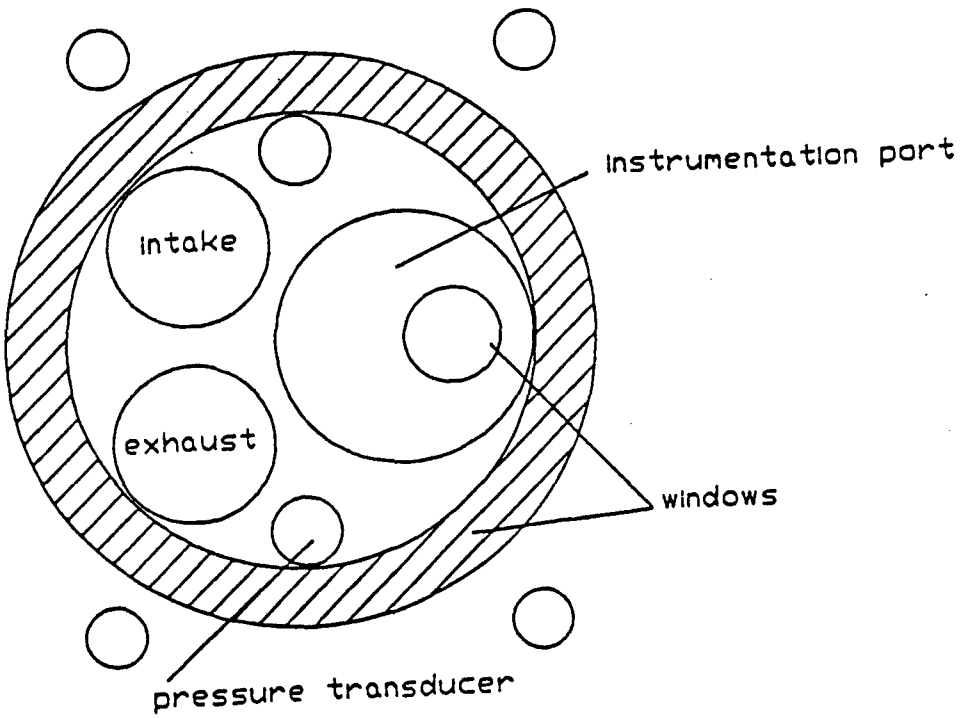

Figure 5-29. Bottom View of Cylinder Head

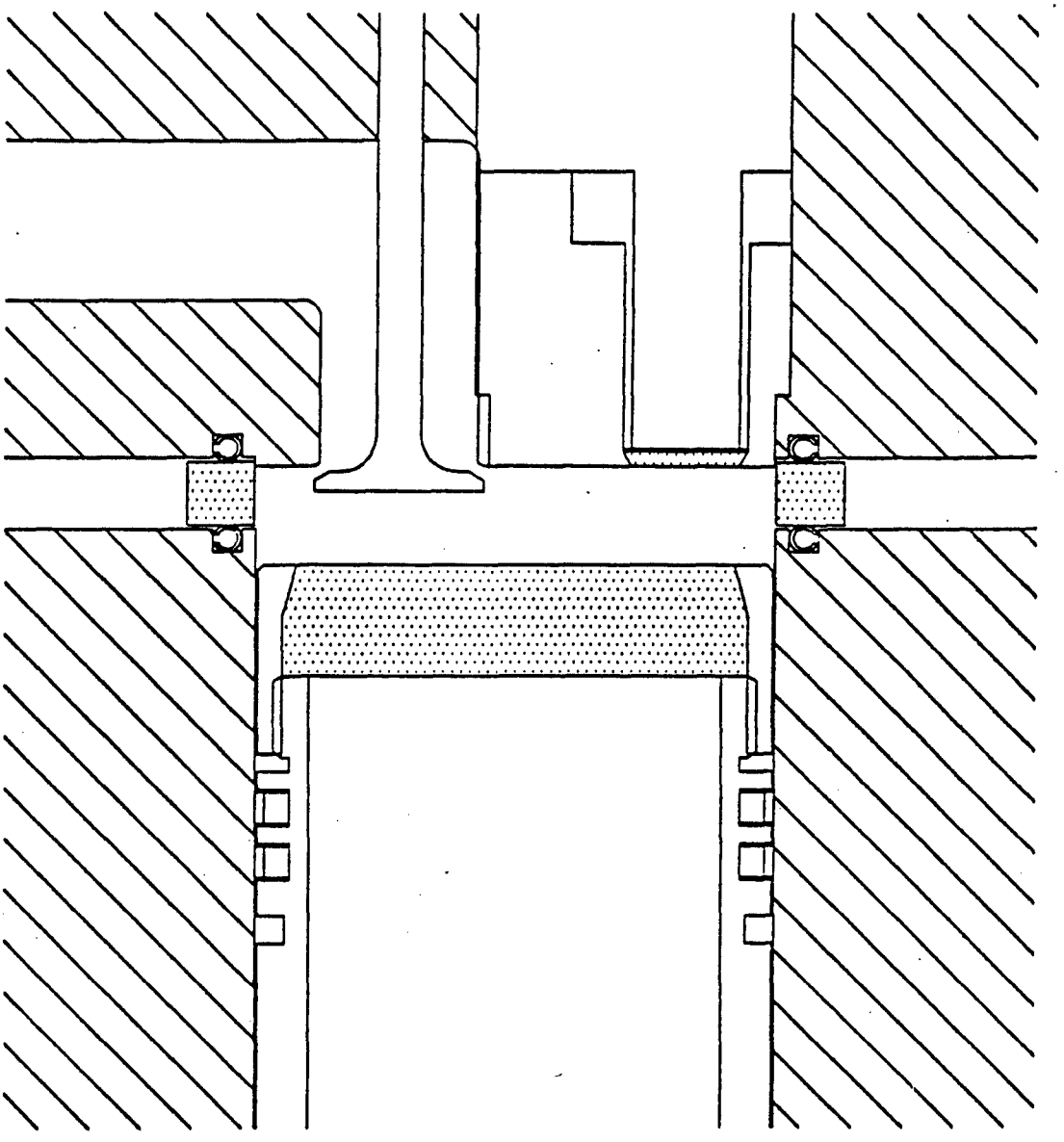

Figure 5-30. Cross-Section of Clearance Volume Showing Location of Windows (Areas With Dots),Valves, and Instrumentation Port

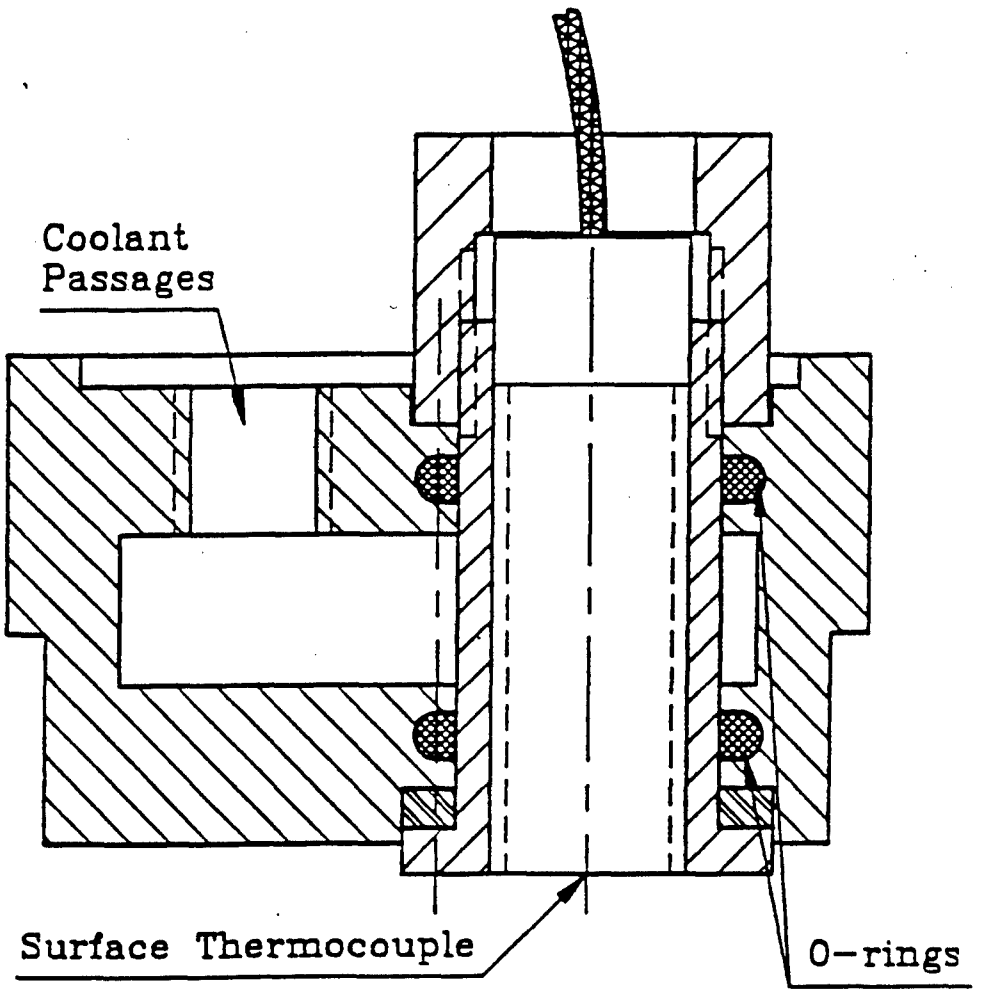

Figure 5-31. Side View of the Instrumentation Plug

The approach taken was to evaluate surface heat transfer from gas side by measuring a gas-phase temperature profile near the surface of interest. For measurements very near the solid surface, an estimate of the temperature gradient near the surface could be used in evaluating the surface heat flux from the surface to the gas phase.

A variety of techniques are available which may be used to make the temperature profile measurements. For the relatively difficult environment of an engine, the techniques considered most likely to succeed were those related to speckle photography and speckle interferometry. Speckle is a phenomena which occurs when collimated light illuminates a diffuse surface or is diffused by a translucent surface like a ground glass plate. As was demonstrated for speckle photography, then speckle interferometry, the behavior of the speckles can be used to infer the gas temperature through which the speckle images have passed. Since speckle interferometry was the primary measurement applied in this work, only this technique will be discussed.

Speckle interferometry for transparent media is a line of sight measurement system which relies on speckle correlation between two speckle photographs to provide full field information on the index of refraction variation of the gas field. A typical experimental set-up is shown in Fig. 5-32. An object beam is passed through the engine containing a gas with a uniform temperature distribution. The beam is diffused by a ground glass plate, and the plate itself is imaged onto a film plane by a lens. In addition, a reference beam is imaged by the same lens onto the film plane. The combination of these two beams at the film plane creates an intensity pattern of speckles representative of the path of the light in the object beam. The test cell then may be modified to include a density profile of interest. A second exposure is then taken on the same piece of film using the same geometry for the object beam and the reference beam. The film is developed and placed in the analyzer of Fig. 5-33. A collimated laser beam illuminates the entire photograph, and the beam is focused by a lens. A low pass filter stops the undiffracted beam at the back focal plane of the lens. The remaining information from the diffracted portion of the beam appears on a viewing screen behind the focal plane. The image that appears is a full field view of a fringe pattern which may be interpreted as regions of speckle correlation and speckle decorrelation. The decorrelation is generated by optical path length variations due to changes in the condition of the test cell between the two exposures.

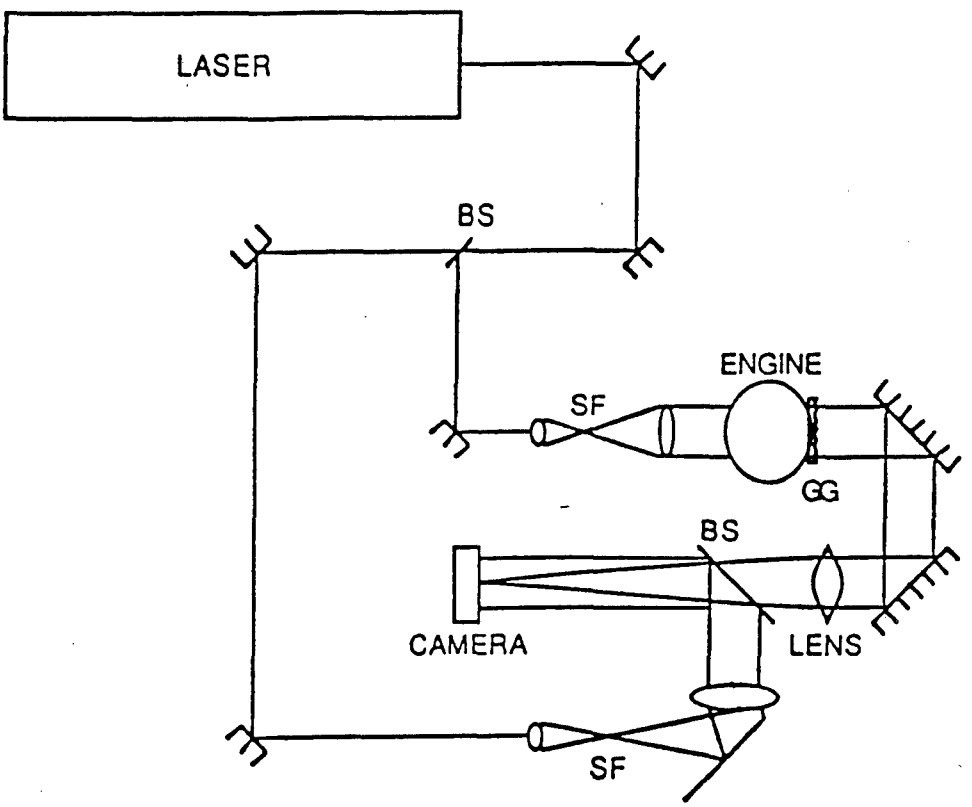

Figure 5-32. Experimental Set Up for Speckle Interferometry in an Engine

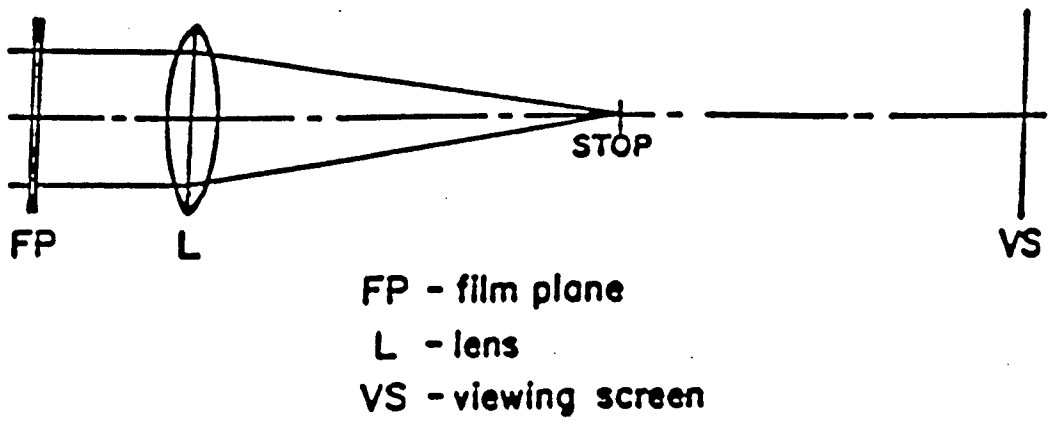

Figure 5-33. Set Up for Reconstruction from Speckle Interferograms

Two series of experiments were performed with the method. The first series was on a 4:1 compression ratio two-stroke engine operated in a motored condition. The engine head was modified to permit optical access by placing a ring of borosilicate glass (Pyrex) between the top cylinder and the cylinder head. A circular copper surface of 44 mm (1.75 in) diameter was attached to the underside of the head in the cylinder bore. The surface was held at constant temperature by circulating water flowing through the support and across the back of the disk.

For a typical test, a first exposure was made with the engine stationary and at room temperature. A second exposure was taken at the appropriate crank angle at 400 rpm. After processing the film, the interferograms were reconstructed using the optical arrangement of Fig. 5-33 and the fringes were recorded on Polaroid positive/negative film. Using the negative in an optical comparator, the fringe numbers and locations were recorded from each interferogram.

A major limitation in the straightforward inversion of the fringe data to solve for the index of refraction occurs if the line integral does not take place along a straight line. In this work, the temperature gradients near the cooled head surface were fairly large, leading to considerable refraction, or ray-bending, of the object beam. Refraction causes two major problems: loss of data due to shadowing; and loss of absolute position location. For a cold surface in a hot medium, light rays will bend toward the cold surface due to index of refraction gradients in the field. Some rays may actually hit the surface, leading to the loss of data.

The path of a ray is defined by the eikonal equation:

$$\frac{\partial}{\partial s}\left(n\frac{\partial r}{\partial s}\right)=\nabla n \tag{32}$$

where n is the local index of refraction, and r is the location of a point on the ray path, s. Since the current problem exhibits a one-dimensional variation of index of refraction (n varies normal to the surface only) Eq. (32) may be simplified somewhat.

The local temperature is calculated for an ideal gas from the Lorenz-Lorentz equation which for $n \approx 1$ gives:

$$T=\frac{3AP}{R\left(n^2-1\right)} \tag{33}$$

where P is the pressure, A is the molar refractivity of the material, and R is the gas constant. The pressure was calculated for a polytropic compression with a polytropic exponent of 1.39.

From the non-dimensional profiles, estimates of thermal boundary layer thickness may be made. These are shown in Fig. 5-34 along with a least-square fit to the data. This figure shows the boundary layer thickness which is based on 90% of the total temperature difference.

Estimates of surface heat transfer, q_w, were made using Fourier's Law:

$$q_w = k\frac{\partial T}{\partial x}\bigg|_{x=0} \tag{34}$$

where the temperature gradient of the gas is taken in the direction x, normal to the surface, and x =0 at the surface. The thermal conductivity of the gas is evaluated at T(0,t). In order to evaluate these gradients, the measured temperature values, corrected for refraction, were fit to a third-order polynomial using the method of least-squares. The resulting surface heat transfer is shown versus crank angle in Fig. 5-35 along with a least squares curve fit.

5.4.2.3. Measurement of the temperature distribution in the see-through engine. Temperature profiles were also measured in the see-through engine described above. A series of double exposure specklegrams was taken at 10 CA degree intervals from 70° BTDC of compression to 60° ATDC of compression for two swirl levels and for two engine speeds. For each crank angle of interest, the first exposure was taken at BDC of a cycle. Each exposure had a duration of 60 μs, which was controlled in duration and timing by a microcomputer. A second exposure was taken at the crank angle of interest, with crank angle information supplied in 1/4° increments to the computer by a shaft encoder. The photograph sequence was repeated five times for each operating condition and crank angle. The resulting specklegrams were filtered as described above, and the interference fringes were recorded on high contrast film which was then analyzed using an optical comparator. For each fringe pattern, the location of the fringes relative to the visible surface of the raised portion of the instrumentation plug was recorded as well as the fringe number. The resulting fringe number and location information was used as input to a ray tracing program designed to iteratively estimate the true location of light rays passing by the specklegram.

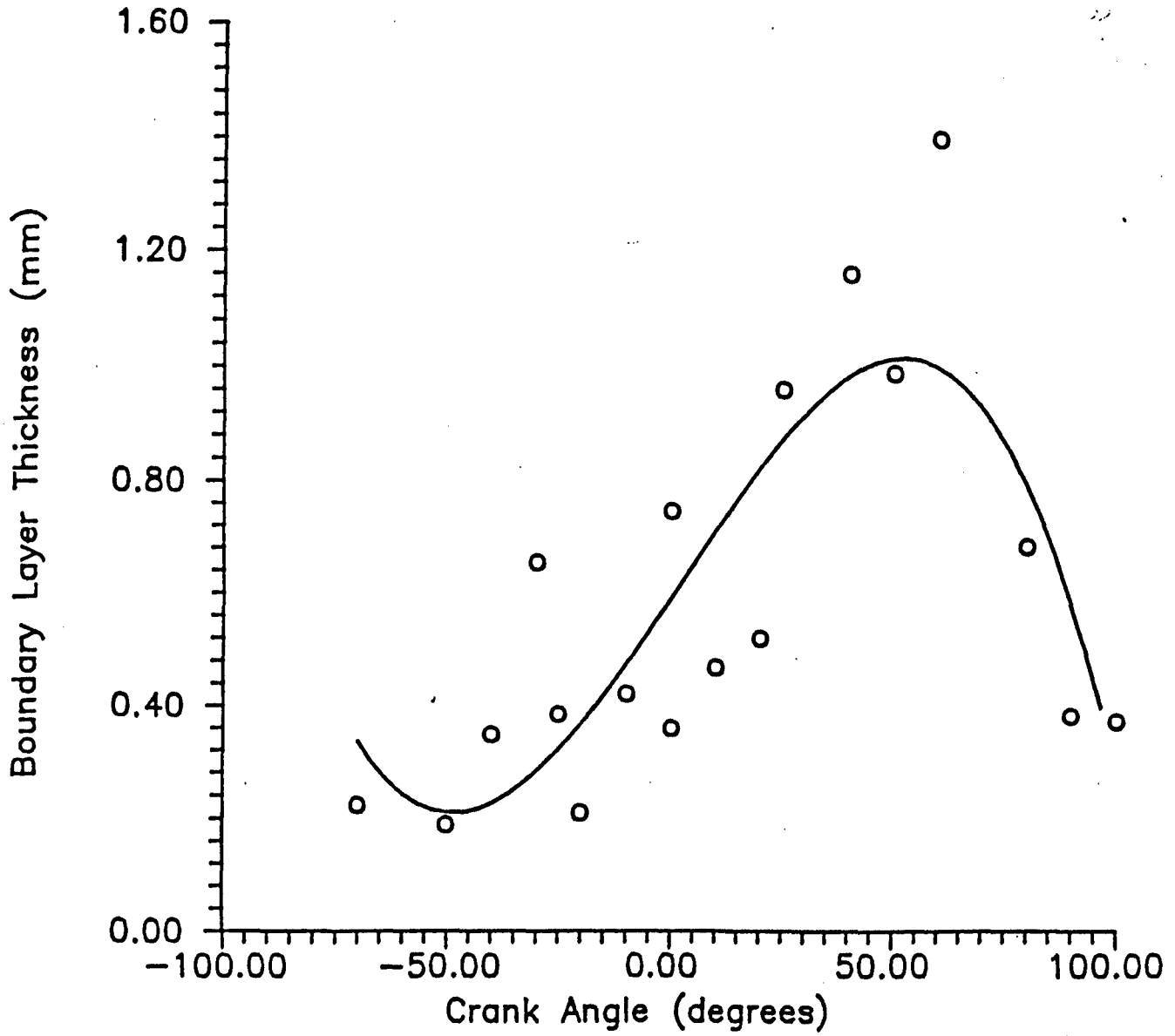

Figure 5-34. Thermal Boundary Layer Thickness Estimates from Speckle Data

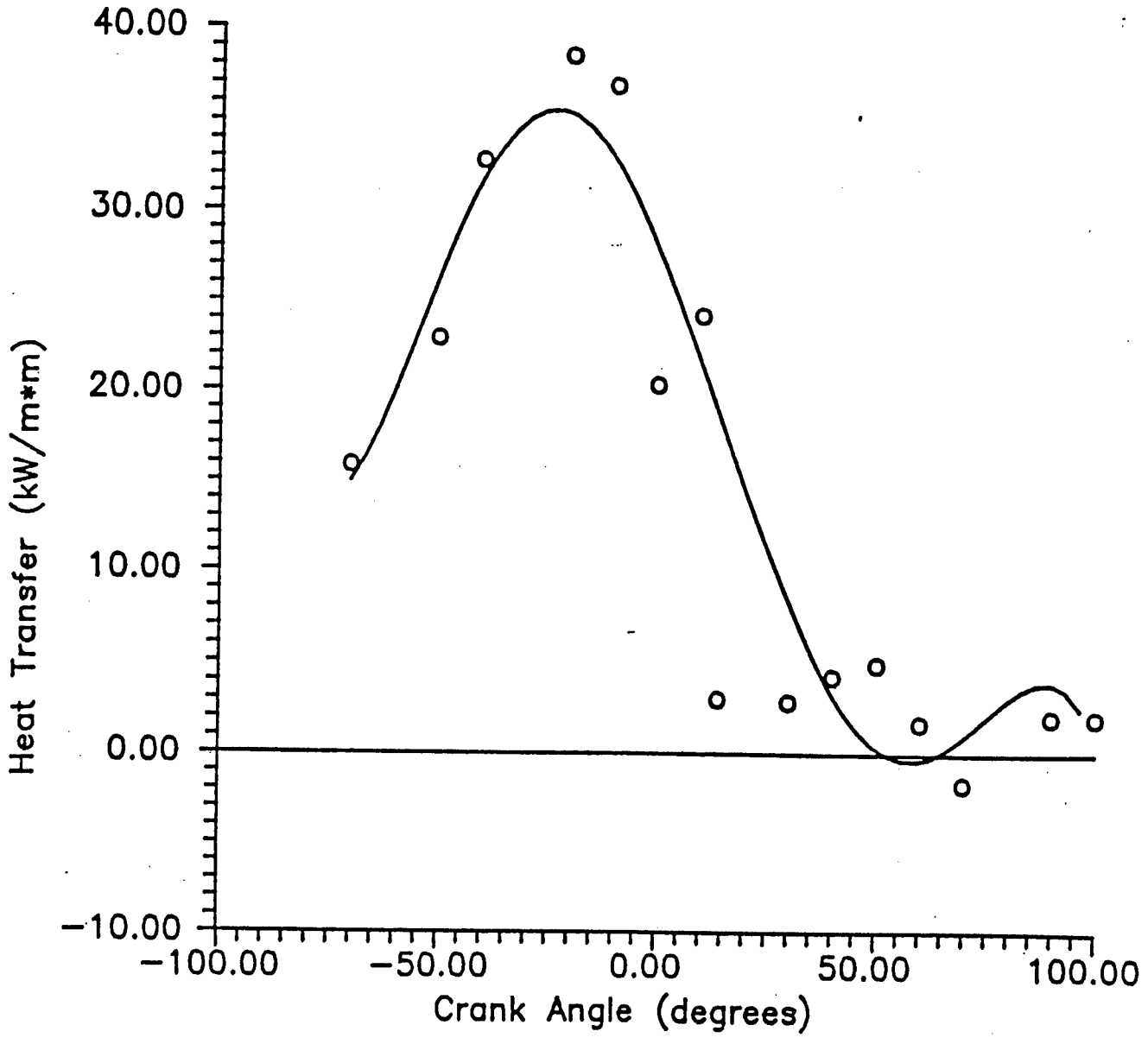

Figure 5-35. Wall Heat Transfer Estimates from Speckle Data

The heat transfer results determined from the temperature measurements for the four test conditions are shown in Fig. 5-36. As was noted, the majority of the data points represent slopes for logarithmic least square fits to five similar data sets. For a few conditions, less than five data sets were acquired. These conditions involving as few as one data set include conditions at 750 rpm high swirl at TDC, and 40° ATDC at 300 RPM for the high swirl case.

The values obtained with speckle interferometry temperature profiles were compared with surface heat flux gage measurements. The measurements were of relative heat flux, indicating that the values given are relative to heat flux defined to be zero at some crank angle (200° before TDC). In order to compare these measurements, the two sets of results were matched at a single point (30° BTDC) by multiplying the speckle interferometry data by an appropriate constant. Other crank angles used the same multiplicative factor. The modified speckle data and the heat flux probe data are given in Fig. 5-37. Overall the shape and peak magnitude of the heat flux curve for 750 RPM and high swirl agrees well with the heat flux gage measurements on the same engine under the same operating conditions. The crank angle location of the peak heat transfer for the current results appears to be somewhat different in character from the heat flux gage results. The speckle data show a generally broader peak value. It should be noted that the heat flux valve at TDC for the speckle data represents one experimental profile, and thus may be less representative than the rest of the data which is the average over 3-5 temperature profiles. No similar comparisons exist for the 750 RPM low swirl case or either of the 300 RPM cases. As mentioned above, the fringe patterns near TDC for the 750 RPM low swirl case are sufficiently distorted by turbulence as to make evaluation impossible. A comparison of the 750 RPM high swirl heat flux data with the 300 RPM data indicate that for these experiments, the higher engine speed causes the heat transfer to increase earlier in the cycle, but decay at about the same crank angle as the low speed.

5.4.2.4 Velocity measurement using laser Doppler velocimetry. Determination of the true velocity distribution from LDV measurements made in the boundary layer of an engine is difficult because of at least five sources of error. First, because these measurements are made close to a wall, the no-slip condition implies that velocity biasing may be a problem. Second, there are steep spatial gradients in the boundary layer which the measurement volume may span.[70] It is possible that there is a systematic bias that appears as a shift in the average location of the measurement volume. Third, the laser beams are traversing a field of fluctuating refractive index gradients that will move and distort the

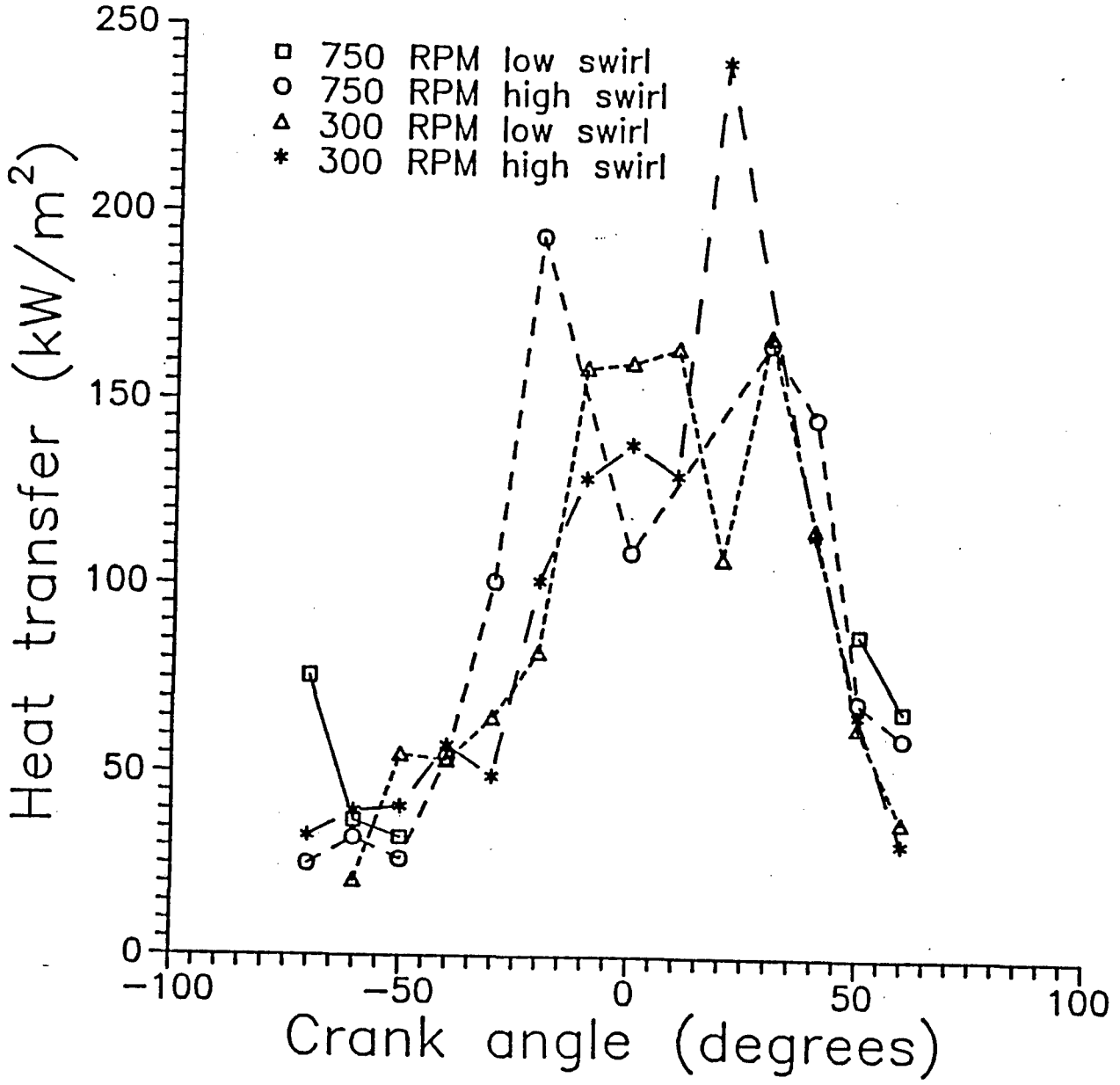

Figure 5-36. Wall Heat Transfer Estimates from Speckle Data for Different Engine Operating Conditions

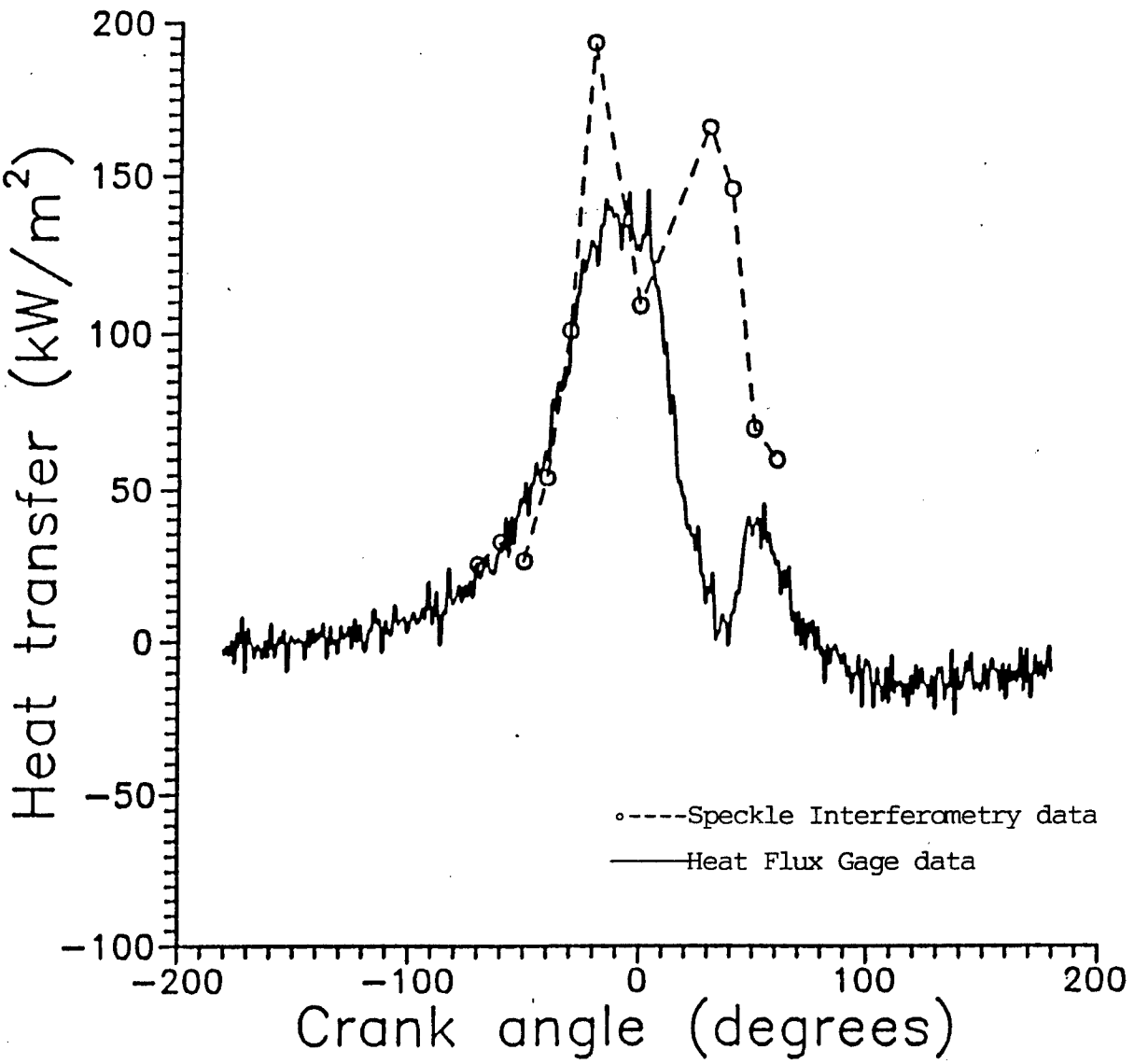

Figure 5-37. Comparison of Heat Flux Estimates from Speckle Interferometry and Heat Flux Probe Measurements

measurement volume.[71-74] Fourth, recent work of Trump, et al.[75] indicates that local temperature variations will affect the local particle density. And finally, cycle-to-cycle variations in the fluid velocity represents a potential source of large errors in the derived quantities.[76]

In the present study, only corrections for velocity biasing were used in the data analysis. Care was taken in the LDV setup to reduce the effect of spatial gradients in the mean velocity by using expansion optics to reduce the measurement volume size. The data was checked to see if there were effects from beam steering by observing if there were regions where velocities appeared to be generated by flare from intersection of the beams with the wall. In addition, data taken with and without spatial filters was compared with no obvious differences. No technique was used to account for the possible bias observed by Trump, et al. Finally, the temperature data and the velocity data were phase-averaged to produce the mean quantities,[77] which assumes that the variation in these quantities from cycle-to-cycle was negligible.

Initially, the 1-D biasing correction proposed by McLaughlin and Tiederman[78] was employed with a weighting function:

$$w = \frac{1}{|u_i|}. \tag{35}$$

However, this correction produces infinite values of the weighting function for zero velocity particles, as shown in Fig. 5-38. On a data set of a finite number of velocity realizations, this correction scheme produces unrealistic weighting of the low-speed particles. To attenuate the sharp increase of the weighting function for low-speed particles, a different weighting function was used, as shown in Fig. 5-38. Thus, for a streamwise velocity realization with a magnitude lower then the uncorrected mean velocity, Um, the weighting function was:

$$W = \frac{1}{|U_m|} - \frac{1}{U_m^2}\left(|U_i| - U_m\right) \tag{36}$$

Individual velocity measurements for the entire cycle from a position approximately 50 μm from the wall are shown in Fig. 5-39. The data shown in this figure were collected over several hundred cycles. Note the strong flow during the intake process, the increase and decrease during the later stages of compression (TDC on compression is at 0 crank-angle degrees), and the large variation that occurs during the expansion stroke. It is instructive to compare

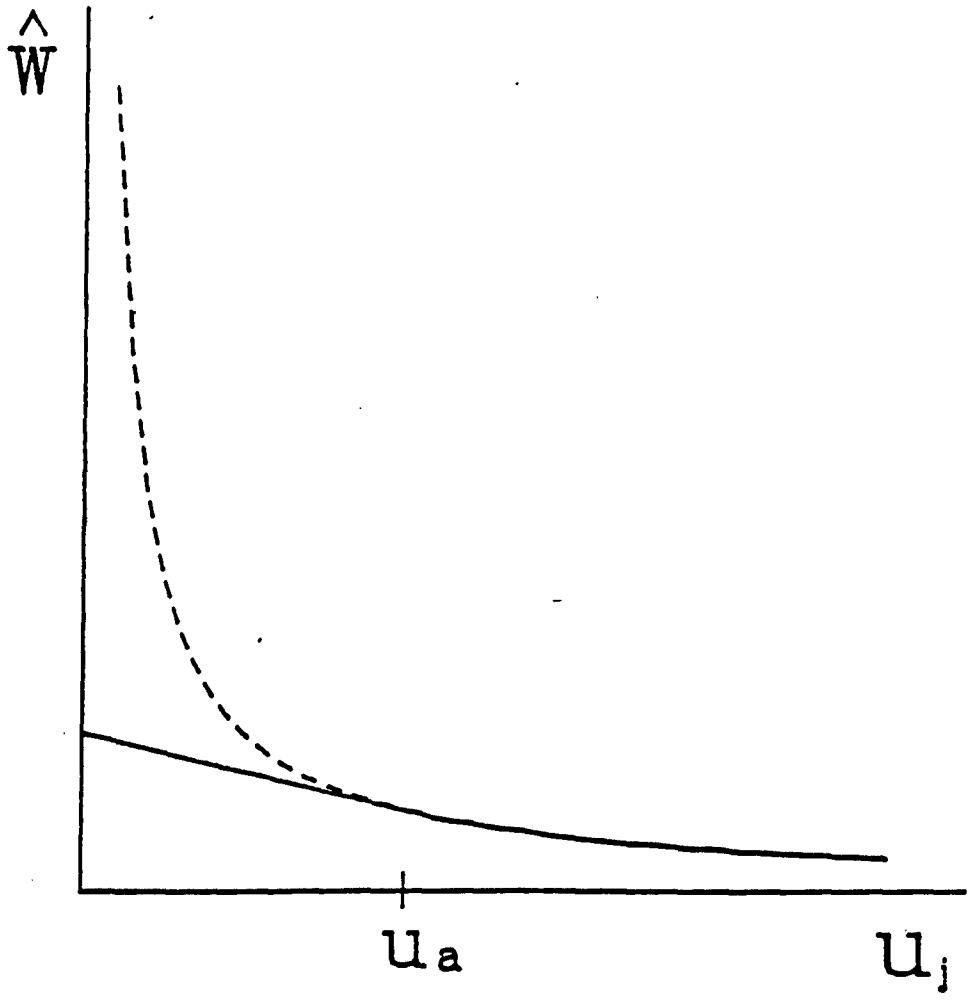

Figure 5-38. McLaughlin and Tiederman weighting function (dashed line) and modified weighting function applied to measurements (solid line)

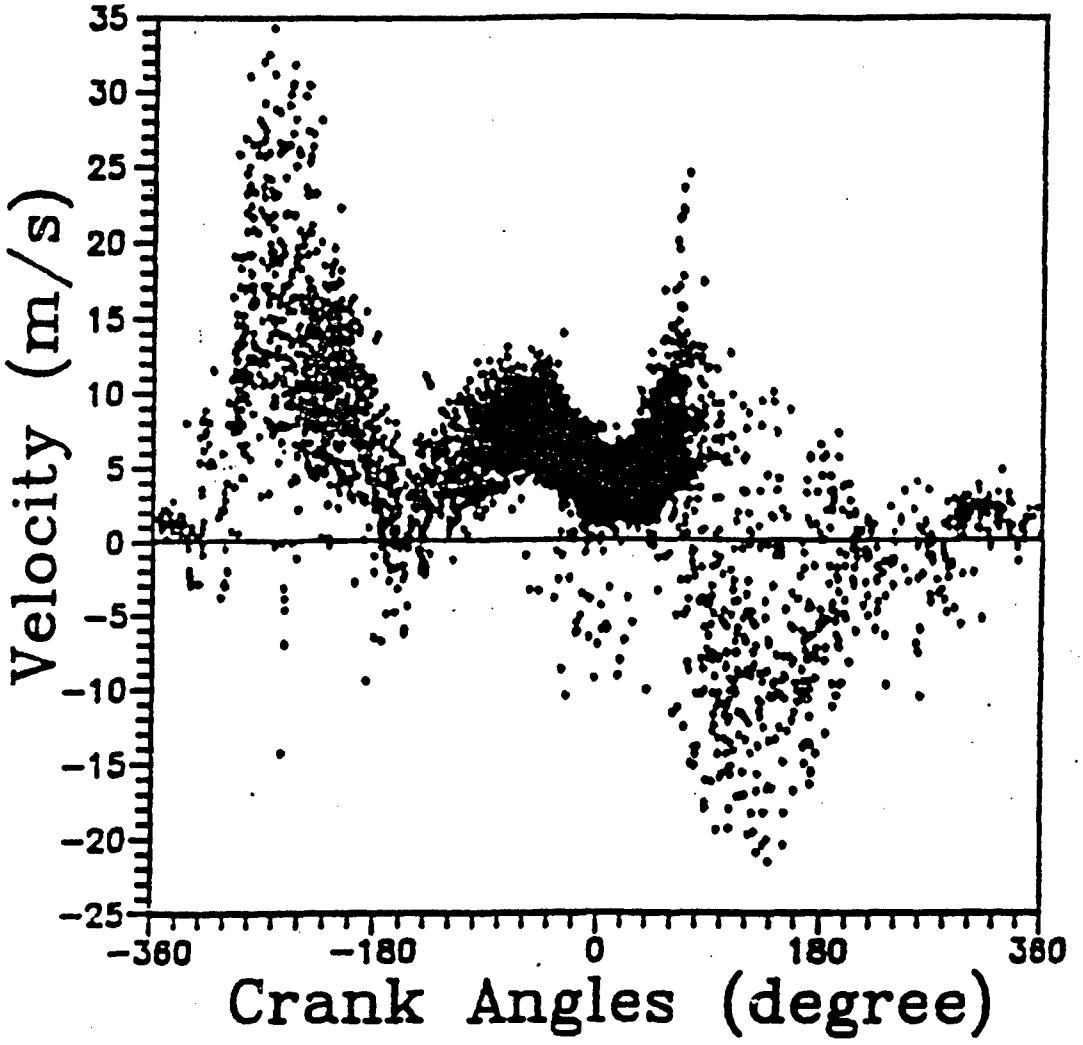

Figure 5-39. Velocity data taken 50 microns from the wall at 750 RPM, high swirl

this figure to the phase-averaged surface temperature measurements shown in Fig. 5-40. The abrupt change in the surface temperature during expansion at 750 rpm occurs at the same time that the velocity data indicates the largest fluctuations. This is not observed nearly as strongly at 1500 rpm.

The phase-averaged velocity for the entire cycle with and without biasing correction are shown in Fig. 5-41 for comparison. The biasing correction is, in general, not more than about 10 percent for most of the cycle. The largest correction occurs again at the region in the cycle where the largest fluctuations occur.

Phase-averaged boundary-layer velocity profiles for the two engine speeds are shown in Fig. 5-42. The velocities at 50 microns are of a magnitude similar with the velocities away from the wall. This may be due to a systematic bias which has not been accounted for, such as the probe protrusion.

Friction velocities were calculated from the measured velocity data using the Spalding's formula[79] for the inner law:

$$y^+ = u^+ + e^{-\kappa B}\left[e^{\kappa u^+} - 1 - \kappa u^+ - \frac{(\kappa u^+)^2}{2} - \frac{(\kappa u^+)^3}{6}\right] \qquad (37)$$

and since $y^+ = \rho u^* y/\mu$ and $u^+ = u/u^*$, once the velocity u at distance y is known, the friction velocity u^* can be calculated. Figure 5-43 shows the friction velocity calculated from the corrected velocity data. If the velocity profiles obey the law-of-the-wall, the calculated friction velocities obtained from using different data points in one velocity profile should be the same. As shown in Fig. 5-43, the calculated friction velocities from data points more than 0.2 mm from the wall were very similar. However, the calculated friction velocities using the data points within 0.2 mm of the wall produced increasing values of the friction velocity as the point chosen for comparison moved to the wall.

These results indicate one of two things. Either the law-of-the-wall for the momentum boundary layer in this flow is not correct, or there are errors biasing the measurements close to the wall that have not been corrected for. Because the friction velocities determined from data points greater than 0.2 mm from the wall were similar, it is assumed that there remains bias errors in measurements close to the wall. Thus to produce the friction velocity to be used in the heat transfer

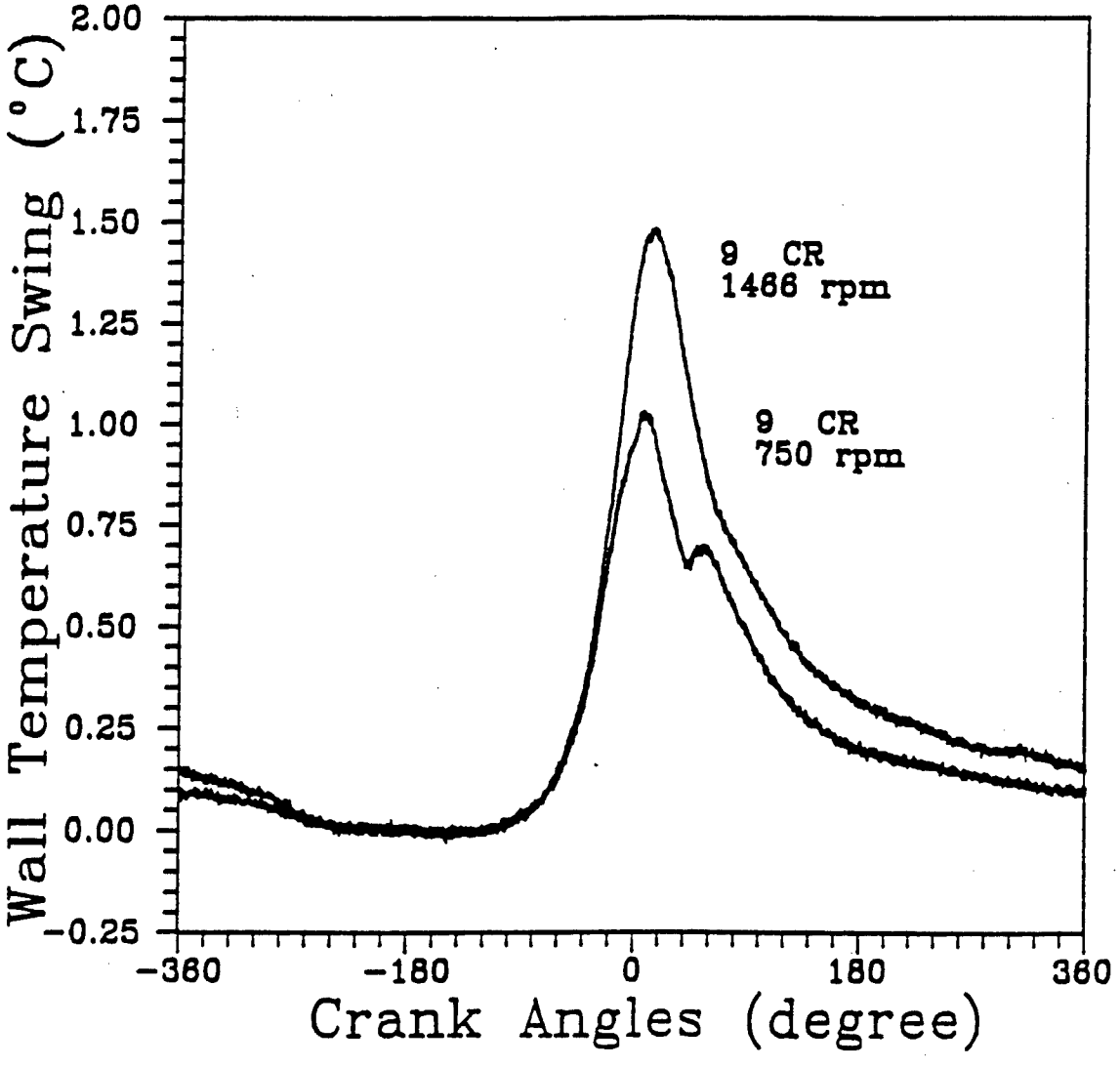

Figure 5-40. Phase-Averaged Surface Temperature Swing

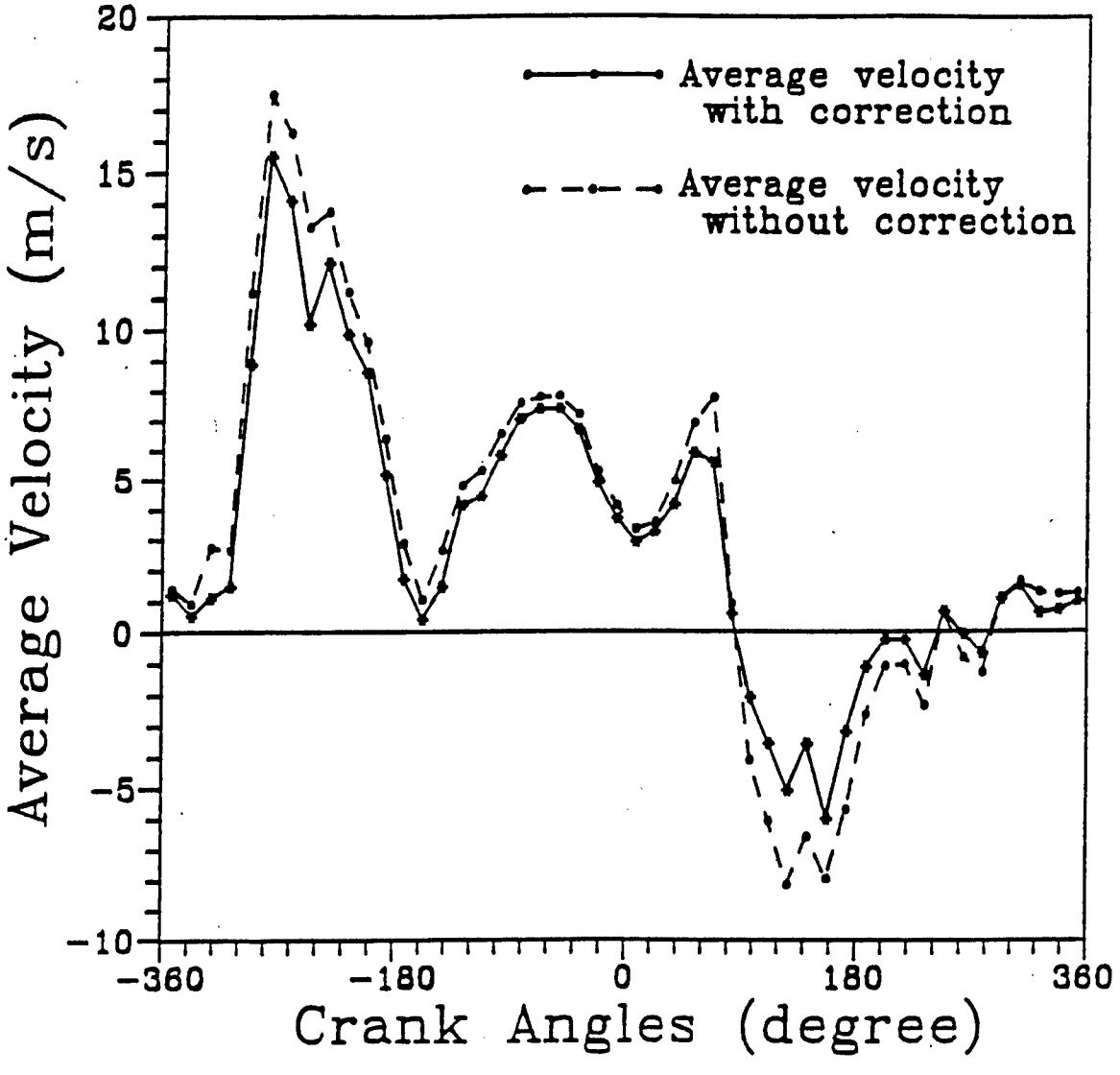

Figure 5-41. Comparison of Bias Corrected and Uncorrected Phase Averaged Velocity Data, 50 Microns from Wall at 750 rpm, High Swirl

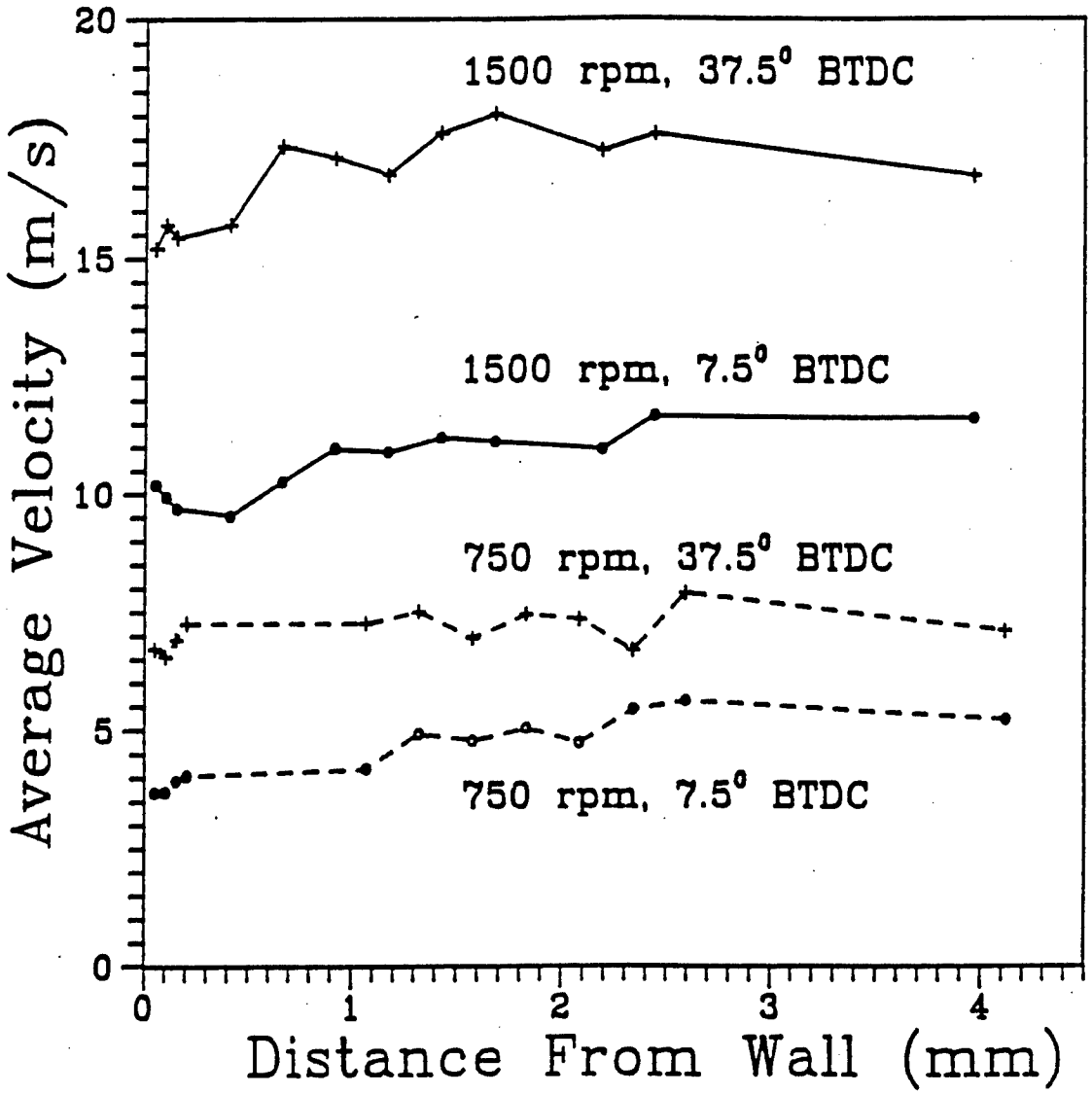

Figure 5-42. Phase-Averaged Velocity Profiles with Bias Correction for Two Different Crank Angles and Two Engine Speed

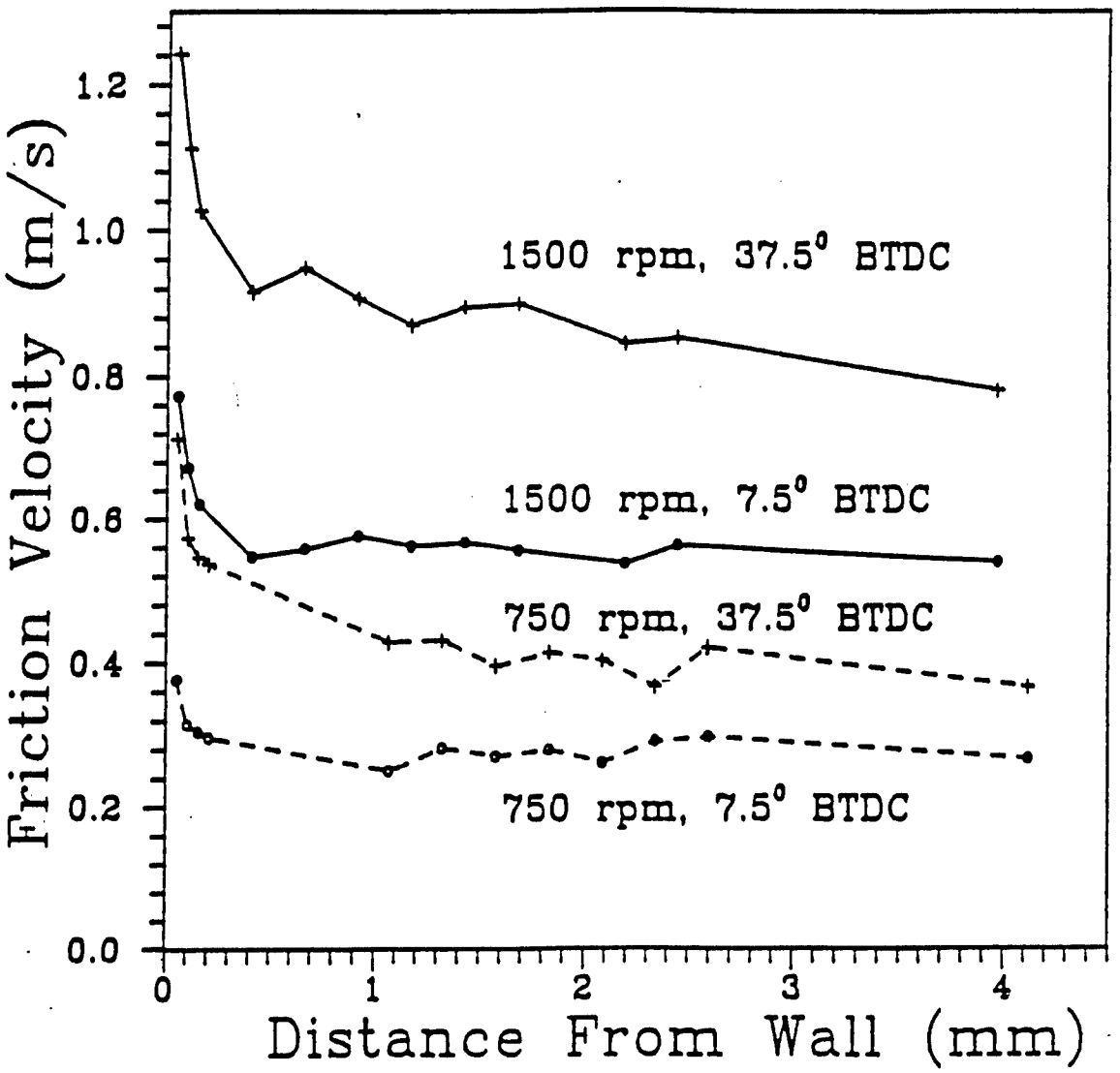

Figure 5-43. Friction Velocities Calculated by Matching Law-of-the-Wall at Different Distance From The Wall

model, the calculated friction velocities determined from data points farther than 200 μm from the wall were averaged. Using this procedure, the friction velocity versus crank angle can be determined. This is plotted in Fig. 5-44. Near TDC on compression, the friction velocities begin to fall, probably due to a combination of boundary layer growth and lower core velocities.

5.4.3. Comparisons with Experimental Data. The first comparisons with experimental data have been confined to the AS1DEE model (described in 5.4.1.2) because this model relies on physical parameters which can be most easily measured or inferred from experimental data. The other models have been used for comparison after substitution into KIVA-II. KIVA-II then produces the necessary details about the fluid mechanics and in-cylinder state. These comparisons will be described in the next section.

In this section, the results of comparisons between the AS1DEE model and two different experiments will be presented. One data set was obtained in the see-through engine facility. In particular, the measured pressure data and calculated friction velocity from the LDV measurement data were used as input to the AS1DEE model. While heat flux measurements have been made for a range of engine swirl ratios, engine speeds, gas properties, and intake gas temperature/wall temperature ratios, it is most appropriate to confine the comparisons with the AS1DEE model to cases where the restrictions used in its development are likely to be met, and accurate velocity data has been obtained. This will most likely be true for the case where the engine fluid mechanics are dominated by a strong swirl motion, with negligible squish flow. Thus the measurements to be compared here were for run conditions of 750 and 1500 rpm, motored, with the shrouded intake valve in a position to produce maximum swirl. The predicted heat flux is compared with the measured heat flux in Fig. 5-45. Very good agreement was obtained. As shown in the figure, magnitudes and phasing were almost identical between the model and experiment for these operating conditions. A second, small peak in the heat flux data observed at the slower engine speed is not captured by the model. This peak probably corresponds to a sudden increase in the velocity fluctuations observed in the velocity measurement data, which would not be accounted for in the model.

Similar to these results, a set of comparisons were performed with data obtained by Dao[80] at the University of Wisconsin-Madison in a previous set of experiments. These measurements were performed on a modified Fairbanks-Morse diesel engine, having a cylinder bore and stroke of 79.4 and 101.6 mm, respectively. The intake valve was shrouded to induce swirl in the cylinder,

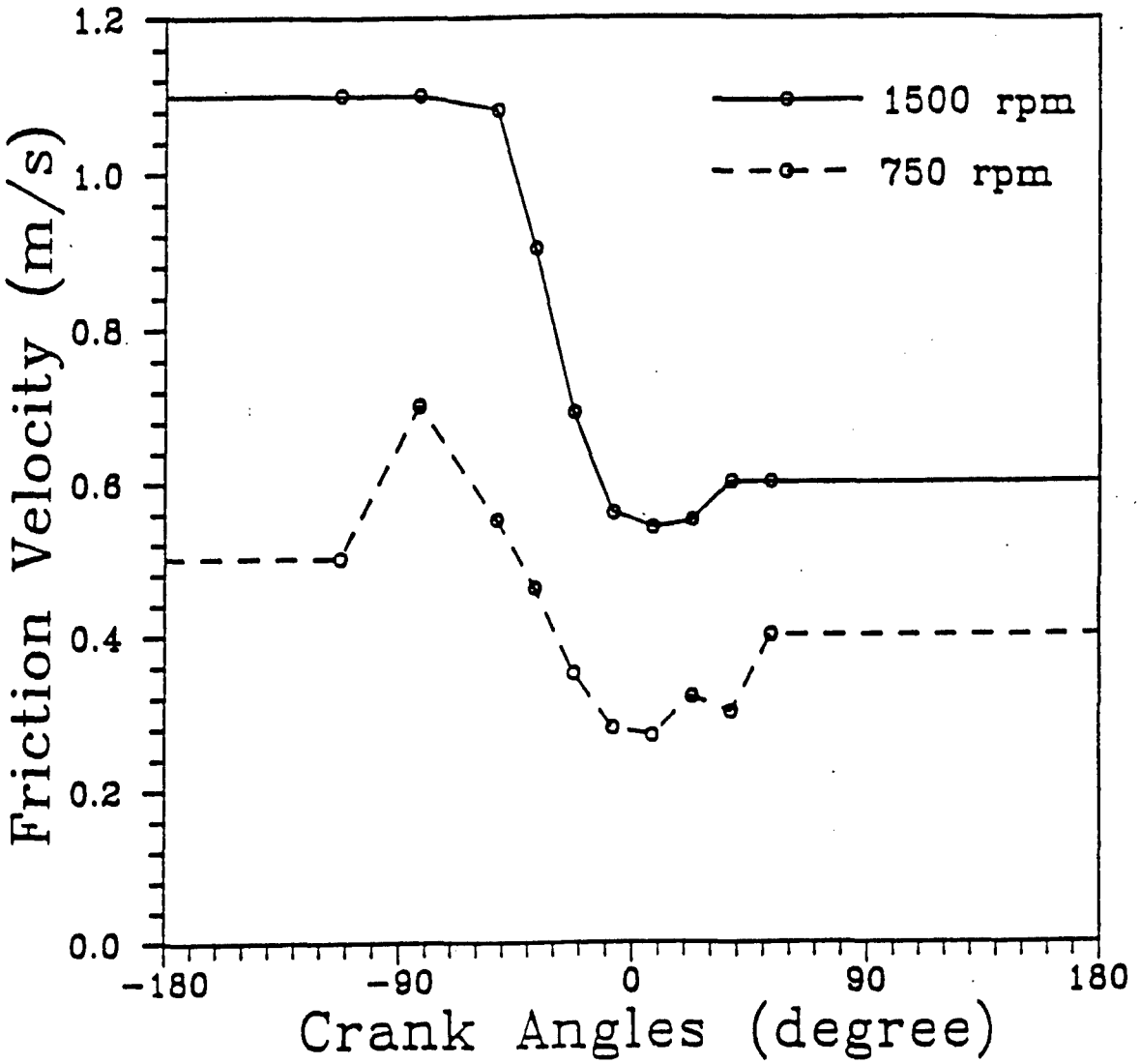

Figure 5-44. Averaged Friction Velocity vs Crank Angles for Two Engine Speed at High Swirl Conditions

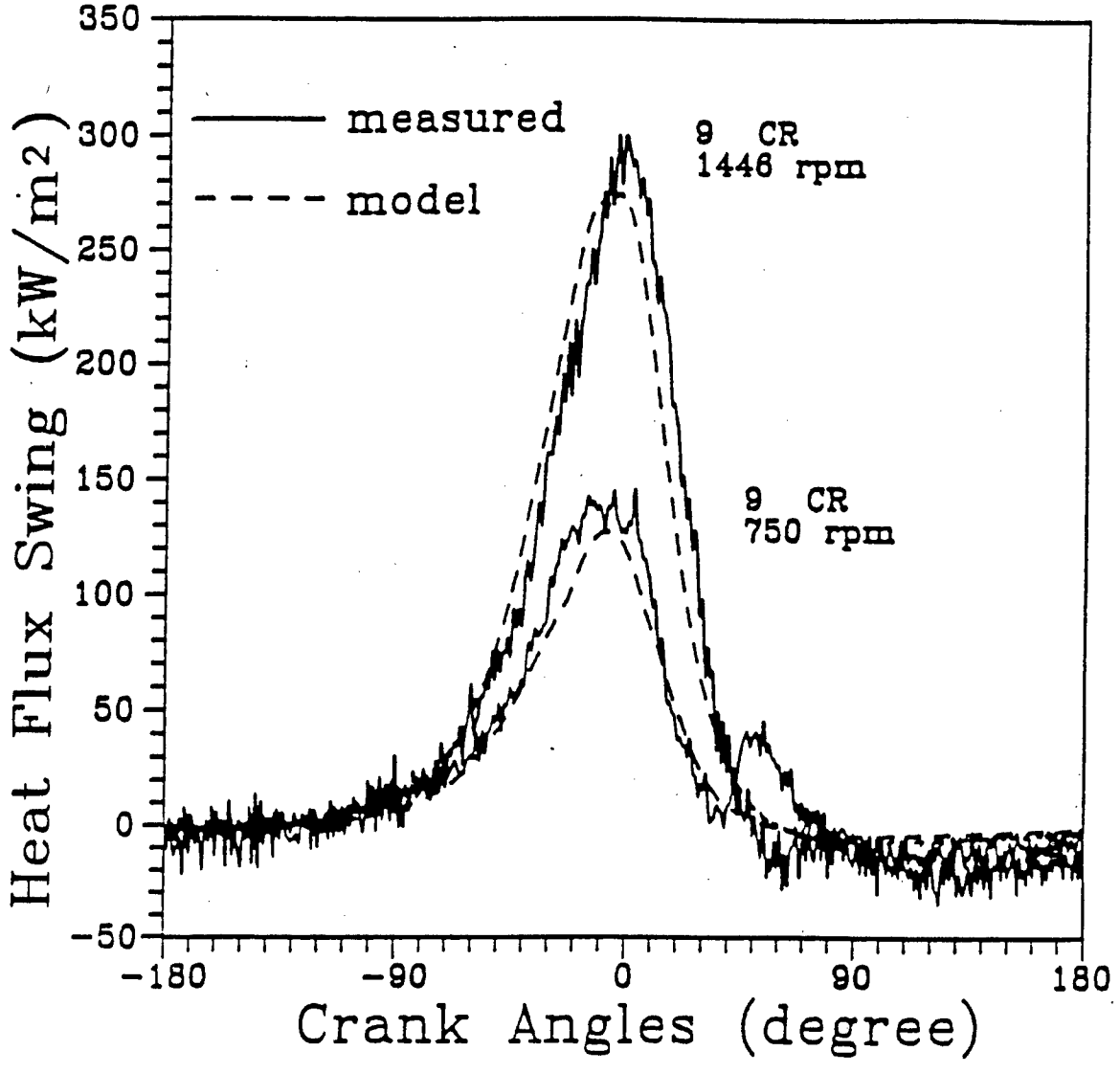

Figure 5-45. Comparisons of Measured Heat Flux with Model Calculations

which for these experiments was positioned such that steady state measurements of the swirl ratio produced a value of 7.15. The head and piston were modified to form a pancake-shaped chamber, similar to the experiments described above. The piston to head clearance was varied to observe effects of compression ratios from 8:1 to 14:1. Surface temperatures were measured with thermistors, one of which was located on each side of a pyrex disk, which was flush-mounted to the cylinder head. An analog RC network was used to determine the heat flux. In all tests the engine was operated in a motored condition.

Comparisons with the model were made for four different engine operating conditions, shown in Table 5-4. As shown in Table 5-4, investigated were changes in engine speed and compression ratio.

For this experiment, the friction velocity was not measured. Thus, it was necessary to estimate the friction velocity at one operating condition, and estimate a relationship between friction velocity and engine speed so comparisons could be made at other operating conditions. An assumption was made that the friction velocity was proportional to the swirl velocity, which is directly related to the engine speed. Using the calibration condition, a relationship relating friction velocity and engine speed was determined:

$$u^* = C \cdot n \tag{38}$$

where n is the engine speed and $C=4.4\times10^{-4}$m/s-rpm.

Shown in Fig. 5-46 is the sensitivity of the model predictions to the value of u^*. For this case the heat flux varies linearly with friction velocity.

Figures 5-47 and 5-48 are the results of the comparison. In general, it appears as if the measured and calculated heat flux agree very well. The fluctuations observed in the experiment are not present in the approximate solution, as would be expected.

5.4.4. Comparison with KIVA-II Predictions.

5.4.4.1. Comparison under simulated motored conditions. For this set of comparisons, KIVA-II has been used to model the hydrodynamics for the first engine case described in section 5.3.6, and for the case of an engine with a bowl-in-piston. These two geometries represent the primary differences in geometry between modern spark-ignition engines and modern diesel engines. All of the chambers are axisymmetric, such that the calculations could be performed on a

Table 5-4. Measurement Conditions

Speed, rpm	CR	T_{in}, °C	P_{tank}, kPa
900	8	24.4	137.8
900	14	24.4	137.8
603	11	23.9	137.8
1202	11	23.9	137.8

Table 5-5. Bowl-in-Piston Geometry Specifications and Operating Conditions

Bore (mm)	79.4
Stroke (mm)	101.6
Displacement (cc)	502.8
Bowl Diameter (mm)	44.7
Bowl Depth (mm)	17.5
Squish Height (mm)	
Compression Ratio	
Engine Speed (rpm)	900
Wall Temperature (K)	297.4
Intake Pressure (kPa)	137.9

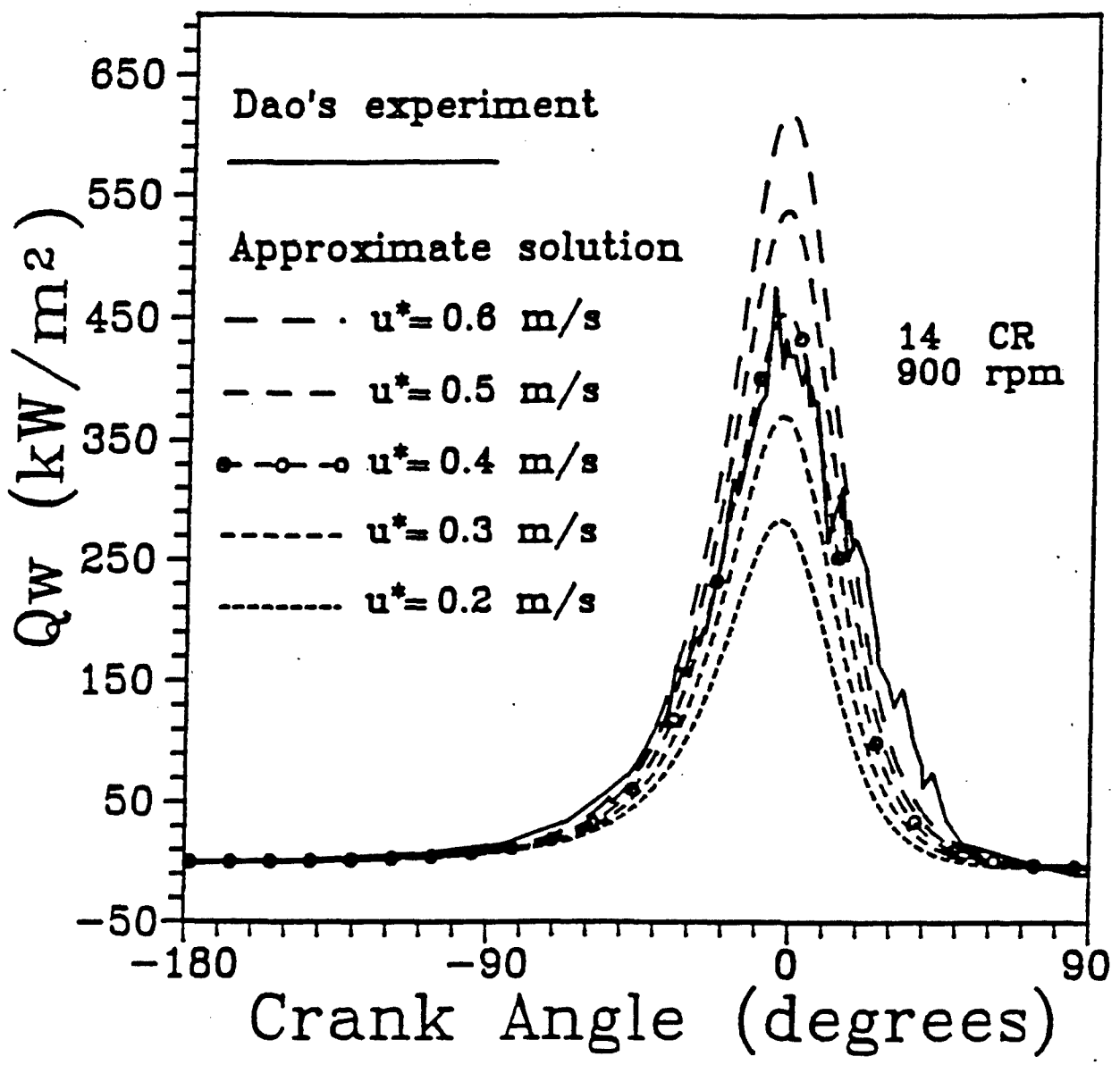

Figure 5-46. Sensitivity of Heat Flux Predictions to Value of u*

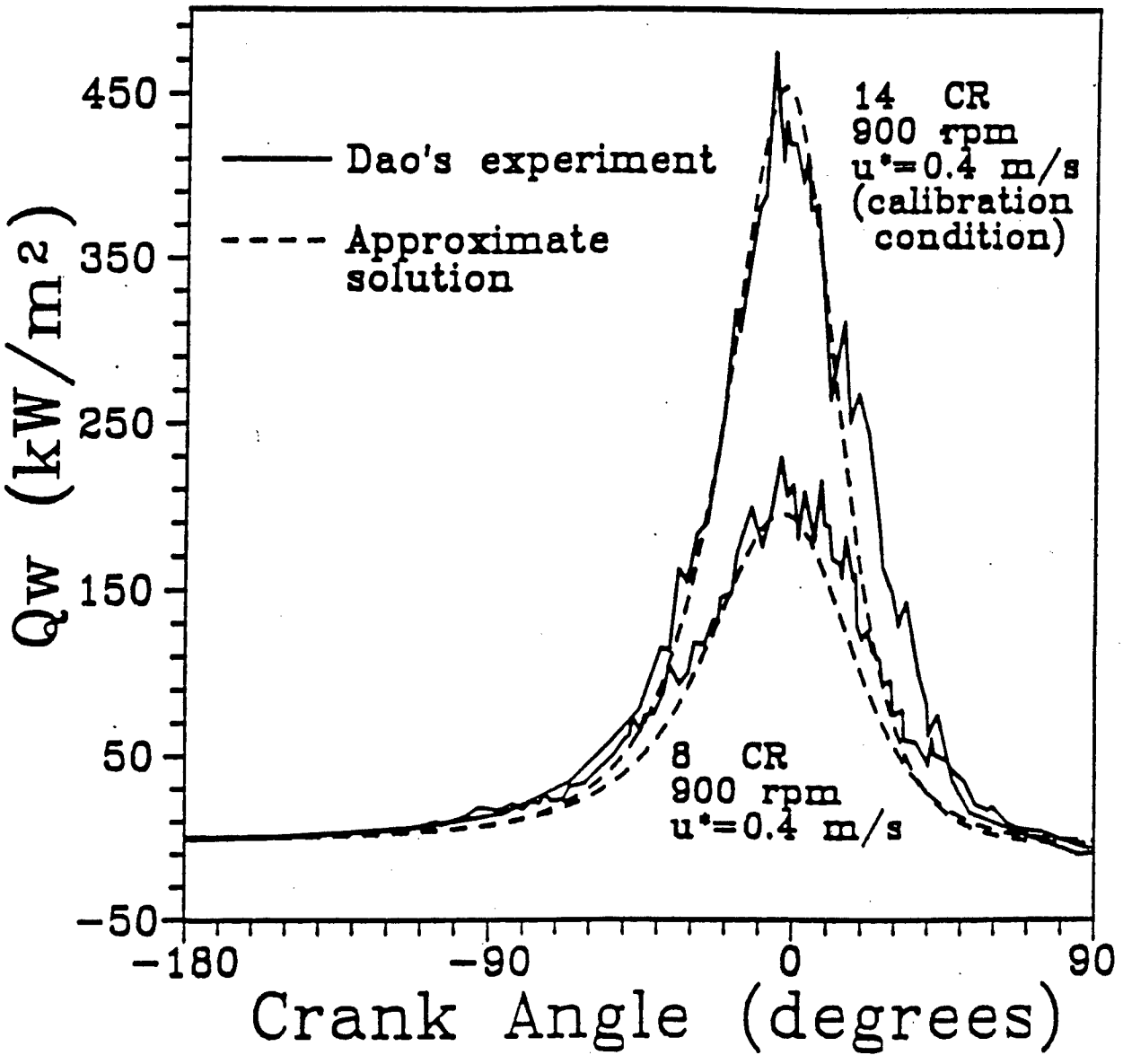

Figure 5-47. Measured and Calculated Values of Heat Flux for a Change in Comparison Ratio

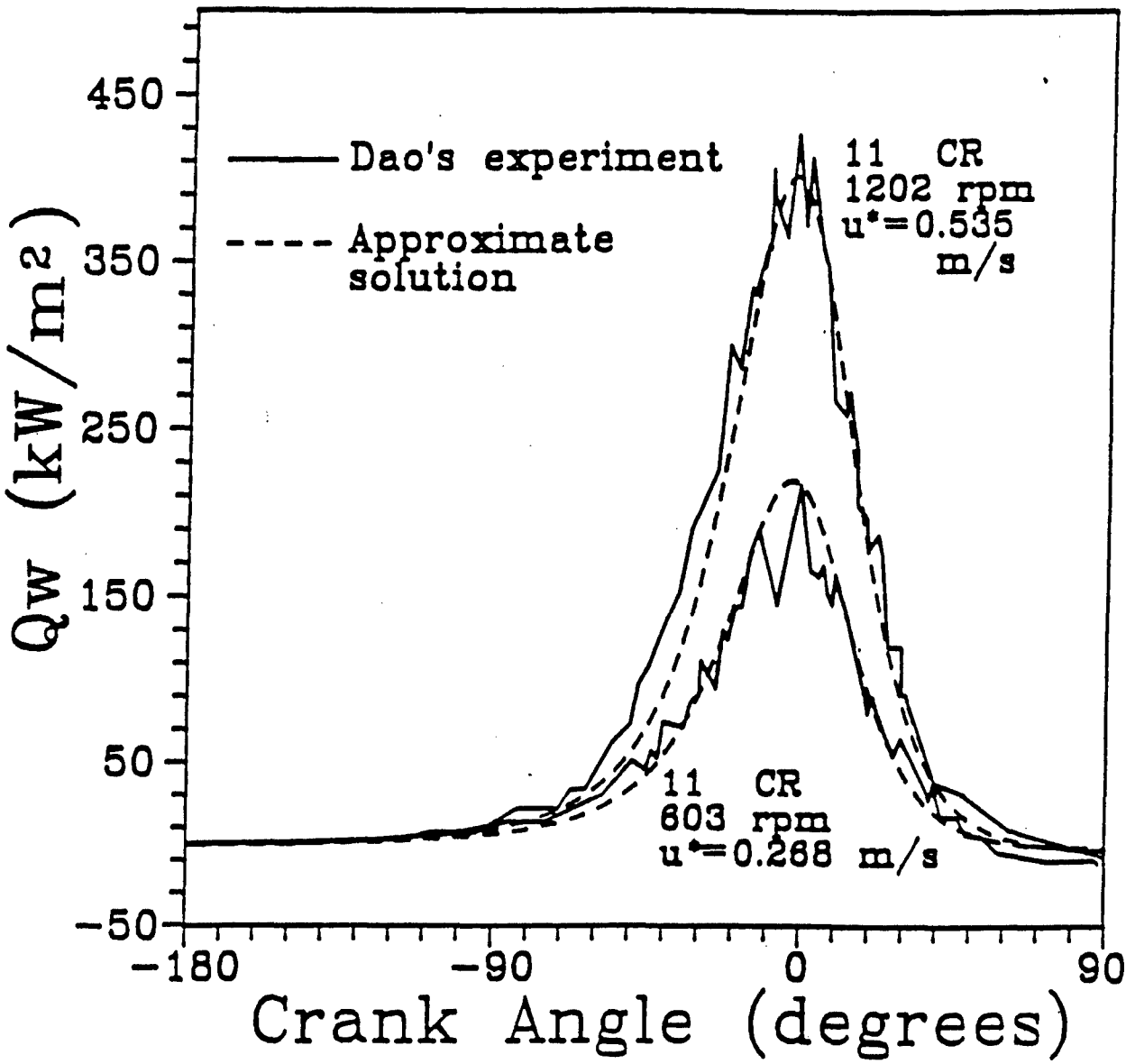

Figure 5-48. Measured and Calculated Values of Heat flux for a Change in Engine Speed

two-dimensional sector of the cylinder to save computing time. The calculations were started at intake valve closure, with the assumption of uniform gas temperature and density. The initial turbulent kinetic energy was assumed to the half the square of the mean piston speed, with the characteristic turbulent length scale assumed to be equal to 7% of the cylinder bore.[81] The initial swirl profile used was a Bessel-function distribution. The boundary condition for the gas velocity is the no-slip condition, and the wall temperature was assumed to be constant throughout the cycle.

5.4.4.2. Comparison for the pancake chamber geometry. The heat flux comparisons shown in Fig. 5-49 for the see-through engine show that the normal wall function underpredicts the peak flux by about 30%, with a phase delay in the time of the peak flux, which is in agreement with the flat piston results from Ikegami, et al.[82] The AS1DEE model and the modified law of the wall model (MLAWAL, 5.4.1.3) produce better results, with differences in the magnitude of peak heat flux of 7% and 10% from the measurements, respectively. The MLAWAL model has a phase difference with the measurements, with the peak value occurring about 15 degrees before the time of the peak observed in the measurements.

5.4.4.3. Comparisons for the bowl-in-piston geometry. A similar set of comparisons for the heat flux models with the data from Dao[83] are shown in Figs. 5-50- 5-51. Specifications of the engine geometry and operating conditions for this data set are given in Table 5-5. As can be seen in Fig. 5-50, at the position on the cylinder head farthest from the bowl (33.02 mm from the bowl center), the models all compare with the measurement results quite well. The peak values are very similar, and the phasing of the peak values are very similar. Secondary peaks observed in the measurement results are again not predicted by any of the models. The source of the these secondary peaks is unknown, and it is not surprising that the models do not predict these characteristics.

At a position at the edge of the bowl (22.35 mm from the bowl center, Fig. 5-51), the PGC model is most similar to the experimental results. There is a double peak in the experimental data that again is not understood and not predicted. Both the normal wall treatment and the MLAWAL overpredict the peak values, probably because these models do not include effects of pressure gradients which will be very important at this position as a result of squish flows.

Finally, at a position 9.40 mm from the bowl center, the MLAWAL and the ordinary law-of-the-wall, produce predictions most similar to the experimental results, as shown in Fig. 5-52. Pressure gradient estimates from the KIVA calculations cause the pressure gradient correction model (PGC model, 5.4.1.4) to produce the behavior shown. Because of the complex flow in this region, it is not

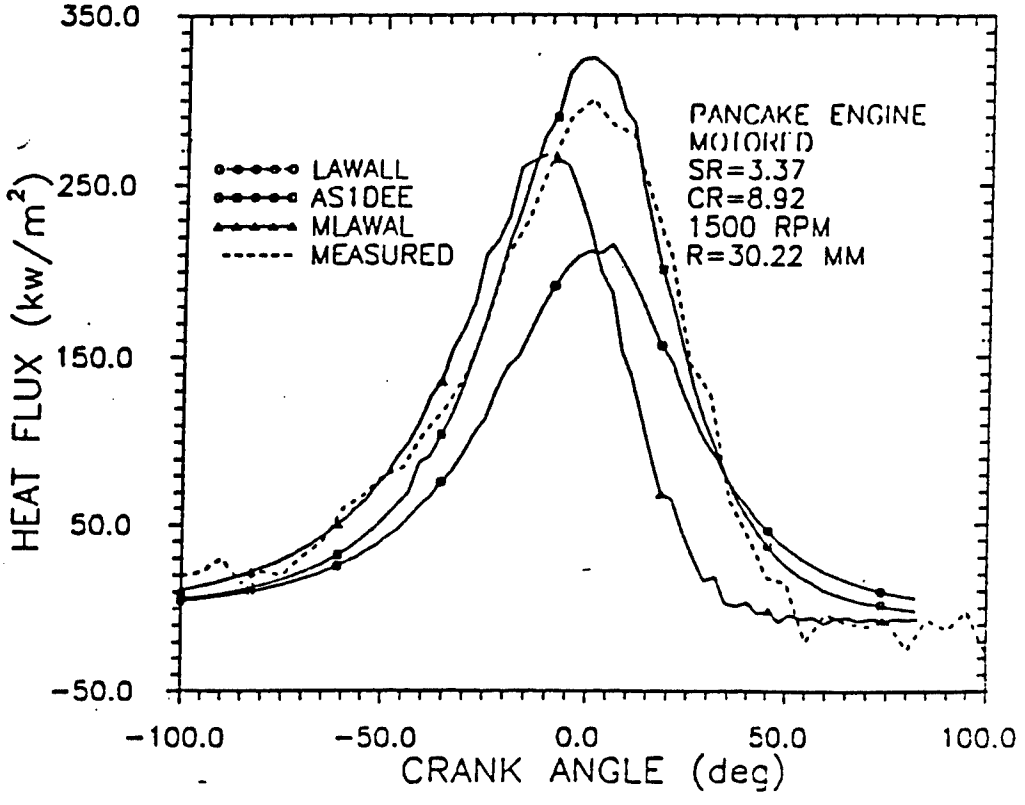

Figure 5-49. Comparison of Heat Flux Predictions and Measurements in the Motored Pancake Engine

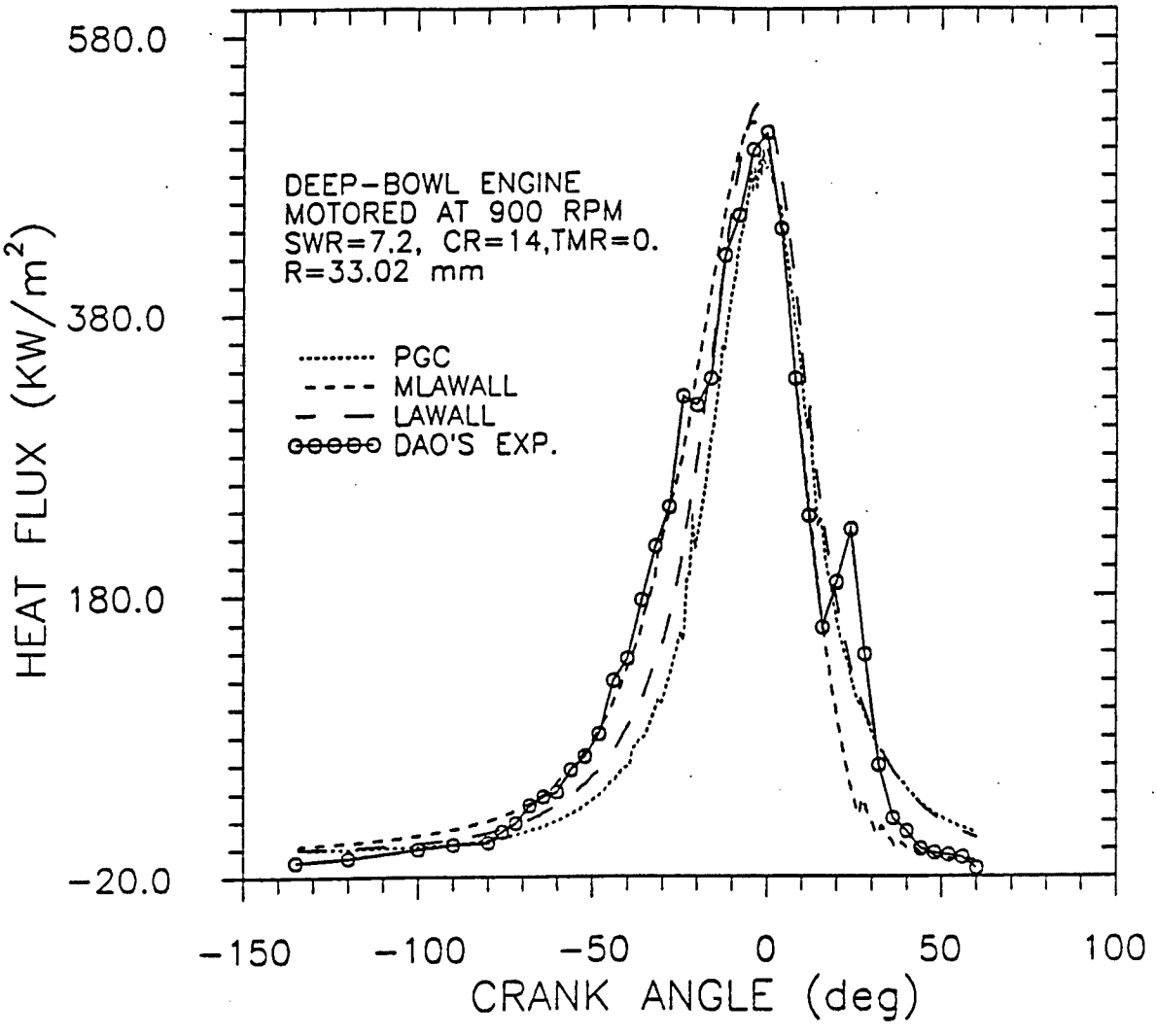

Figure 5-50. Comparison of Different Heat Flux Model Predictions on the Cylinder Head of a Motored Deep-Bowl Engine

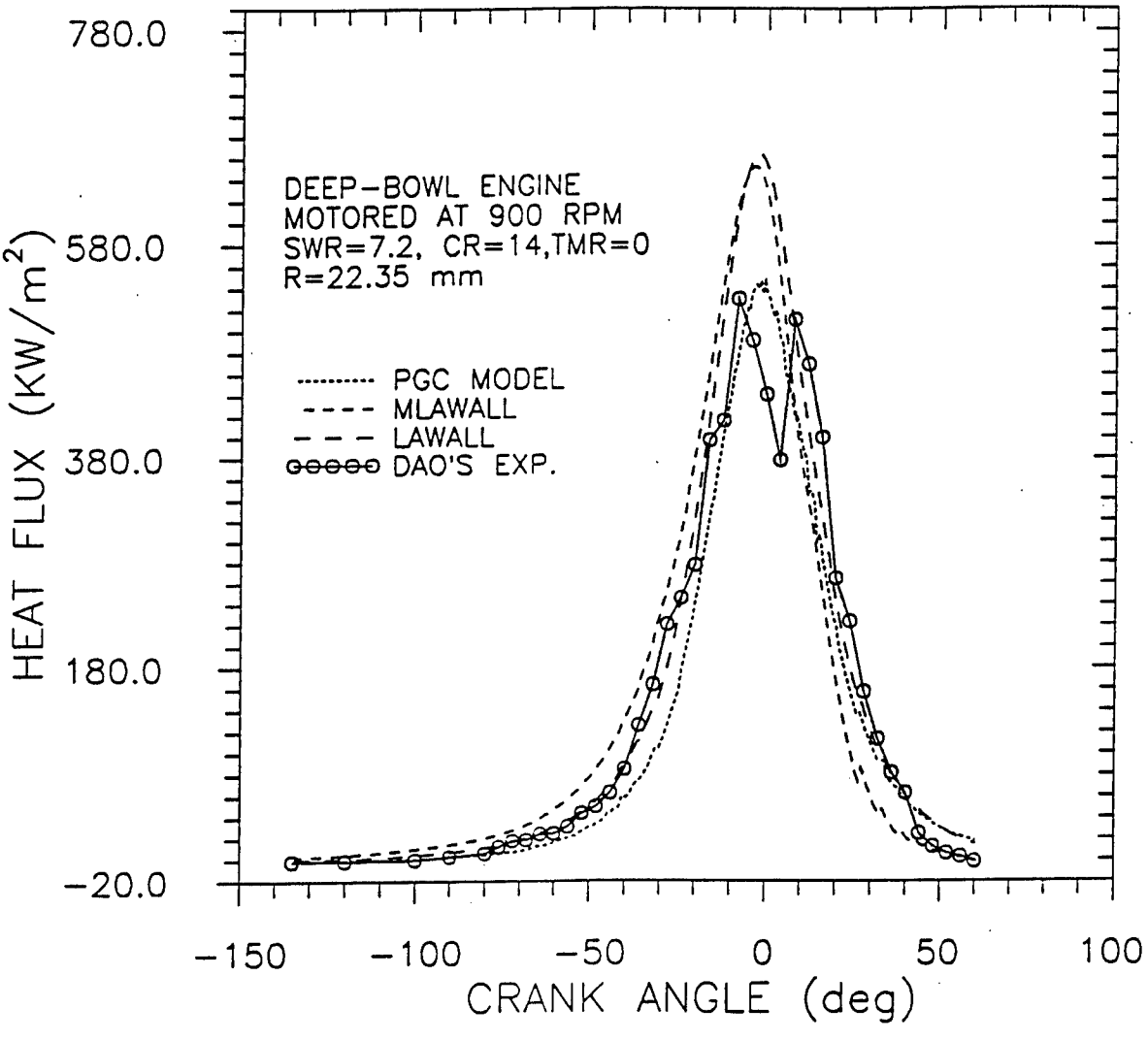

Figure 5-51. Comparison of Different Heat Flux Model Predictions on the Cylinder Head of a Motored Deep-Bowl Engine

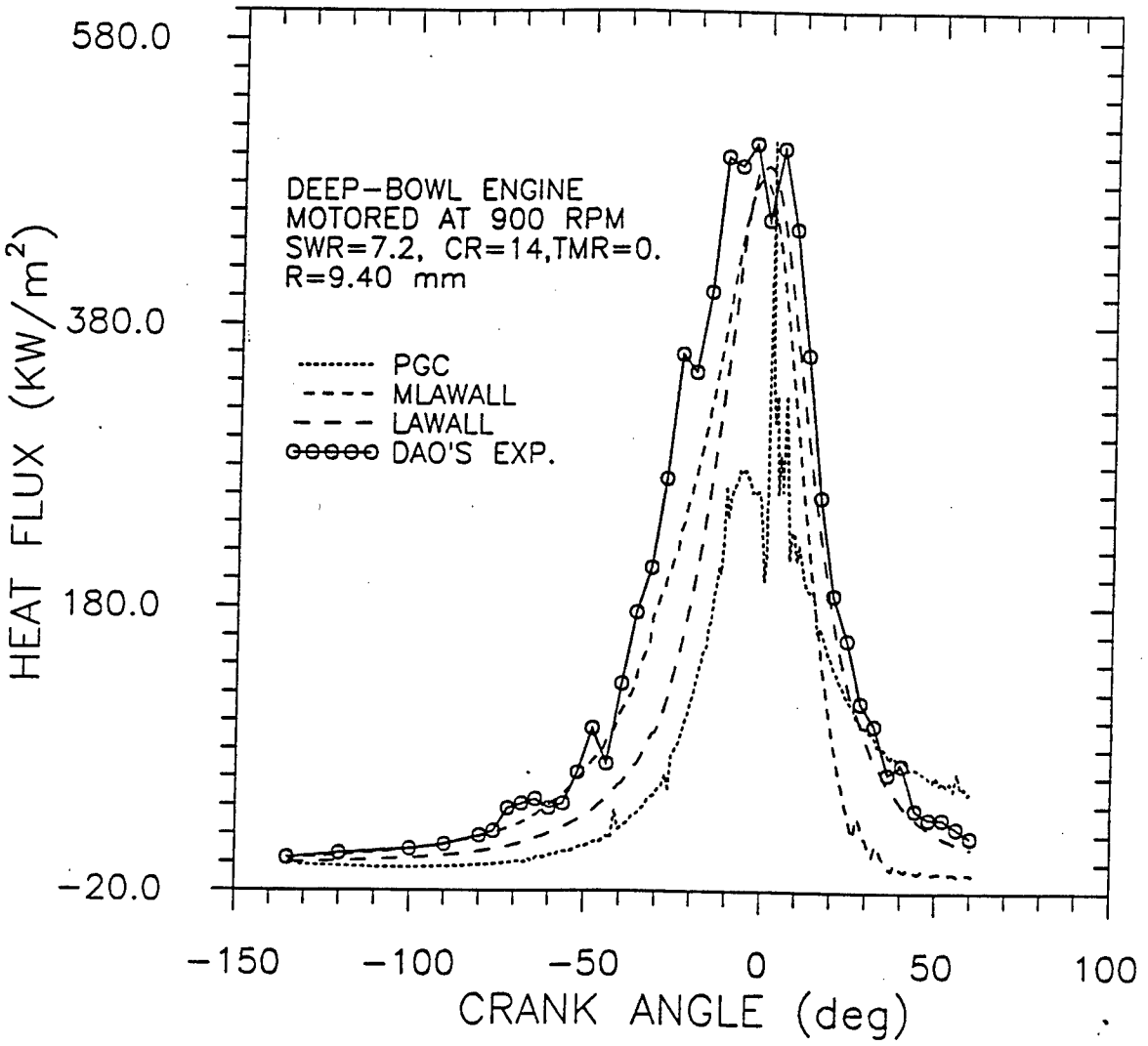

Figure 5-52. Comparison of Different Heat Flux Model Predictions on the Cylinder Head of a Motored Deep-Bowl Engine

recommended to use the PGC model for predictions where the flow will be dominated by inner-bowl effects.

All of these calculations will be dependent on the initial conditions used for the in-cylinder flow. For example, KIVA-II is able to produce solid-body and other swirl-velocity profiles as initial conditions, however, these flows are assumed not to be axially-dependent. In-cylinder flows that are dominated by tumble will not be modeled correctly with these profiles, meaning that heat transfer predictions for flows that are dominated by tumble will likely have errors. Thus, it is very important to recognize that the deviations between the models and experiments in the comparisons described above are, at best, qualitative. Better in-cylinder flow modeling will be necessary for true quantitative comparisons and direct verification of the best heat transfer models.

5.4.4.4. Simulated fired conditions using KIVA-II. For simulated fired conditions using a multidimensional code such as KIVA, the situation just described is further confounded. In addition to the uncertainties in the hydrodynamics, the combustion process in a diesel relies on accurate submodels for the fuel spray, vaporization, ignition, and subsequent reaction. Currently each of these submodels used are under development and have not been validated to the extent that the models can be described as predictive. Of course, the accuracy of heat transfer predictions in engines will be dependent on the accuracy at which combustion is simulated because combustion effects are such an important part of engine heat transfer.

Given these constraints, suitable comparisons under fired conditions are not presented here because of the uncertainties in the combustion modeling, and the appropriate methods to include the effects of combustion on the heat transfer.

LIST OF REFERENCES

1 Chang, I-Ping, "Predictions of Pressure-Gradient Effects on Heat Transfer Predictions for Engine-Type Environments," Ph.D. Thesis, University of Wisconsin-Madison (1991)

2 Cook, D., "Transient Cycle Simulation Program of a Research Diesel Engine," M.S. Thesis, University of Wisconsin-Madison, (1986)

3 Lin, C-S., "Experimental Study of Combustion and Heat Transfer of a Diesel Engine Under Dynamic Operating Conditions," Ph.D. Thesis, University of Wisconsin-Madison (1988)

4 Mueller, M., "In-Cylinder Flame Temperature, Soot Concentration, and Heat Transfer Measurements in a Low-Heat-Rejection Diesel Engine," M.S. Thesis, University of Wisconsin-Madison (1990)

5 Lei, Ning, "A Cycle Simulation Program for the Dynamic Operation of a Single Cylinder Direct Injection Diesel," M.S. Thesis, University of Wisconsin-Madison (1988)

6 Pierce, P., Near-Wall Velocity Characteristics in a Motored Four-Stroke Engine," Ph.D. Thesis, University of Wisconsin - Madison (1991)

7 Verhoeven, Dean D., "Application of Laser Speckle Methods to Temperature Measurements in Engines," M.S. Thesis, University of Wisconsin-Madison (1986)

8 Yang, J., "Convective Heat Transfer Predictions and Experiments in an IC Engine," Ph.D. Thesis, University of Wisconsin-Madison (1988)

9 Borman, G.L., "In-Cylinder Heat Transfer Research at the U.W. Engine Research Center," Int. Symp. COMODIA 90: 1-10, 1990.

10 Borman, G.L. and Nishiwaki, K., "Internal-Combustion Engine Heat Transfer," Prog. Energy Combust. Sci., Vol. 13, pp. 1-46 (1987)

11 Huh, K., Chang, I.-P. and Martin, J.K., "A Comparison of Boundary Layer Treatments for Heat Transfer in IC Engines," SAE Paper No. 900252, (1990)

12 Lin, C.S. and Foster, D.E., "An Analysis of Ignition Delay, Heat Transfer and Combustion During Dynamic Load Changes in a Diesel Engine," SAE Paper No. 892054 (1989)

13 Mueller, M.A., Foster, D.E. and Myers, P.S., "Energy Balances and Particulate Temperature Measurement in an Insulated Engine," Proceedings DOE Workshop, "Coatings for Advanced Heat Engine," August 6-9, 1990, Castile, Maine

14 Verhoeven, D. and Farrell, P., "Speckle Interferometry in Transparent Media," Applied Optics 25 (1986)

15 Verhoeven, D. and Farrell, P., "Heat Transfer Measurements in a Motored Engine Using Speckle Interferometry", SAE Paper 870456, SAE Transactions (1988)

16 Yamada, S., Paulsen, H, and Farrell, P., "Heat Transfer Measurements in a Motored Engine", SAE Paper 890319, SAE Transactions (1990)

17 Yang, J. and Martin, J.K., "Approximate Solution - 1D Energy Equation for Transient, Low-Mach Number, Compressible, Turbulent Boundary Layer Flows," ASME Journal of Heat Transfer, Vol. 111(3), pp.619-624 (1989)

18 Yang, J., Pierce, P., Martin, J.K., and Foster, D.E., "Heat Transfer Predictions and Experiments in a Motored Engine," SAE Paper 881314, SAE Transactions, pp. 1608-1623, Vol. 97 Jour. of Engines (1988)

19 Borman, G.L. and Nishiwaki, K., "Internal-Combustion Engine Heat Transfer," Prog. Energy Combust. Sci., Vol. 13, pp. 1-46 (1987)

20 Borman, G.L., "In-Cylinder Heat Transfer Research at the U.W. Engine Research Center," Int. Symp. COMODIA 90: 1-10, 1990.

21 Borman, G.L., "Mathematical Simulation of Internal Combustion Engine Processes and Performance Including Comparisons with Experiment," CAE Report No. 954, (1964)

22 Borman, G.L, Myers, P.S., and Uyehara, O.A., "Engine Simulation Studies conducted at The University of Wisconsin," TACOM Technical Report No. 11398, (1972)

23 Borman, G. L., "Modeling of Flame Propagation and Heat Release," Combustion Modeling in Reciprocating Engines, Plenum Press, Ed. I. Mattavi & C. Amann (1978)

24 Amsden, A.A., "KIVA - A Comprehensive Model for 2-D and 3-D Engine Simulations," SAE Paper No. 850554 (1985)

25 Amsden, A.A., O'Rourke, P.J. and Butler, T.D., "KIVA-II: A Computer Program for Chemically Reactive Flows with Sprays," Los Alamos Report No. LA-11560-MS, May (1989)

26 Borman, G.L., "Mathematical Simulation of Internal Combustion Engine Processes and Performance Including Comparisons with Experiment," CAE Report No. 954, (1964)

27 Borman, G.L, Myers, P.S., and Uyehara, O.A., "Engine Simulation Studies conducted at The University of Wisconsin," TACOM Technical Report No. 11398, (1972)

28 Lei, Ning, "A Cycle Simulation Program for the Dynamic Operation of a Single Cylinder Direct Injection Diesel," M.S. Thesis, University of Wisconsin-Madison (1988)

29 Watson, N., "Transient Performance Simulation and Analysis of Turbocharged Diesel Engines," SAE Paper No. 810338 (1981)

30 Woschni, G., "Heat Insulation of Combustion Chamber Walls - A Measure to Decrease the Fuel Consumption of I.C. Engines," SAE Paper No. 870339 (1987)

31 Cook, D., "Transient Cycle Simulation Program of a Research Diesel Engine," M.S. Thesis, University of Wisconsin-Madison, (1986)

32 Lei, Ning, "A Cycle Simulation Program for the Dynamic Operation of a Single Cylinder Direct Injection Diesel," M.S. Thesis, University of Wisconsin-Madison (1988)

33 Borman, G.L, Myers, P.S., and Uyehara, O.A., "Engine Simulation Studies conducted at The University of Wisconsin," TACOM Technical Report No. 11398, (1972)

34 IMSL Library, Edition 9, IMSL, Inc., Houston, Texas (1982)

35 Lei, Ning, "A Cycle Simulation Program for the Dynamic Operation of a Single Cylinder Direct Injection Diesel," M.S. Thesis, University of Wisconsin-Madison (1988)

36 Borman, G.L., "Mathematical Simulation of Internal Combustion Engine Processes and Performance Including Comparisons with Experiment," CAE Report No. 954, (1964)

37 Borman, G.L, Myers, P.S., and Uyehara, O.A., "Engine Simulation Studies conducted at The University of Wisconsin," TACOM Technical Report No. 11398, (1972)

38 Watson, N., "Transient Performance Simulation and Analysis of Turbocharged Diesel Engines," SAE Paper No. 810338 (1981)

39 Cook, D., "Transient Cycle Simulation Program of a Research Diesel Engine," M.S. Thesis, University of Wisconsin-Madison, (1986)

40 Miyamoto, N., "Description and Analysis of Diesel Engine Rate of Combustion and Performance using Wiebe's Functions," SAE Paper No. 850107 (1985)

41 Krieger, R.B. and Borman, G.L., "The Computation of Apparent Heat Release for Internal Combustion Engines," ASME, 66-WA/DGP-4 (1966)

42 Miyamoto, N., "Description and Analysis of Diesel Engine Rate of Combustion and Performance using Wiebe's Functions," SAE Paper No. 850107 (1985)

43 Mohammad, I.S. and Borman, G.L., "Measurement of Soot and Flame Temperature Along Three Directions in the Cylinder of a Direct Injection Engine," SAE Paper No. 910728 (1991)

44 Watamabe. Y., Fujisaki, H., Tsuda, T., "DI Diesel Engine Becomes Noisier at Acceleration - The Transient Noise Characteristics of Diesel Engine," SAE 790269 (1979)

45 Sawa, N., "Transitional Character of Diesel Engines," Nai Nan Ki Kan (Internal Combustion Engine, Japan), p. 57, vol. 19, no. 235, 1980.4 (1980)

46 Samria, W.K., Kostin, A.K., Larionov, V.V., Kvasov, E.E., "Study of Heat Release Rate in Diesel Engine Cylinder Under Unsteady Regimes," 8 NCICEC-83, paper HT-1 (1983)

47 Watamabe. Y., Fujisaki, H., Tsuda, T., "DI Diesel Engine Becomes Noisier at Acceleration - The Transient Noise Characteristics of Diesel Engine," SAE 790269 (1979)

48 Huehn, W., Berendes, H., Sauevteig, J.E., "Charge Air Cooling for Duetz Diesel Engines - System Arrangements and Effect on Performance and Emissions," SAE 861943 (1986)

49 Van Gerpen, J., "The Effects of Air Swirl and Fuel Injection System Parameters on Diesel Combustion," Ph.D. Thesis, Mechanical Engineering Department, University of Wisconsin-Madison (1984)

50 Watamabe. Y., Fujisaki, H., Tsuda, T., "DI Diesel Engine Becomes Noisier at Acceleration - The Transient Noise Characteristics of Diesel Engine," SAE 790269 (1979)

51 Krieger, R.B. and Borman, G.L., "The Computation of Apparent Heat Release for Internal Combustion Engines," ASME, 66-WA/DGP-4 (1966)

52 Murayama, T., Miyamoto, N., Tsuda, T., Suzuki, M., and Hasegawa, S.I., "Combustion Behaviors under Accelerating Operation of an IDI Diesel Engine," SAE 800966 (1980)

53 Morel, T., Keribar, R. and Blumberg, P., "Cyclical Thermal Phenomena in Engine Combustion Chamber Surfaces," SAE 850360 (1985)

54 Lin, C.S., "Experimental Study of Combustion and Heat Transfer of a Diesel Engine Under Dynamic Operating Conditions," Ph.D. Thesis, Mechanical Engineering Department, University of Wisconsin-Madison (1988)

55 Huang, J.C. and Borman, G.L., "Measurements of Instantaneous Heat Flux to Metal and Ceramic Surfaces in a Diesel Engine," SAE 871055 (1987)

56 Woschni, G., Spinder, W., and Kolisa, K., "Heat Insulation of Combustion Chamber Walls - A Measure to Decrease the Fuel Consumption of I.C. Engines?" SAE 870339 (1987)

57 Morel, T., Wahiduzzaman, S., and Fort, E.F., "Heat Transfer Experiments in an Insulated Diesel," SAE 880186 (1988)

58 Alkidas, A.C., "Performance and Emission Achievements with an Uncooled, Heavy-Duty, Single-Cylinder Diesel Engine," SAE 890144 (1989)

59 Gatowski, J.A., "Evaluation of a Selectively-Cooled, Single-Cylinder, 0.5-L, Diesel Engine," SAE 900693 (1990)

60 Yang, J. and Martin, J.K., "Predictions of the Effects of High Temperature Walls, Combustion, and Knock on Heat Transfer in Engine-Type Flows," SAE 900690 (1990)

61 Mueller, Mark, "In-Cylinder Flame Temperature, Soot Concentration, and Heat Transfer Measurements in a Low-Heat-Rejection Diesel Engine," M.S. Thesis, Mechanical Engineering Department, University of Wisconsin-Madison (1990)

62 Gatowski, J.A., "Evaluation of a Selectively-Cooled, Single-Cylinder, 0.5-L, Diesel Engine," SAE 900693 (1990)

63 Borman, G.L. and Nishiwaki, K., "Internal-Combustion Engine Heat Transfer," Prog. Energy Combust. Sci., Vol. 13, pp. 1-46 (1987)

64 Yang, J. and Martin, J.K., "Heat Transfer Predictions with High Temperature Walls and Combustion," SAE Paper No. 900690, (1990)

65 Yang, J., "Convective Heat Transfer Predictions and Experiments in IC Engines," Ph.D. Thesis, University of Wisconsin - Madison, (1988)

66 Launder, B.E. and Spalding, D.B., The Numerical Computation of Turbulent Flows, Computer Methods in Appl. Mech. and Eng., Vol. 3, (1974)

67 Chang, I-Ping, "Predictions of Pressure-Gradient Effects on Heat Transfer Predictions for Engine-Type Environments," Ph.D. Thesis, University of Wisconsin-Madison (1991)

68 Verhoeven, D. and Farrell, P., "Heat Transfer Measurements in a Motored Engine Using Speckle Interferometry", SAE Paper 870456, SAE Transactions (1988)

69 Durst, F., Melling, A., and Whitelaw, J.H.,: Principles and Practice of Laser-Doppler Anemometry, 2nd ed., Academic Press, (1981)

70 Kreid, D.K., "Laser-Doppler Velocimeter Measurements in Nonuniform Flow: Error Estimates," Applied Optics, Vol. 13, No. 8. (1974)

71 Hong, N.S., Jones, A.R., and Weinberg, F.J., "Doppler Velocimetry Within Turbulent Phase Boundaries," Proc. R Soc., Lond., A, 353, 77, (1977)

72 Witze, P.O. and Baritaud, T.A., "Influence of Combustion on Laser Doppler Signal qulaity in a Spark Ignition Engine," Int. Sym. on Laser Anemometry, ASME FED 33, 3, (1985)

73 Hall, M.J., Bracco, F.V., and Santavicca, D.A., "Cycle-resolved Velocity and Turbulence Measurements in an IC Engine with Combustion," SAE Paper No. 860320, (1986)

74 Hashimoto, M., Hamamoto, Y., Ohkawa, H., and Sato, O., "Laser Doppler Velocimetry - Effective of Refractive Index Change at Flame Front," Bull., JSME, 26, 1908, (1983)

75 Trump, D.D., Goss, L.P., and Chen, T.H., "Combined CARS-LDV System for Turbulent Flame Studies," Technical Meeting, Central States Section, Combustion Institute, Combustion Fundamentals and Applications, Indianapolis, (May 1988)

76 Witze, P.O. and Martin, J.K., "Cyclic-variation Bias in Spark Ignition Engine Turbulence Measurements," Proceedings of the Second International Symposium on Applications of Laser Anemometry to Fluid Mechanics, Lisbon, (July 1984)

77 Rask, R.B., "Laser Doppler Anemometer Measurements in an Internal Combustion Engine," Trans. SAE, Vol. 88, P. 371, (1979)

78 McLaughlin, D.K. and Tiederman, W.G., "Biasing Correction for Individual Realization of Laser Anemometer Measurements in Turbulent Flows," The Physics of Fluids, Vol. 16, No. 12, (1973)

79 Spalding, D.B., "A Single Formula for the 'law-of-the-wall'," J. Appl Mech., Vol. 28, pp. 455-457, (1961)

80 Dao, K., "Heat Transfer with Cyclic Pressure Variations in Piston Engines," Ph.D. Thesis, University of Wisconsin-Madison, (1972)

81 Ikegami, M., Kidoguchi, Y., and Nishiwaki, K., "A Multidimensional Prediction of Heat Transfer in Non-Fired Engines," SAE 860467, (1986)

82 Ikegami, M., Kidoguchi, Y., and Nishiwaki, K., "A Multidimensional Prediction of Heat Transfer in Non-Fired Engines," SAE 860467, (1986)

83 Dao, K., "Heat Transfer with Cyclic Pressure Variations in Piston Engines," Ph.D. Thesis, University of Wisconsin-Madison, (1972)

DISTRIBUTION LIST

	Copies
Commander Defense Technical Information Center Building 5, Cameron Station ATTN: DDAC Alexandria, VA 22304-9990	12
Manager Defense Logistics Studies Information Exchange ATTN: AMXMC-D Fort Lee, Va 23801-6044	2
Commander U.S. Army Tank-Automotive Command ATTN: ASQNC-TAC-DIT (Technical Library) Warren, MI 48397-5000	2
Commander U.S. Army Tank-Automotive Command ATTN: AMSTA-CF (Dr. Oscar) Warren, MI 48397-5000	1
Director U.S. Army Material Systems Analysis Activity ATTN: AMXSY-MP (Mr. Cohen) Aberdeen Proving Grounds, MD 21005-5071	1
U.S. Army Tank-Automotive Command ATTN: AMSTA-RGR- (E. Schwarz) Warren, MI 48397-5000	6